INDUCTION OF PARTIAL EMT WITH NUTRIENT RESTRICTION AND
LYSOSOMAL ALKALINIZATION IN CACO-2
COLORECTAL CANCER CELLS

A THESIS SUBMITTED TO
THE GRADUATE SCHOOL OF NATURAL AND APPLIED SCIENCES
OF
MIDDLE EAST TECHNICAL UNIVERSITY

BY

HEPŞEN HAZAL HÜSNÜGİL

IN PARTIAL FULFILLMENT OF THE REQUIREMENTS
FOR
THE DEGREE OF DOCTOR OF PHILOSOPHY
IN
BIOLOGY

AUGUST 2022

Approval of the thesis:

INDUCTION OF PARTIAL EMT WITH NUTRIENT RESTRICTION AND LYSOSOMAL ALKALINIZATION IN CACO-2 COLORECTAL CANCER CELLS

submitted by **HEPŞEN HAZAL HÜSNÜGİL** in partial fulfillment of the requirements for the degree of **Doctor of Philosophy** in **Biology, Middle East Technical University** by,

Prof. Dr. Halil Kalıpçılar
Dean, Graduate School of **Natural and Applied Sciences**   _____

Prof. Dr. Ayşe Gül Gözen
Head of the Department, **Biological Sciences**   _____

Prof. Dr. Sreeparna Banerjee
Supervisor, **Biological Sciences, METU**   _____

Examining Committee Members:

Prof. Dr. Ayşe Elif Erson Bensan
Biological Sciences, METU   _____

Prof. Dr. Sreeparna Banerjee
Biological Sciences, METU   _____

Assoc. Prof. Dr. Özlen Konu Karakayalı
Molecular Biology and Genetics, Bilkent University   _____

Assoc. Prof. Dr. Tülin Yanık
Biological Sciences, METU   _____

Assist. Prof. Dr. Onur Çizmecioğlu
Molecular Biology and Genetics, Bilkent University   _____

Date: 26.08.2022

I hereby declare that all information in this document has been obtained and presented in accordance with academic rules and ethical conduct. I also declare that, as required by these rules and conduct, I have fully cited and referenced all material and results that are not original to this work.

Name Last name : Hepşen Hazal Hüsnügil

Signature :

ABSTRACT

INDUCTION OF PARTIAL EMT WITH NUTRIENT RESTRICTION AND LYSOSOMAL ALKALINIZATION IN CACO-2 COLORECTAL CANCER CELLS

Hüsnügil, Hepşen Hazal
Doctor of Philosophy, Biology
Supervisor : Prof. Dr. Sreeparna Banerjee

August 2022, 126 pages

Limited availability of nutrients to cancer cells can result in metabolic rewiring, manifesting in the activation of processes such as autophagy for survival. Our study shows for the first time that Caco-2 cells incubated in a nutrient-restriction (NR) medium of low glucose, glutamine and serum for 48h were viable but less proliferative, demonstrated robust autophagy induction and lower sensitivity to 5-Fluorouracil. However, the cargo protein p62 was not degraded efficiently, suggesting a slower autophagic flux. Perturbation of lysosomal acidification with Bafilomycin A1 (Baf) revealed the strong activation of partial epithelial to mesenchymal transition (EMT) with changes in gene expression and cellular morphology in NR cells. Different from these observations, post-confluent Caco-2 cells that were spontaneously differentiated, showed autophagy induction with functional autophagic flux and more epithelial characteristics.

Culture of Caco-2 cells as 3D spheroids revealed that with NR, the spheroids were loosely formed while addition of Baf led to a complete loss of spheroid formation with loss of cell-cell adhesion. Our data with early- and late-stage autophagy inhibitors suggest that rather than autophagy induction itself, the slower autophagic

flux, perhaps via p62 accumulation, could be implicated in the development of partial EMT and lower drug sensitivity in NR Caco-2 cells.

Overall, our data suggest that low availability of nutrients may lead to the activation of a partial EMT program, particularly if the lysosomes are less acidic.

ÖZ

CACO-2 KOLON KANSERİ HÜCRELERİNDE BESİN AÇLIĞI VE LİZOZOMAL ALKALİZASYON İLE KISMİ EMT İNDÜKSİYONU

Hüsnügil, Hepşen Hazal
Doktora, Biyoloji
Tez Yöneticisi: Prof. Dr. Sreeparna Banerjee

Ağustos 2022, 126 sayfa

Kısıtlı besin mevcudiyetine maruz kalan kanser hücrelerinde, hayatta kalmak için otofaji gibi süreçlerin aktivasyonu ile kendini gösteren metabolik yeniden yapılandırmalar gerçekleşmektedir. Çalışmamız ilk kez, 48 saat boyunca kısıtlı glikoz, glutamin ve serumdan oluşan bir besin açlığı (NR) ortamında inkübe edilen Caco-2 hücrelerinin hayatta kaldığını ancak daha az proliferatif olduğunu, güçlü otofaji indüksiyonu ile birlikte 5-Fluorourasil'e karşı daha dirençli olduğunu göstermektedir. Bununla birlikte, besin açlığında kargo proteini p62 seviyesinin beklenildiği şekilde azalmadığı ve otofajik akışta yavaşlama olduğunu gösterdik. Ayrıca Bafilomycin A1 (Baf) ile lizozomal asiditenin bozulması, NR hücrelerinde gen ekspresyonu ve hücresel morfolojideki değişikliklerle kısmi epitelyalden mezenkimal geçiş (EMT) aktivasyonu gerçekleştiğini ortaya çıkardı. Bu gözlemlerden farklı olarak, konflüensiye bağlı kendiliğinden farklılaşan Caco-2 hücreleri, otofaji indüksiyonu, fonksiyonel otofajik akış ve daha fazla epitelyal özellik gösterdi.

Caco-2 hücrelerinin 3D sferoid kültürü, NR muamelesi sonucunda sıkı olmayan sferoidlerin oluştuğunu, Baf ilavesinin hücre adezyon kaybıyla birlikte sferoid oluşumunun tamamen kaybına yol açtığını ortaya çıkardı. Erken evre ve geç evre

otofaji inhibitörleri ile elde ettiğimiz veriler, otofaji indüksiyonunun kendisinden ziyade, belki de p62 birikimi yoluyla daha yavaş otofajik akışın, NR Caco-2 hücrelerinde kısmi EMT ve daha düşük ilaç duyarlılığı gelişiminde rol oynayabileceğini göstermektedir.

Genel olarak, verilerimiz, düşük besin mevcudiyetinin, özellikle lizozomlar daha az asidik ise, kısmi EMT programının aktivasyonuna yol açabileceğini göstermektedir.

Anahtar Kelimeler: Kolon Kanseri, Besin Açlığı, Otofaji, Lizozomal Alkalizasyon, Kısmi EMT

To my beloved ones,

For their endless love and support

ACKNOWLEDGEMENTS

Las but not least, I owe my deepest gratitude to my family. I am the person as I am today because of my parents, Arife Hüsnügil and Mehmet Enver Hüsnügil, who have been my role models since my childhood and always encouraged me to pursuit my goals. Their unconditional love has always been a constant source of drive and motivation for me. I wish to thank my brother, İsmail Aslan Hüsnügil who has always been my side and helped to keep my spirit up especially with the fun videos and memes he shared with me. My greatest thanks go to them for their never-ending support and understanding, which is beyond what anyone could ever ask for.

TABLE OF CONTENTS

xiv

LIST OF TABLES

TABLES

LIST OF FIGURES

FIGURES

LIST OF ABBREVIATIONS

ABBREVIATIONS

3-MA 3-Methyladenine

3'UTR 3' Untranslated Region

5-FU 5-Fluorouracil

ATG Autophagy-Related Genes

CMA Chaperone-Mediated Autophagy

CRC Colorectal Cancer

ECM Extracellular Matrix

EMT Epithelial-Mesenchymal Transition

FBS Fetal Bovine Serum

NEAA Non-Essential Amino Acids

PAGE Polyacrylamide Gel Electrophoresis

PBS Phosphate-Buffered Saline

PVDF Polyvinylidene Fluoride

ROS Reactive Oxygen Species

SDS Sodium Dodecyl Sulfate

TBS-T Tris-buffered Saline and Tween-20

TCA Tricarboxylic Acid

TFEB Transcription Factor EB

TME Tumor Microenvironment

WCE Whole cell extract

CHAPTER 1

INTRODUCTION

1.1   Tumor Microenvironment

The emergence and growth of the tumor are shaped by both the intrinsic and extrinsic factors. Intrinsic factors comprise the genetic and epigenetic changes within the tumor cells while extrinsic factors are defined as the components of tumor microenvironment (TME) (Baghban et al., 2020). Cancer cells exist in an environment consisting of both cellular (stromal cells) and non-cellular components (extracellular matrix/ECM). Tumor cells interact with surrounding tumor stromal cells and immune cells through complex signaling mechanisms, as well as with the noncellular components of the ECM such as fibronectin, collagen, and laminin (Spill, Reynolds, Kamm, & Zaman, 2016). The dynamic interactions of tumor cells with the components of the TME affect the emergence and progression of tumors and define the characteristics like multidrug resistance, epithelial to mesenchymal transition (EMT) and metastasis (Baghban et al., 2020).

The interaction of tumor cells with the surrounding non-tumoral cells in the TME is mutually beneficial (Baghban et al., 2020). Tumor cells, by secreting signaling molecules, affect the metabolism of neighboring cells so that they continue to support the high proliferation rate of the tumor itself (Comito, Ippolito, Chiarugi, & Cirri, 2020). Therefore, the composition of the nutrients in TME can be highly affected by these interactions and is continuously fluctuating through malignant progression.

1.2 Metabolism in Cancer

During tumor development and progression, exogenous nutrient sources fluctuate greatly. Cancer cells undergo several metabolic adaptations to strengthen their ability to survive and proliferate under these circumstances. These alterations in metabolism are influenced by oncogenic signaling mechanisms as well as the intercellular crosstalk based on nutrient availability (Comito et al., 2020).

The metabolic state of cancer cells is altered significantly when compared to non-tumorigenic cells. Cancer cells require high levels of macromolecules to support elevated biosynthesis reactions that are required for rapid proliferation. These nutrients are also important for the maintenance of redox homeostasis and signaling mechanisms that can enable cell survival (Comito et al., 2020).

Cancer cells also exhibit variabilities in nutrient dependency as some have altered glucose metabolism, some possess altered one carbon metabolism or increased dependency on amino acid metabolism (Bose, Allen, & Locasale, 2020). Various nutrient deprivation strategies have been utilized to mimic the low nutrient availability in tumor microenvironment. Numerous nutrient restriction protocols for cultured cells have been reported in the literature, most of which depend on either the complete removal or reduced amounts of main carbon sources: glucose, non-essential amino acids such as L-glutamine, and serum. However, it should be considered that the effect of nutrient starvation on cell behavior may vary depending on the available nutrients and the duration of starvation. Since the nutrient requirements may varying among different cell types, they may behave differently in response to nutrient deprivation in culture (Ahmadiankia, 2020).

It is worth to note that the complete removal of the main sources of nutrients can lead to activation of oxidative stress response pathways in cells, as shown in numerous studies (Y. Chen et al., 2011; Spitz, Simons, Mattson, & Dornfeld, 2009; C. A. Wu, Chao, Shiah, & Lin, 2013).

1.2.1 Glucose Metabolism

Glucose availability is the primary factor in determining the metabolic activity of cells. With glycolysis, glucose is mainly metabolized to pyruvate, which then enters the tricarboxylic acid (TCA) cycle for energy production (Pavlova & Thompson, 2016). Cancer cells are highly dependent on glucose to support uncontrolled proliferation. High levels of glucose uptake, mainly through the upregulation of GLUT1-3 transporters, provides metabolic intermediates for biomass production, in addition to ATP (Pavlova & Thompson, 2016).

Elevated glucose uptake and activation of glycolysis despite the presence of oxygen, followed by increased lactate secretion is also known as Warburg metabolism (Liberti & Locasale, 2016). Warburg metabolism is one of the most deregulated mechanisms observed in the cells with high proliferation rate such as cancer cells and non-transformed T lymphocytes (Comito et al., 2020).

Glucose withdrawal strategies have been utilized to study various aspects of cell behavior. Cell cycle arrest, change in survival, increased sensitivity to chemotherapy and also chemoresistance was observed with glucose-restriction in different cell types including colorectal cancer (Conacci-Sorrell, Ngouenet, Anderson, Brabletz, & Eisenman, 2014; Hu et al., 2016; L. Wang et al., 2018).

1.2.2 Amino Acid Metabolism

High proliferation rate of tumor cells can alter amino acid demands and affects the related metabolic pathways (Bose et al., 2020). Cancer cells utilize amino acids both for protein synthesis and as metabolic intermediates. They help to maintain redox balance by serving as catabolic substrates in the TCA cycle. Amino acid availability also affects the proliferation rate and growth by modulating mTORC1 signaling (Kanarek, Petrova, & Sabatini, 2020).

In cancer cells, glutamine is reportedly metabolized more abundantly than other non-essential amino acids (Miyo et al., 2016). Increased glutamine metabolism is mainly mediated by the activities of the oncogene c-Myc (Comito et al., 2020). Increased uptake of glutamine by cancer cells is mediated through SLC1A5/ASCT2 transporter; and its catabolism is regulated by the activities of mitochondrial glutaminolytic enzymes. c-Myc regulates the levels of these enzymes and hence glutamine metabolism (Ohshima & Morii, 2021)

In addition to providing carbons to TCA cycle, glutamine also acts as nitrogen source for the synthesis of purines and pyrimidines, and other non-essential amino acids. Glutamine is first converted to glutamate, then α-ketoglutarate (α-KG) which is also used as a fuel in TC cycle (Jiaqi Li et al., 2020). By contributing to the synthesis of glutathione, glutamine also functions in redox balance (Hensley, Wasti, & DeBerardinis, 2013). Various extents of glutamine dependency have been reported in several cancers; high glutamine dependency is generally associated with more aggressive phenotype and therapy resistance (Hensley et al., 2013).

The dependency of cancer cells on the uptake of amino acids may vary and tumors often exhibit auxotrophy for specific amino acids (Bose et al., 2020). For example, asparagine dependency has been associated with various cancer models (Pavlova et al., 2018). Asparagine is known to activate the mTORC1 pathway and its modulation has been shown to limit cancer cell proliferation and metastatic potential (Hettmer et al., 2015; Knott et al., 2018). Serine and glycine feed one-carbon metabolism which provides building blocks for biosynthesis of proteins, nucleic acids and lipids. Increased uptake of these amino acids has been reported in cancer; and withdrawal of serine and glycine has been associated with decreased tumor growth (Maddocks et al., 2017; Sullivan et al., 2019).

1.2.3 Growth Factors and Cytokines (Serum)

Serum contains several cytokines and growth factors that are required for signaling functions of the cells. Serum starvation is a common protocol applied especially in signal transduction studies, and for cell cycle synchronization experiments (Langan, Rodgers, & Chou, 2016). Serum starvation is generally associated with reduced basal activity, so serum withdrawal makes cell populations more homogenous by causing G0/G1 cell cycle arrest. The withdrawal of growth factors directly affects the mTORC1 activity and hence the cell growth (Palm & Thompson, 2017). The effects of serum starvation on cell cycle, proliferation and induction of apoptosis, has been studied in several malignancies including colorectal cancer (Huang et al., 2018; Jin, Ewton, Park, Hu, & Friedman, 2009; S. H. Lee et al., 2011; J. Tong et al., 2016).

The changes in PI3K and MAPK pathways and associated apoptosis-resistant phenotype were reported in 24 h serum-starved glioma and adenocarcinoma cell lines (Levin et al., 2010). In another study with LoVo CRC cell line it was reported that prolonged (96h) serum starvation significantly altered the transcriptional levels of certain metabolites of the TCA cycle, fatty acid and glucose metabolism and nucleic acid metabolism, as well as cell death and proliferation-related pathways (N. Zheng et al., 2016). Enhanced chemoresistance with serum starvation was reported in CRC and breast cancer cells (Tavaluc, Hart, Dicker, & El-Deiry, 2007; Yakisich, Venkatadri, Azad, & Iyer, 2017). In another study with pancreas and breast cancer cells, serum starvation resulted in decreased invasiveness. In these cells, a marked increase in E-cadherin and decrease in Twist1 RNA and protein expression were observed with serum-deprivation (Rasool et al., 2017).

1.3 Nutrient Restriction and Autophagy

Autophagy is an evolutionarily conserved catabolic mechanism that is important for recycling of biomolecules through elimination of long-lived, aggregated, and misfolded proteins or damaged organelles (Ravanan, Srikumar, & Talwar, 2017).

Autophagy is fundamental for all cells in performing housekeeping functions and is involved in diverse biological processes including development, pathogen defense and cellular differentiation (Kocaturk et al., 2019). Cancer cells exploit the autophagy machinery to deal with stressful situations in the tumor microenvironment such as nutrient deprivation or hypoxia (Kenific & Debnath, 2015). At onset of tumorigenesis, autophagy mainly functions as tumor suppressor by limiting cytoplasmic damage and inflammation. On the other hand, when activated at later stages it can promote the survival of cancer cells by providing a continuous supply of energy and biomolecules under stress conditions (Liu & Ryan, 2012). In fact, metastatic cancer cells rely on autophagy to adapt to the new environmental conditions (Jiaqi Li et al., 2020). The factors that determine the autophagic response includes the type of the stress, the timing of the stress, the genetic make-up of the cells, and the nature of the microenvironment. Autophagy typically functions as an anti-apoptotic mechanism in non-malignant cells, but if it is induced in tumor cells or is aberrantly activated, it may result in cell death or induce apoptosis (Amaravadi, Kimmelman, & Debnath, 2019).

Autophagy is a multistep process in which cells degrade or recycle internal constituents including macromolecules and organelles. It is initiated by the formation of double membrane vesicles called autophagosomes. Later, the selected cargo is engulfed in these vesicles. Finally, autophagosomes fuse with lysosomes and form autophagolysosomes in which the degradation occurs via lysosomal hydrolases (Kocaturk et al., 2019). It is divided into three main classes: macroautophagy, microautophagy and chaperon-mediated autophagy (CMA) (Kocaturk et al., 2019). Macroautophagy (hereafter referred to as autophagy) can be divided into bulk and selective autophagy according to the type of cargo. In non-selective bulk autophagy, degradation targets are enclosed in autophagosomes. On the other hand, selective autophagy targets specific cytoplasmic constituents into the autophagosome, including mitochondria, lysosomes, endoplasmic reticulum (ER) and ribosomes (Levine & Kroemer, 2019). Through selective autophagy, cells are able to control the number of organelles and eliminate dysfunctional compartments.

1.3.1 Molecular Mechanisms of Autophagy

The autophagy process is generally divided into 5 steps, namely: Initiation, Nucleation, Maturation, Fusion, and Degradation (Parzych & Klionsky, 2014). Different protein complexes and autophagy-related genes (ATGs) function in these processes (Fig 1.1).

Initiation of autophagy is mediated through the ULK1/2 complex, which is composed of ULK1 or ULK2 kinase, ATG13, FIP200 and ATG101. Upon activation, ULK1/2 dissociates from mTORC1 and interact with the class III PI3K complex for the nucleation of autophagosome membranes. This complex consists of several proteins including VPS34, Beclin-1, AMBRA1 and ATG9. Beclin-1 interacts with BCL2 to activate apoptosis and inhibits autophagy, whereas its interaction with VPS34 lipid kinase leads to autophagic membrane nucleation. VPS34 mediates generation of phosphatidylinositol 3-phosphate (PtdIns3P) which provides a platform for phosphatidylinositol 3-phosphate (PI3P)-binding domain-containing autophagy proteins (Pattingre et al., 2005).

Accumulation PIP3-binding domain-containing proteins at the autophagosome membrane is followed by the binding of several other ATGs for the enclosure and maturation of autophagosomes. Two ubiquitin-like conjugation systems function in maturation: the first complex consists of ATG7/ATG10 and ATG12-ATG5-ATG16L1 proteins and is important for the function of the second system which mediates the conjugation of the protein LC3 to phosphatidylethanolamine (PE) (Tanida, Ueno, & Kominami, 2004). Prior to this, ATG4 cleaves the precursor form of LC3, which exposes the C-terminus glycine residue for PE conjugation. ATG7 and ATG3 proteins mediate LC3-PE conjugation, and the PE conjugated form of the protein is known as LC3-II. The presence of LC3-II in a cell is therefore considered to be a marker for of formation of autophagosomes and induction of autophagy (Yoshii & Mizushima, 2017).

p62 is an ubiquitin-binding autophagic adaptor that selectively recognizes autophagic cargo such as mitochondria, intracellular pathogens and subset of cytosolic proteins and mediate its engulfment into autophagosomes (Katsuragi, Ichimura, & Komatsu, 2015). Since the adaptor proteins are also degraded along with the contents of the autophagosome, successful degradation via autophagy (autophagic flux) is therefore associated with a decrease in the protein levels of p62.
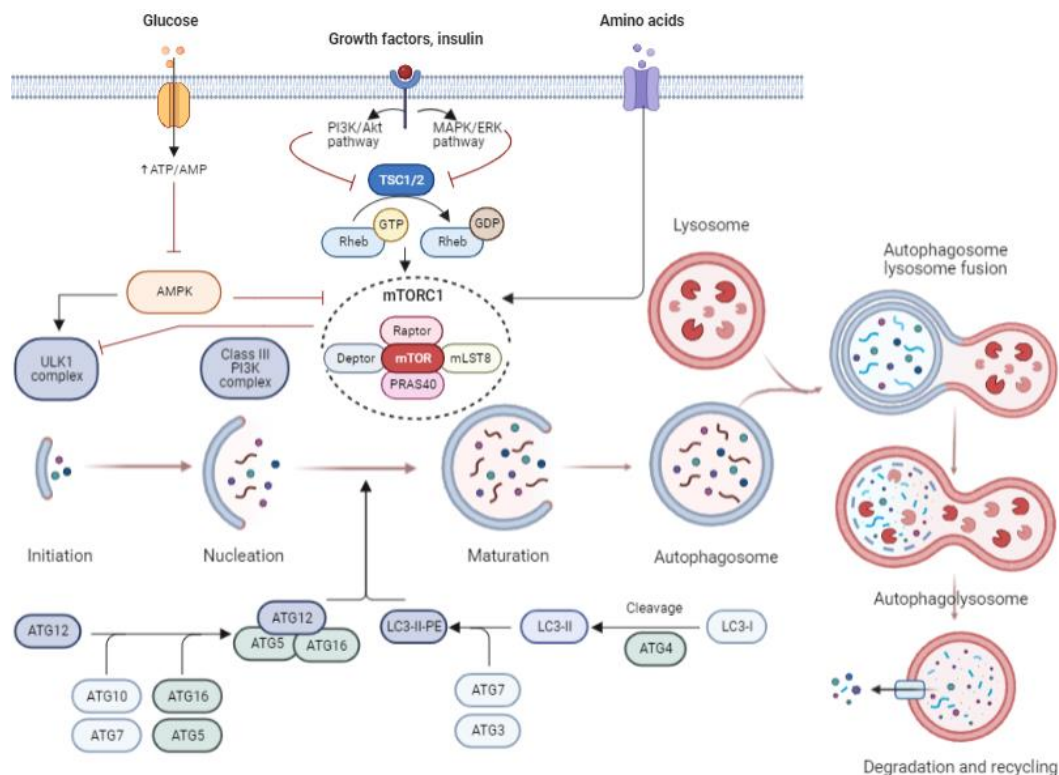
Figure 1.1 Autophagic machinery

Autophagy takes place in a series of steps. Initiation is induced when the ULK1 complex dissociates from the mTORC1 under nutrient-restricted conditions. Activated ULK1 complex drives the formation of the isolation membrane also known as phagophore. Then, nucleation is induced by the PI3K complex. The maturation step is mediated by the Atg5-Atg 12-Atg16L and LC3II-PE conjugates. The autophagic cargo is enriched and encapsulated upon maturation of phagophore into autophagosomes. The autophagosomes then fuse to the lysosomes to form autophagolysosomes. The cargo present within the autophagolysosome is then degraded by the lysosomal enzymes. Created with BioRender.com.

1.3.2   Regulation Mechanisms and Signaling Pathways of Autophagy

In response to different stress stimuli, the autophagic process is initiated with the crosstalk of the two primary nutrient sensing complexes: the mammalian target of rapamycin (mTOR) and AMP Kinase (AMPK) (González, Hall, Lin, & Hardie, 2020).

mTOR is an evolutionary conserved serine/threonine kinase that integrates several signals to modulate energy homeostasis in cells. mTOR forms two distinct complexes namely mTOR complex 1 (mTORC1) and mTOR complex 2 (mTORC2). mTORC1 activity is regulated by PKB/Akt pathway (Ward & Thompson, 2012). mTORC1 directly or through regulatory proteins senses and is phosphorylated in response to nutrient signals. Under nutrient-rich conditions, mTORC1 is active, suppresses catabolic process like autophagy and drives anabolic processes for cell growth. When nutrient deprivation occurs, mTORC1 becomes inactive through phosphorylation of TSC2 and RAPTOR and autophagy is activated (Gwinn et al., 2008).

AMPK is another major energy sensor in cells that can activate autophagy when the AMP/ATP or ADP/ATP ratios are high, such as under nutrient-deprived conditions. In response to high AMP/ATP levels, an upstream kinase LKB1 activates AMPK. Active AMPK causes inactivation of mTORC1 activity through phosphorylation and activation of the inhibitory TSC1/2 complex (Inoki, Zhu, & Guan, 2003). In addition, AMPK activity causes cell cycle arrest through activation of p27^{kip1}, a cyclin-dependent kinase inhibitor in order to activate protective autophagy (McKay & White, 2021).

At the transcriptional level, autophagy is regulated via several transcription factors. FoxO (Forkhead box transcription factor class O) was the first transcription factor that was shown to induce autophagy through transcription of multiple autophagy genes including LC3B, BECN1, ULK2 and VPS34 (Ravanidis et al., 2021). Other important transcription factors that induce the autophagy genes include TFEB, TFE3

and MITF (Napolitano et al., 2018). Various steps of the autophagy process from initiation to elongation, cargo capture to trafficking and fusion with lysosomes are regulated by these factors. The activity of these transcription factors can also be mediated through phosphorylation by the mTORC1 complex in response to stress stimuli (Szabo & Bala, 2018). In a recent study, it was demonstrated that nutrient availability regulates the TFEB activity and nuclear translocation via mTOR (Napolitano et al., 2018). According to this model, the active mTOR complex sequesters TFEB close to the lysosome and prevents its nuclear translocation. When mTOR activity is inhibited, the TFEB is free to translocate to the nucleus and transcriptionally upregulates CLEAR (Coordinated Lysosomal Expression and Regulation) motif containing genes.

Autophagy can also be regulated at the post transcriptional level through microRNAs (miRNAs) (Gozuacik, Akkoc, Ozturk, & Kocak, 2017). miRNAs are short (17-23 nt) non-coding RNAs that are involved in post-transcriptional regulation of gene expression by affecting both the stability and translation of mRNAs. They impact several fundamental cellular processes such as proliferation, differentiation, metabolism, and apoptosis. Recent studies suggest that miRNAs are important regulators of autophagy (Akkoc & Gozuacik, 2020). They affect the protein levels of numerous proteins involved in different steps of autophagy. For example, miR-7, miR-199a and miR-101 directly regulates several components of mTOR1 pathway including p70S6K and eukaryotic translation initiation factor 4E (eIF4E) in different cell types. miR-885-3p and miR-26b mediated regulation of ULK1/2, miR-30a, miR-376 and miR-384-5p mediated regulation of BECN1, miR-204 mediated regulation of LC3B and miR-17/20/93/106 miRNA families mediated regulation of p62 can be given as examples to indicate the involvement of miRNAs in the autophagy regulation (Akkoc & Gozuacik, 2020).

1.3.3 Autophagy and Differentiation

Autophagy can be active at a basal level in all cells, providing a continuous turnover of damaged or aged cellular components and maintaining cellular homeostasis (Ravanan et al., 2017). It was also indicated by several studies that autophagy is involved in cellular differentiation in various cell models. For example, the involvement of autophagy in adipocyte differentiation was shown in 3T3-L1 preadipocytes and mouse models. It was noted that this process was regulated via C/EBP, a crucial transcription factor involved in adipocyte development (Ni et al., 2013). Another study with MCF-7 human breast cancer cells showed that differentiation followed by autophagy induction was observed in response to the phytochemical Pterostilbene (Chakraborty et al., 2012).

Autophagy is also important for homeostasis in the gut epithelium. The small and large intestinal epithelial layer is formed from the intestinal endoderm by the formation of a crypt-villus axis. Due to cell differentiation occurring along the crypt-villus axis, the epithelial layer of the small and large intestine is in a regular state of destruction-regeneration cycle (Gehart & Clevers, 2019). The crypt-villi axis of the intestinal mucosa exhibits distinct features from undifferentiated cells to terminally differentiated cells. The autophagic machinery is utilized for the removal of terminally differentiated apoptotic cells (Levine, Mizushima, & Virgin, 2011). Our lab has shown that autophagy was activated during the differentiation of intestinal epithelial cells via the upregulation of ER stress as the cells acquired a more secretory phenotype (Tunçer et al., 2020).

Cells forming epithelial tumors enter the process of "loss of differentiation", which is caused by factors such as loss of expression of epithelial markers and an increase in the expression of genes that cause the acquisition of abilities such as proliferation and metastasis (Rodrigues et al., 2018; Solanas et al., 2008). Understanding the mechanisms of loss of differentiation (dedifferentiation) in the intestinal epithelial layer will contribute to understanding of the causes of malignant growth. However, since apoptosis is observed shortly after separation from the tissue in primary

11

intestinal epithelial cells (anoikis), it is technically challenging to investigate the differentiation process (Hofmann et al., 2007). For this reason, colon cancer cell lines like Caco-2, which show spontaneous and reversible differentiation into enterocytes, are frequently used as a model of intestinal differentiation (Devriese et al., 2017; Rousset, 1986).

1.4   Effects of Nutrient Restriction on Cancer Cell Behavior

Cancer cells are highly proliferative, especially at early stages of their development. In order to sustain viability under nutrient-deprived conditions, cancer cells can rewire their metabolism and signaling mechanisms (C. Li et al., 2015; Xu et al., 2015). As a result, the progression through cell cycle and proliferation of the cells are affected and several adaptive responses such as autophagy, epithelial to mesenchymal transition (EMT) and chemoresistance are induced (Vaziri-Gohar et al., 2022).

1.4.1   Cell Cycle and Proliferation

The impact of nutrient restriction on cancer cell survival and proliferation has been investigated by numerous studies in different cancer models including colorectal cancer (CRC). The findings of these studies are divergent and context specific, depending on the type of nutrient restriction, the duration of treatment and the cellular status.

For example, Jin et al. showed that HT29 CRC cells cultured in serum-free medium for 48 hours entered a reversible quiescent G0 state through increased expression of minibrain-related kinase (Mirk)-mediated destabilization of G1 cyclins (Jin et al., 2009). Similarly, it was reported that the short term (6 h and 12 h) treatment of HCT-116 CRC cells with serum-free medium resulted in decreased viability through a Smad4/PUMA-mediated mechanism (S. H. Lee et al., 2011). In another study conducted with various cell lines from different cancers including CRC, the

12

increased expression of apoptotic proteins was observed in response to 24 h culturing of cells in 0.5 % FBS-supplemented medium, thus making the cells more sensitive to apoptotic cell death (C. Li et al., 2015).

On the other hand, some studies reported the increased cell survival in response to nutrient-restriction with CRC cells. For example, amino-acid deprivation of CRC cell lines SW48, SW620, DLD-1 and LoVo for 24 h resulted in activation of autophagy as a protective mechanism (Sato et al., 2007). Likewise, DLD-1 cells cultured in medium without glucose, glutamine and serum, individually, for 24 h, 48 h and 96 h showed increased survival and apoptosis evasion via proteolytic cleavage of Myc (Conacci-Sorrell et al., 2014). Interestingly, these authors reported that Myc-nick promoted survival through the induction of autophagy. It was reported that CRC cells were able modulate their metabolism to continue survival under glucose deprivation, while the viability of pancreatic cells was decreased (Miyo et al., 2016).

1.4.2   Sensitivity to Drugs

In order to continue their survival under stressful conditions, cancer cells modulate various signaling mechanisms. This can also affect the sensitivity of these cells to chemotherapeutics. Moreover, while sensitizing the tumor cells to drugs, nutrient starvation can act as a protective mechanism decrease the cytotoxic effects of drugs in normal cells (Naveed, Aslam, & Ahmad, 2014).

The sensitization of cancer cells to chemotherapeutics via glucose, amino acid and serum starvation has been reported in several studies (Shi et al., 2012; Thomas, Davis, Nell, Sishi, & Engelbrecht, 2020; L. Wang et al., 2018). The elevated ROS generation and oxidative stress introduced with serum starvation was shown as a mechanism to enhance sensitivity to chemotherapeutics (Pandey, Lopez, & Jammu, 2003; Zhuge & Cederbaum, 2006). In another study the increased sensitization of breast cancer cells to Doxorubicin with amino acid starvation was demonstrated. The same study also reported that upon Doxorubicin treatment, autophagy induction was

observed which played a central role in the increased chemosensitivity (Thomas et al., 2020).

In various other studies, the opposite effect of nutrient starvation was reported where it increased chemoresistance. For instance, the resistance of lung and breast cancer cells to a number of conventional chemotherapeutic agents in response to prolonged serum starvation was reported. The mechanism of resistance was revealed as increased stemness characteristics via upregulation of Sox2, MDR1 and Bcl-2 factors (Yakisich et al., 2017). In addition, nutrient-deprivation-induced Myc cleavage in CRC cells was indicated as another mechanism which could prevent apoptotic cell death after treatment with chemotherapeutic drugs such as etoposide and cisplatin (Conacci-Sorrell et al., 2014). In another study with CRC cells, glucose-restriction-induced chemoresistance was observed in an ATF4-dependent mechanism, a key gene involved in ER stress and the unfolded protein response (Hu et al., 2016).

1.4.3 Epithelial to Mesenchymal Transition

Epithelial to mesenchymal transition (EMT) is a highly complex sequence of events that includes loss of contact between adherent epithelial cells, change of morphology by acquisition of mesenchymal characteristics and enhanced motility (Yang et al., 2020). EMT is functional both during development and metastasis. In this program, epithelial cells change their shape from a cobblestone like morphology to a more spindle like shape by acquiring the ability to survive after detachment from other cells or the basement membrane (anoikis resistance), gain the ability of reorganization of the cytoskeleton and degradation of the extracellular matrix. These changes in cancer are known to enhance metastatic spread, resistance to chemotherapeutic drugs and is associated with the recurrence of cancer (Yang et al., 2020). EMT-related resistance to drugs is one of the major causes of treatment failure (Hill & Wang, 2020).

Conventional EMT is characterized by a complete loss of epithelial characteristics such as the expression of junctional proteins E-cadherin and Occludin and acquisition of mesenchymal properties such as the expression of the cytoskeletal protein Vimentin and N-cadherin (Sinha, Saha, Samanta, & Bishayee, 2020). Recent studies, however, suggest that rather than the binary process of a complete transition from epithelial to a mesenchymal phenotype, disseminating cells may acquire a hybrid phenotype whereby there is a gradual conversion of epithelial cells, through a number of intermediate stages, to a mesenchymal form (Sinha et al., 2020) (Fig 1.2). Cells that show characteristics of partial/hybrid EMT pose greater risk of metastatic spread compared to cells showing complete EMT and are associated with poor clinical prognosis in cancer (Pastushenko & Blanpain, 2019; Saitoh, 2018).
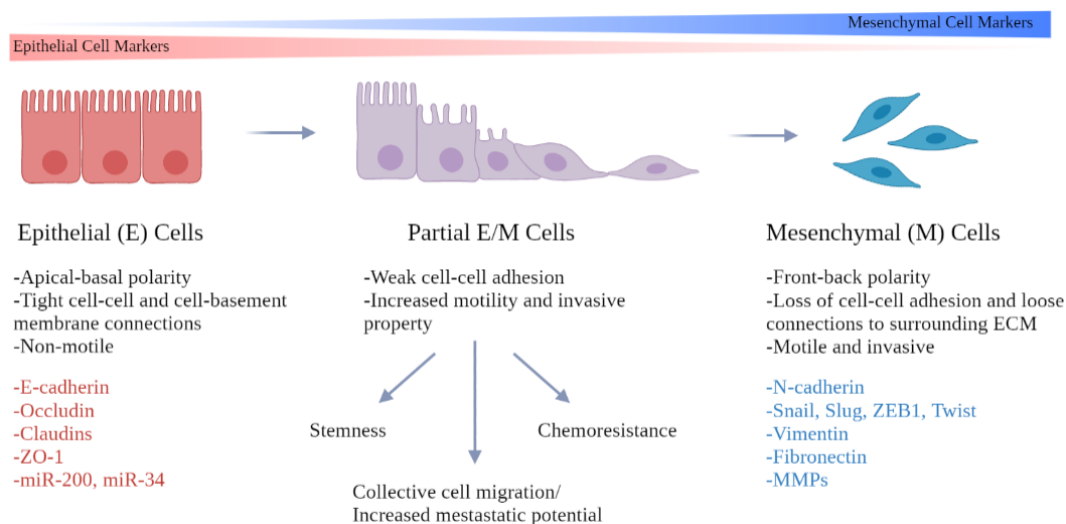
Figure 1.2 Overview of partial EMT

In the course of EMT process epithelial markers (e.g., E-cadherin, occludin) are gradually lost, while mesenchymal markers (e.g., N-cadherin, vimentin) are expressed. This process is regulated by transcription factors Snail/Slug, ZEB1 and Twist. Partial EMT is an intermediate stage in the EMT spectrum possessing both epithelial and mesenchymal signatures. Cells undergoing partial EMT have the capacity to undergo collective migration, enhanced stemness, and are unresponsiveness to chemotherapy. Created with BioRender.com.

The limited availability of nutrients affects the invasive and metastatic properties of cancer cells as shown by various studies. It was revealed that nutrient-restriction, through modulation of EMT-related genes, resulted in enhanced cell migration. For example, elevated TGF-ß signaling and induction of EMT were observed in hepatocellular carcinoma and bladder cancer with HBSS starvation. In addition, the importance of starvation-induced autophagy in the EMT-mediated invasion and migration was reported (Jun Li et al., 2013; H. Tong et al., 2019). When the cells were treated with early- and late-stage autophagy inhibitors, 3-MA and Chloroquine, the expression of TGF-β Smad3 was decreased and EMT was suppressed (H. Tong et al., 2019). Genetic inhibition of Atg3 or Atg7 with siRNA under starvation conditions also resulted in decreased EMT which was rescued by the exogenous administration of TGF-β (Jun Li et al., 2013). In colorectal cancer cells, increased motility and metastatic capacity with glucose and glutamine restriction was demonstrated through enhanced expression of actin bundling protein fascin. The elevated levels of autophagosomal protein LC3-II were reported in starved cells, which was further accumulated with the autophagy inhibitor Chloroquine. In addition to the activation of EMT, starved cells also exhibited resistance to apoptosis, which was reversed by the autophagy inhibitor Chloroquine (Conacci-Sorrell et al., 2014).

The interplay between EMT and autophagy have been reported in different contexts for both cancerous and noncancerous cells (Gugnoni, Sancisi, Manzotti, Gandolfi, & Ciarrocchi, 2016). Cytoskeletal reorganization, mitochondrial dysfunction, and selective degradation of EMT proteins have been suggested as the regulator of the two processes. Considering the dual effect of autophagy on cancer progression, the autophagy-EMT crosstalk also appears to be context dependent and varies depending on the type and/or the stage of the tumor.

1.5 Scope, Aim and Novelty of This Study

Limited availability of nutrients to cancer cells can result in metabolic rewiring. As a result of these metabolic changes, several aspects of cancer cell growth and survival are affected and adaptive responses such as autophagy and EMT can be activated.

Our lab previously reported the induction of autophagy in spontaneously differentiating Caco-2 cells (Tunçer & Banerjee, 2019; Tunçer et al., 2020). Nutrient restriction and differentiation can both alter the metabolic state of a cell considerably. In this thesis, I hypothesized that metabolic rewiring resulting from nutrient-restriction-induced stress may affect the EMT process. For this, I chose Caco-2 cells as the model cell line. Our lab has previously shown that confluency dependent differentiation in Caco-2 cells over a period of 20 days can enhance mesenchymal features, which can be reversed when the cells undergo dedifferentiation (Yilmaz-Ozcan et al., 2014). Based on the previous findings and my hypothesis I examined the following:

1. Whether the restriction of the three major carbon sources: glucose, L-glutamine and serum could activate autophagy in proliferating Caco-2 cells.
2. Whether the induction of autophagy and the underlying cellular signaling pathways were comparable when Caco-2 cells underwent to two divergent autophagy-inducing processes: spontaneous differentiation and nutrient restriction.
3. Whether nutrient restriction and subsequent activation of various signaling mechanisms in the cell could activate EMT and affect the sensitivity of the cells to chemotherapy drugs.

Overall, this study showed for the first time that culture of Caco-2 cells with limiting amounts of glucose, glutamine and serum could activate partial EMT, which was further exacerbated when lysosomal signaling was perturbed. The nutrient restricted cells also showed lower sensitivity to chemotherapy drugs, most likely due to the induction of partial EMT

CHAPTER 2

MATERIALS AND METHODS

2.1   Cell Culture

Caco-2 cells purchased from Şap Enstitüsü (Ankara, Turkey) and HCT-116 cells purchased from DKFZ (Heidelberg, Germany). Caco-2 cells were cultured in 1 g/L glucose-containing Eagle's minimum essential medium (EMEM) (Biological Industries) with addition of 20% fetal bovine serum (FBS), 1mM sodium pyruvate, 2 mM L-glutamine, 0.1 mM non-essential amino acids and (NEAA) and 1% penicillin/streptomycin (P/S). HCT-116 cells culturing media was prepared with RPMI 1640 medium without phenol red (Biological Industries) with addition of 10% FBS, 1% P/S and 2mM L-glutamine. Culturing conditions for the cells were 37 °C with 5% CO_2. Routine mycoplasma control was performed to all cells, and they were treated with 2.5 µg/mL Plasmocin® (Invivogen, France) continuously for prophylaxis.

2.1.1   Caco-2 Cell Line

Caco-2 cells which was initially isolated from a patient with colon adenocarcinoma have the ability to undergo a process of spontaneous differentiation in culture (Sambuy et al., 2005). Caco-2 cells acquire morphological and functional enterocyte-like features upon differentiation such as formation of microvilli and secretion of brush border enzymes (Astarci, Sade, Çimen, Savaş, & Banerjee, 2012; Devriese et al., 2017), and is frequently used in barrier formation and intestinal differentiation studies a model (Rousset, 1986).

When cultured in monolayer under two-dimensional (2D) culture conditions, Caco-2 cells exhibit epithelioid or cobblestone-like morphology and characterized as a fast-growing cell line (De Both, Vermey, Dinjens, & Bosman, 1999). Caco-2 cell line presents wild-type KRAS, BRAF, PIK3CA and PTEN copies; and it harbors TP53 mutation (E204X) (Ahmed et al., 2013). Under *in vitro* culture conditions, Caco-2 cells exists as a heterogenous population consisting of subpopulations with different morphologies and genetic makeup (Sambuy et al., 2005).

2.1.2 HCT-116 Cell Line

HCT-116 cell line was originally generated from the colon of an adult male as three subpopulations (Brattain MG, Fine WD, Khaled FM, Thompson J, 1981). Unlike Caco-2 cells, they don't have the ability to spontaneous differentiate upon growth to confluency (Yeung, Gandhi, Wilding, Muschel, & Bodmer, 2010). HCT-116 is a fast-growing cell line and harbors KRAS (G13D) and PIK3CA (H1047R) mutations while it is wild type for BRAF; PTEN and TP53 (Ahmed et al., 2013).

2.2 Spontaneous Differentiation Protocol

Control Caco-2 cells were always kept at sub-confluent conditions (50-60% confluency) to prevent differentiation. For differentiation induction, cells were inoculated at high density and grown until confluency. When 100% confluency was achieved, cells were denoted at day 0 of differentiation. Then, post-confluent Caco-2 cells were cultured for 20 days and harvested at various intervals (0, 5, 10 and 20 days upon reaching confluency). 10th day of differentiation was denoted as differentiated.

2.3   Real-time Measurement of Differentiation with xCELLigence

To examine the continuous changes occurring in differentiated cells in real time, the xCELLigence Real Time Cell Analyzer (Agilent, USA) was used. For this, Caco-2 cells were plated in 96-well gold microelectrode-covered plates and changes in proliferation index and cell number were monitored continuously until the 20th day of differentiation. As the number of cells increased, an increase in the impedance was observed; the day on which the impedance reaches a plateau was designated as Day 0 of differentiation. At the 10th day of differentiation, 6% EtOH treatment was performed for 3 h to disrupt the cell barrier function (tight junctions), followed by 24 h recovery in complete growth medium. As control, cells were treated with 2.5 mM EDTA for 3 h was to analyze the effect of loss of adherens junction on the impedance value measured.

2.4   Nutrient Restriction Protocol

The nutrient-restriction medium was prepared by using glucose and glutamine free Dulbecco's Modified Eagle Medium (DMEM) that was supplemented with 1% FBS, 0.2 mM L-glutamine, 0.1 g/L glucose, 1mM sodium pyruvate, 0.1 mM NEAA and 1% P/S. Cells were seeded into tissue culture flasks or 6-well plates and allowed to attach overnight. The next day, the complete growth medium was removed, and cells were washed with PBS before addition of the starvation medium. Cells were incubated in nutrient-restriction medium for 48 h. For these studies, the cells were kept in sub-confluent state to prevent the cells from undergoing spontaneous differentiation.

For replenishment experiments, after 48h of treatment, the starvation medium was replaced with complete growth medium or the medium replenished with respective nutrient (FBS, glucose or L-glutamine). Cells were harvested after additional incubation of 6 h or 24 h.

21

2.5   Treatments

Treatments of Caco-2 cells were performed at 37° C as follows: Sub-confluent cells were treated with 100 nM Bafilomycin A1 (in DMSO), 50 µM 5-FU (in DMSO), 5 mM 3-MA (in medium) for 48 h in complete growth medium and/or nutrient-restriction medium. Drug treatments were started simultaneously with nutrient-restriction, unless stated otherwise. Rapamycin (500 nM) and Chloroquine (30 µM) co-treatments were performed for 24 h in complete growth medium. The list of drugs used in the study is given in Table 2.1.

Table 2.1 Information of chemicals used in this study

Chemical	Function	Mechanism of Action	Vehicle	Concentration
Bafilomycin A1	Autophagy inhibitor	Lysosomal V-ATPase inhibition	DMSO (0.01%)	100 nM
3-Methyladenine (3-MA)	Autophagy inhibitor	Class III PI3K inhibition	Medium (100%)	5 mM
5-Fluorouracil (5-FU)	Anti-cancer agent	Thymidylate synthase inhibition	DMSO (0.05%)	50 µM
Chloroquine	Autophagy Inhibitor	Lysosomal alkalinization	dH$_2$O (0.01%)	30 µM, 24 h 100 µM, 3 h
Rapamycin	Autophagy Activator	mTOR inhibition	DMSO (0.01%)	500 nM

For the Bafilomycin treatments, cells were co-treated with Bafilomycin and nutrient-restriction for 48 h. At the end of the treatment duration, the medium was either replaced with complete growth medium (complete recovery) or with nutrient-

restriction medium not containing Bafilomycin (Bafilomycin recovery); and cells were incubated for an additional 24 h.

2.6   Alkaline Phosphatase Activity

The alkaline phosphatase enzymatic activity was determined as a marker of spontaneous differentiation. Since Caco-2 cells differentiate into enterocytes, these cells start expressing digestive enzyme when the differentiate. Caco-2 cells were collected at pre-confluent state and at the 0, 5, 10 and 20th day of differentiation and lysed with a freeze-thaw cycle. For this, pellets were collected and washed with PBS, then samples were frozen at -80°C for 20 min followed by 20 min thawing at 37°C. After 2 cycles, 75 µl of cell lysate was mixed with 75 µl of p-nitrophenylphosphate (pNPP) substrate and 25 µl $MgCl_2$ solution. The mixture was incubated at 37°C in the dark for 60 min in an orbital shaker with shaking at150 rpm. Absorbance measurement was performed at 405 nm. For the calculation of specific enzyme activity, absorbance values were divided to the amount of protein present in the samples.

2.7   RNA Isolation and cDNA Synthesis

For the isolation of RNA, cells were collected by centrifuging at 1500 x *g* for 5 min at 4°C and washed with PBS. Total RNA was isolated with using NucleoSpin RNA Kit (Macherey Nagel, Germany) following the manufacturer's protocol and the isolated RNAs were kept at -80 °C until use. 1 µg RNA was used to synthesize cDNA with RevertAid First Strand cDNA Synthesis Kit (Thermo Scientific) with using random hexamers. DNase I treatment was carried out within the protocol of the kit, and the synthesized cDNAs were stored at -20 °C.

2.8   Quantitative Real-time PCR (qRT-PCR)

qRT-PCR was carried out in Rotor GeneQ 6000 series (Qiagene) with using 0.1 mL 4-strip Rotor Gene style Tubes. Real time PCR reactions were prepared in 10 µL volumes using 5 µL of 2X GoTaq qPCR Master Mix (Promega, Madison, WI, USA), 1 µM forward and reverse primers and 2 µL cDNA. Standard curves for each primer pair were generated and threshold cycle (C_t) values were calculated after 45 cycles using relative standard curve method. The fold change in transcriptional expressions was calculated by Pfaffl method (Pfaffl, 2001). The primers used in the study are given in Table 2.2.

Table 2.2 List of primers used in this study

Gene	Forward Primer Sequence	Reverse Primer Sequence	TM (°C)
ACTB	TGTCCACCTTCCAGCAGATGT	AGCTCAGTAACAGTCCGCCTAGA	59
B2M	AGCAGCATCATGGAGGTTTG	AGCCCTCCTAGAGCTACCTG	59
RAB5	CAAGGCCGACCTAGCAAATAA	GATGTTTTAGCGGATGTCTCCAT	56
RAB7A	AGTGTTGCTGAAGGTTATCATCC	TTCCTGTCCTGCTGTGTCC	56
SQSTM1	ATGAGGACGGGGACTTGGTT	TTGCAGCCATCGCAGATCA	57
SNAI1	TGGTTCTTCTGCGCTACTGC	GCTGCTGGAAGGTAAACTCTGG	58
SI	CAAATGGCCAAACACCAATG	CCACCACTCTGCTGTGGAAG	57

Table 2.2 (cont'd)

OCLN	AAGAGTTGACAGTCCC ATGGCATAC	ATCCACAGGCGAAGTT AATGGAAG	59
MCOLN1	CATGAGTCCCTGCGAC AAGT	ACCACGGACATACGCA TACC	60
CDH1	TGCCCAGAAAATGAAA AAGG	GTGTATGTGGCAATGC GTTC	59
VIM	CCAGCCGGAGCTACGT GACTA	GTGCGGGTGTTCTTGAA CTCG	59

2.9 Protein Isolation and Western Blot

2.9.1 Total Protein Isolation

For the isolation of total protein, lysis buffer was prepared with addition of 1X protease and phosphatase inhibitors (Roche, Germany) to M-PER Mammalian Protein Extraction Kit (Thermo Fisher Scientific). The cell pellets were collected and washed with PBS and then centrifuged at 1500 x g for 5 min at 4 °C. Next, MPER lysis mixture was added at a volume of 30-50 µL according to the size of the pellet. Pellets were mixed by vortexing for 30 sec followed by ice incubation for 10 min. This procedure was repeated two more times. After lysis, cells were centrifuged at 14000 x g for 10 min at 4 °C. Supernatants were collected, and the proteins were stored at -80 C until use.

2.9.2 Cytoplasmic and Nuclear Protein Isolation

To determine the nuclear translocation of TFEB and thereby its activity, cytoplasmic and nuclear protein isolation of Caco-2 cells was performed. After washing with PBS, the collected cells were centrifuged at 500 x g for 5 min at 4 °C. The pellets

were lysed with 300 µL hypotonic buffer. After ice incubation for 15 min, lysed cells were mixed with 75 µL 10% NP-40 (Pan-Reac AppliChem, Germany). The mixture was centrifuged at the 14000 x g for 30 sec at 4 °C. The supernatant, which was considered to be the cytoplasmic fraction, was transferred to a fresh Eppendorf tube. The remaining pellet containing the nuclear proteins was re-suspended with 80 µl nuclear extraction buffer, was vortexed for 30 sec followed by 15 min ice incubation on an orbital shaker. After repeating this procedure for 2 more times, the mixture was centrifuged at 14000 x g for 10 min at 4 °C. Supernatant was collected in a fresh Eppendorf tube, which was considered to contain the nuclear fraction.

2.9.3 Protein Quantification

Protein concentration determination was carried out with Coomassie Protein Assay Reagent (Thermo Fisher Scientific) in 96-well microplates. After isolation, proteins were diluted 1:5 in MPER mixture. 5 µL of the diluted proteins was mixed with 250 µl Coomassie reagent. For each sample, 3 replicates were prepared, and the absorbance was measured at 595nm with MultiSkan GO Microplate Spectrophotometer (Thermo Scientific). Then, the concentration of proteins was calculated with using the pre-generated standard curve which was prepared with bovine serum albumin (BSA) at various concentrations.

2.9.4 Western Blot

Protein separation was carried out with 12% SDS-PAGE gels which were run at 100V for 2 h and 30 min. Then, wet western blot transfer was performed with polyvinylidine fluoride (PVDF) membranes at 115V for 1 h and 30 min. Then 5% BSA (AppliChem) in 0.1% TBS-T was used for membrane blocking for 1 h at RT on a shaker. Membranes were incubated with primary antibodies at 4 °C O/N on an orbital shaker. The next day, membranes were washed with 0.1% TBS-T for 10 min, 3 times. Then incubation with the respective secondary antibody was carried out for

1 h at RT on a shaker. Clarity ECL Substrate (Bio-Rad) mixture was prepared at dark, and the membranes were incubated for 2 min in this solution for the visualization of protein bands. Images were taken by using ChemiDoc MP Imaging System (Bio-Rad) until saturation. Band intensity measurement was carried out with ImageLab software. The adjusted band intensities were calculated and normalized to that of housekeeping proteins to determine the change in expression. All antibodies used in the study are given in Table 2.3.

Table 2.3 List of antibodies used in this study

Antibody	Size (kD)	Origin	Brand	Catalog No
ß-actin (C4)	45	Mouse	Santa Cruz Biotechnolgy	sc-47778
Lamin B1	66	Mouse	ProteinTech	66095-1-Ig
LC3 A/B (D3U4C)	14,16	Rabbit	Cell Signaling Technology	12741S
p62/SQSTM1	62	Mouse	Santa Cruz Biotechnology	sc-28359
Beclin-1	60	Mouse	Santa Cruz Biotechnology	sc-48341
Rab5	25	Rabbit	Cell Signaling Technology	3547
Rab7a	23	Rat	Biolegend	850401
LAMP1 (H4A3)	90-120	Mouse	Santa Cruz Biotechnology	sc-20011
p-RPS6 (S235/236)	32	Rabbit	Cell Signaling Technology	2211S
p70S6K (49DS7)	70, 85	Rabbit	Cell Signaling Technology	2708P

Table 2.3 (cont'd)

p-p70S6K (T289)	70, 85	Rabbit	Cell Signaling Technology	9234S
AMPKα1/2	62	Mouse	Santa Cruz Biotechnology	sc-74461
p-AMPKα (T172)	62	Rabbit	Cell Signaling Technology	2535S
TFEB	65-70	Mouse	Biolegend	852001
CEA	150-180	Mouse	Invitrogen	11365133
E-cadherin	135,120/80	Mouse	Santa Cruz Biotechnology	sc-8426
Goat α-Rabbit			Advansta	R05071 500
Goat α-Mouse			Advansta	R05072 500
Goat α-Rat			Advansta	R05075 500

2.10 Proliferation and Cell Viability Assays

For the assessment of changes in cell viability and proliferation in response to nutrient-restriction and/or drug treatments, three different assays were used.

2.10.1 MTT Assay

In order to analyze changes in the number of viable cells after treatments, MTT [3-(4, 5-dimethylthiazol-2-yl)-2, 5-diphenyltetrazolium bromide] assay was used, according to the manufacturer's recommendations (Thermo Fisher Scientific, USA). Briefly, 10,000 cells per well were seeded on 96-well plates, with 5 technical

replicates. The next day, drug treatments or nutrient-restriction was started, and cells were incubated for 48 hours (treatment duration was total of 72 hours for recovery/replacement experiments). The MTT solution was prepared with dissolving 5mg MTT powder in 1 mL PBS, which then diluted 1:10 with complete growth medium. After treatment period was finished, the medium was discarded and the MTT mixture was added to the wells. The cells were incubated with MTT solution for 4 hours at 37°C, then 1% SDS in 0.01M HCl solution was added to each well. After O/N incubation at 37°C, absorbance was measured at 570 nm with Multiskan-GO microplate spectrophotometer (Thermo Fisher Scientific, USA).

2.10.2   BrDU Cell Proliferation Assay

In order to measure the changes in the number of actively dividing cells after nutrient-restriction and Bafilomycin treatment, BrDU Cell Proliferation Assay (Sigma Aldrich, Germany) was used according to manufacturer's instructions. 10,000 cells per well (100 µL) were seeded on 96-well plates, with 3 technical replicates. The next day, drug treatments or nutrient-restriction was started, and the cells were incubated for 48 hours. When the treatment was completed, the cells were labeled with 10µM BrDU solution and anti-BrdU-POD antibody. After addition of the chemiluminescent substrate, luminescence measurement was carried out using SpectraMax ID3 Microplate Reader (Molecular Devices, UK) at 492 nm.

2.10.3   Muse Cell Viability Assay

To measure cell death after nutrient-restriction as well as treatment with Bafilomycin and 5-FU, the Muse Cell Count and Viability Assay was carried out according to manufacturer's instructions. Cells were seeded into 6-well plates and treatments were started the day after seeding. At the end of treatment duration, cells were collected with scraping in the respective treatment media; and mixed with Count and Viability Reagent (1:20 fold dilution). After 5 min incubation at room temperature,

measurement was caried out with Muse Cell Analyzer (Merck, Germany) by selecting pre-adjusted reading parameters in the equipment (Cell Count and Viability Assay parameters). The live and dead populations were automatically plotted, and respective percentages were displayed on the graph.

2.11   Spheroid Formation Assay

To evaluate the ability of nutrient restricted and Bafilomycin co-treated cells to form spheroids in 3D culture conditions and to determine their size, spheroid formation assay was performed. Cells were seeded at 50,000 cells/well density in 200 µL complete medium or nutrient-restriction medium with or without Bafilomycin to 96-well Ultra-Low Attachment (ULA) plates (Corning, USA) and cultured at 37ºC for 96 h. At the end of incubation period, each individual spheroid formed in the 96-well ULA plate was imaged and then collected as pellet for RNA isolation.

To evaluate the ability of the cells to reform spheroids after passaging, cells were seeded at 50,000 cells/well density in 200 µL complete medium to 96-well Ultra-Low Attachment (ULA) plates (Corning, USA) and cultured at 37ºC. Spheroid formation was observed after 24 h of incubation. Spheroids were collected after 48 h in a 1.5 mL Eppendorf tubes and centrifuged at 500 x g for 5 min at 4ºC. After washing with PBS, spheroids were dissociated into single-cell suspensions with 1 mL 2.6-gauge (G) needle. Cells were centrifuged at 500 x *g* for 5 min, PBS was removed, and cells were re-suspended in complete growth medium or nutrient-restriction medium with or without Bafilomycin and re-plated in ULA plates. After culturing for additional 48 h, each individual spheroid formed in the 96-well ULA plate was imaged and then collected as pellet for RNA isolation.

2.12   Phalloidin Staining Protocol

Phalloidin staining was performed to evaluate the phenotypic changes and cytoskeletal reorganization in response nutrient restriction, Bafilomycin A1

treatment and the combination of the two. For this, Caco-2 cells were plated on glass coverslips placed in 12-well plates. After allowing overnight attachment to the glass surface, nutrient-rich and nutrient-restricted Caco-2 cells were incubated in the absence or presence of 100 nM Bafilomycin A1 for 48 h, and recovery from Bafilomycin A1 treatment was performed for 24 h in complete growth medium. At the end of the experimental duration, light microscopy images were taken first. Then, cells were fixed with 4% paraformaldehyde in PBS and permeabilized with 0.1% Triton X-100 (Sigma). Afterwards, the fixed cells were stained with Alexa Fluor® 405 phalloidin for cytoplasmic distribution of F-actin and counterstained with 4', 6-diamidino-2-phenylindole (DAPI) for nuclear staining which was present in the mounting medium that was used to preserve the slides. Images were gathered with Zeiss LSM 800 Laser Scanning Microscope (Germany) at 63× magnification at BIOMATEN, ODTÜ.

For the quantification of F-actin stress fibers, number of fibers were manually counted in approximately 50 cells; none of the fibers counted twice, and the final numbers were divided by number of nuclei to calculate the numbers of fibers/cell.

2.13 Statistical Analyses

GraphPad Prism 6 software package (Prism, CA, USA) was used for the analysis of the data and the drawing of the representative graphs. Experiments were performed with 5 technical replicates (MTT and BrdU assays) and 3 technical replicates (qRT-PCR) and repeated with at least 3 biological replicates (unless indicated otherwise). Data were expressed as mean ± SEM. The statistical significance between experimental results was analyzed with Students' t-test, one-way ANOVA using Dunnett's multiple comparison test, or two-way ANOVA using Sidak's multiple comparisons test. Significant difference was statistically considered at the level of $p < 0.05$. * $p < 0.05$, ** $p < 0.01$, *** $p < 0.001$, **** $p < 0.0001$, ns: non-significant.

CHAPTER 3

RESULTS

3.1 Differentiation of Caco-2 Cells

Caco-2 cells are known to undergo spontaneous differentiation into enterocytes when grown to 100% confluency for 5-20 days (Ding, Ko, & Mark Evers, 1998). When the cells reached 100% confluency, they were collected at the 5th, 10th and 20th day for gene expression analysis. As the cells differentiated, their morphology changed, and they started to grow in multilayers. Domes structures are formed in 2D cultured Caco-2 cells when the cells become absorptive as they differentiate into enterocyte type cells. Fluids are accumulated between the surface and the cells, in turn they result in the local detachment of cells (Fantini, Abadie, & Tirard, 1986). Domes were seen around the 10th day of differentiation and were still present until Day 20. Representative pictures of Caco-2 cells in their undifferentiated (control) and differentiated states, as well as the presence of domes are shown in Figure 3.1.
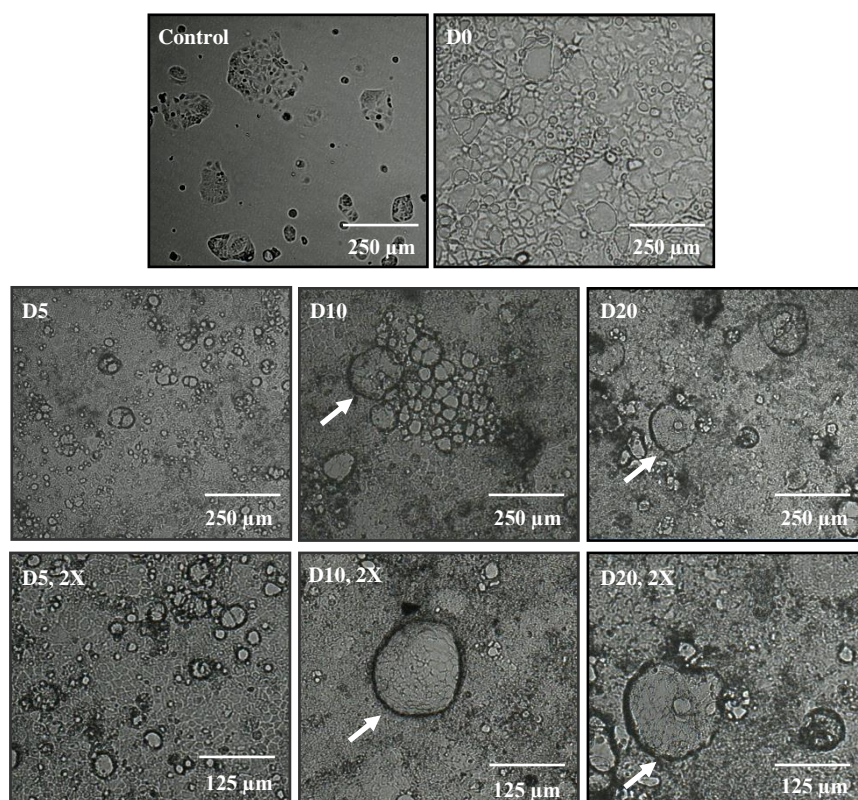
Figure 3.1 Spontaneous differentiation of Caco-2 cells

The morphological changes during spontaneous differentiation of Caco-2 cells were assessed with an inverted light microscope. Representative images of 3 biological replicates are given for sub-confluent/control cells, 100% confluent (D0) cells, and differentiated cells collected 5 (D5), 10 (D10) and 20 (D20) days after reaching confluency. Domes in the differentiated cells are indicated with arrows.

Differentiation of Caco-2 cells was also confirmed with the expression of different markers and activities of enzymes. The activity of the enzyme alkaline phosphatase (ALP), which is expressed in differentiated enterocytes, was assessed colorimetrically using p-nitrophenylphosphate (pNPP) as a substrate (Fig 3.2A). A significant increase in the specific activity of the enzyme was observed from Day 5 onwards. Additionally, mRNA levels of the well-established differentiation marker sucrose isomaltase (SI) was examined with qRT-PCR (Fig 3.2B), Again, a significant increase in expression was observed from Day 5 onwards, reaching a ~

2000-fold increase in expression by Day 20. Finally, protein levels of carcinoembryonic antigen (CEA), another intestinal epithelial differentiation marker and the junctional protein E-cadherin was analyzed with western blot. We observed an increase in the expression of CEA from Day 5 and an increase in the mature form of E-cadherin (that is found at cell-cell junctions) from Day 10 onwards.
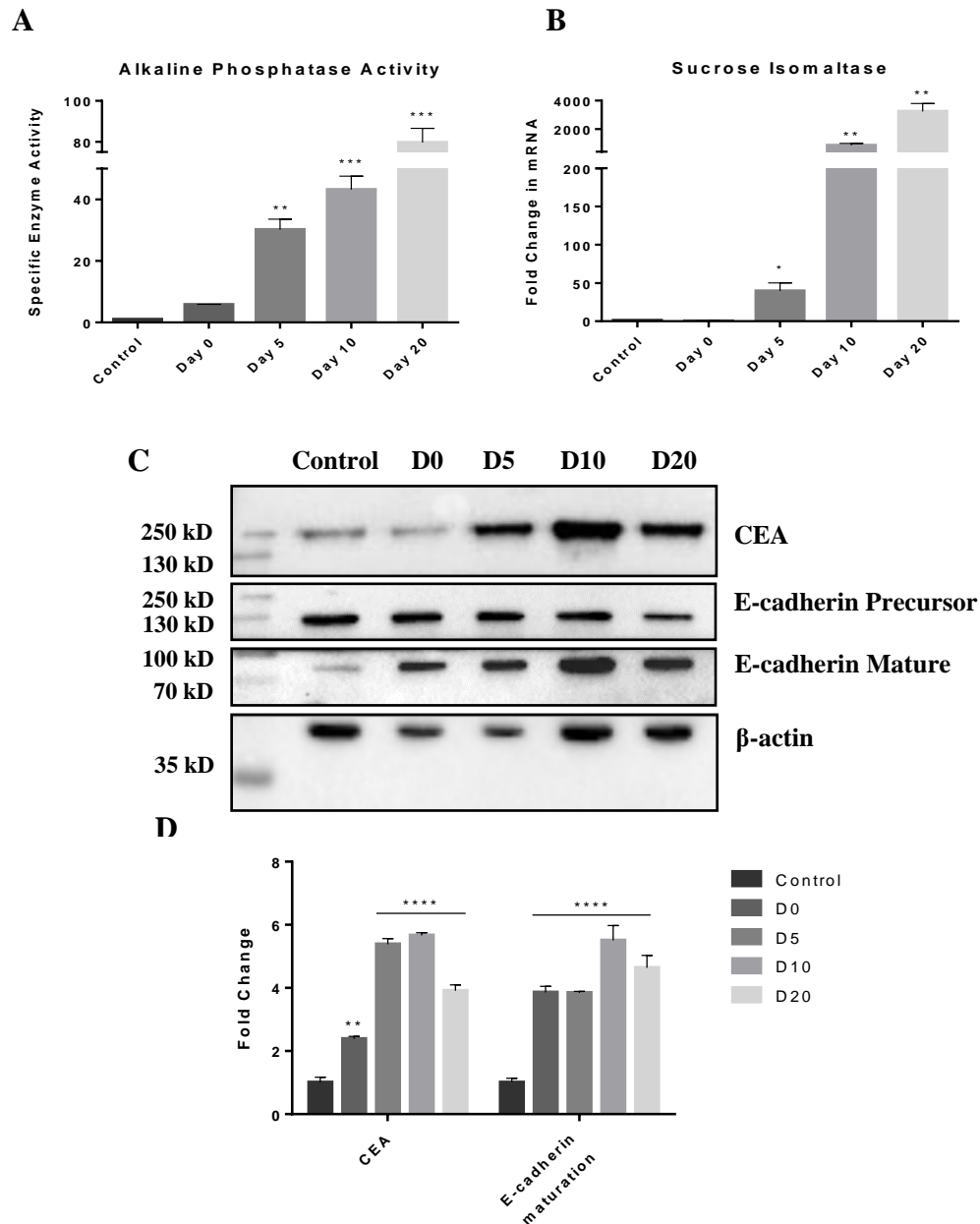
Figure 3.2 Confirmation of differentiation in spontaneously differentiating Caco-2 cells

Figure 3.2 (cont'd) *Induction of spontaneous differentiation in Caco-2 cells was confirmed with increasing alkaline phosphatase activity through pNPP colorimetric assay (A), increase in sucrase isomaltase mRNA levels (B) and increase in CEA protein and E-cadherin maturation levels (C). Figures are representative of 3 independent biological replicates. Bars represent mean ± SEM (n=3). **p<0.01, ****p<0.0001.*

Next, to examine the continuous changes occurring in differentiated cells in real time, the xCELLigence Real Time Cell Analyzer was used which provides real-time tracking of cell-cell adhesion formation during differentiation (Sun et al., 2012). As the number of cells increased due to proliferation, the measured impedance also increased and the day the impedance reached a plateau was designated as day 0 (Fig 3.3A), suggesting that the cells had reached confluency. As the cells were cultured further, it was expected that the impedance would increase with the increased formation of tight junctions that is a known characteristic of differentiated cells. However, due to the continuing growth of cells as multilayers, we observed no change in impedance in the 10 days following the plateau (Fig 3.3A).

A loss in tight junction is expected to decrease the impendence. Therefore, we disrupted the tight junction barrier with 6% EtOH (Ying et al., 2014). For this, Caco-2 cells at the 10th day of differentiation (after the plateau was reached) were treated with 6% EtOH for 3h, and the medium was replaced with complete growth medium. EtOH treatment caused a decrease in impedance (Fig 3.3B). Cells re-exposed to regular growth medium after 3h regained tight junctions over time and reached impedance levels close to the control cells. In addition to tight junctions, intestinal epithelial cells also show the formation of adherens junctions; these junctions rely on the presence of Ca^{2+} ions (Harris, Daeden, & Charras, 2014). We treated cells with 2.5mM EDTA for 3h to chelate the Ca^{2+} ions to and observed a modest change in impedance (Figure 3.3B), confirming that treatment with ethanol mostly affected the tight junctions and thereby the impedance measured by the device.
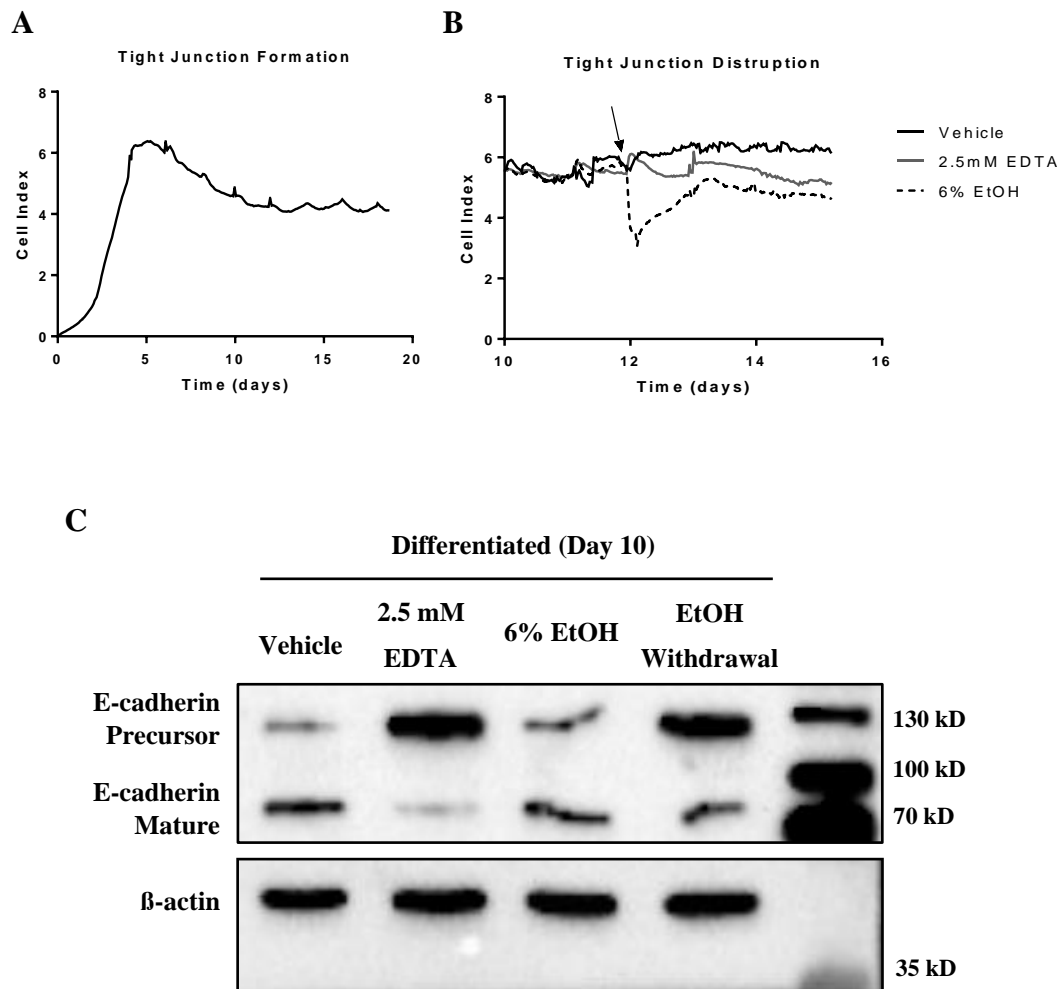
Figure 3.3 Real-time monitoring of differentiation in Caco-2 cells using xCELLigence system

Tight junction formation in Caco-2 cells were monitored continuously until Day 20 of differentiation (A). For the tight junction disruption, differentiated cells (Day 10, D10) were treated with 6% ethanol. Vehicle-treated and 2.5 mM EDTA-treated control cells are also shown (B). The time point for ethanol and EDTA treatment was indicated with the arrow. The measured impedance value was shown as the cell index on the y axis. Western blot results showing the E-cadherin levels after ethanol treatment/withdrawal and EDTA treatment in differentiated Caco-2 cells. Representative data from 3 independent biological replicates is shown.

E-cadherin is a Ca^{2+}-dependent cell adhesion protein that plays a key role in adherence junctions (Shibata-Seki, Nagaoka, Goto, Kobatake, & Akaike, 2020). Treatment with EDTA resulted in a dramatic increase in the precursor form of E-cadherin, confirming the importance of Ca^{2+} ions in the maturation and membrane localization of the protein (Fig 3.3C). Of note, treatment of differentiated Caco-2 cells with 6% ethanol for 3h did not lead to any change in the mature or precursor form of E-cadherin, further confirming that ethanol treatment affected tight junctions rather than adherens junctions. Withdrawal of ethanol and replenishment with complete medium, however, led to an increase in the expression of the precursor form of E-cadherin.

Taken together, these results indicate that spontaneous differentiation was successfully induced in the Caco-2 cell line.

3.2 Induction of Autophagy in Differentiated Caco-2 Cells

In order to determine autophagy in differentiating Caco-2 cells, autophagy markers LC3, Beclin-1 and p62; and the mTOR pathway protein pS6 were examined by Western blot (Klionsky et al., 2012) (Fig 3.4).
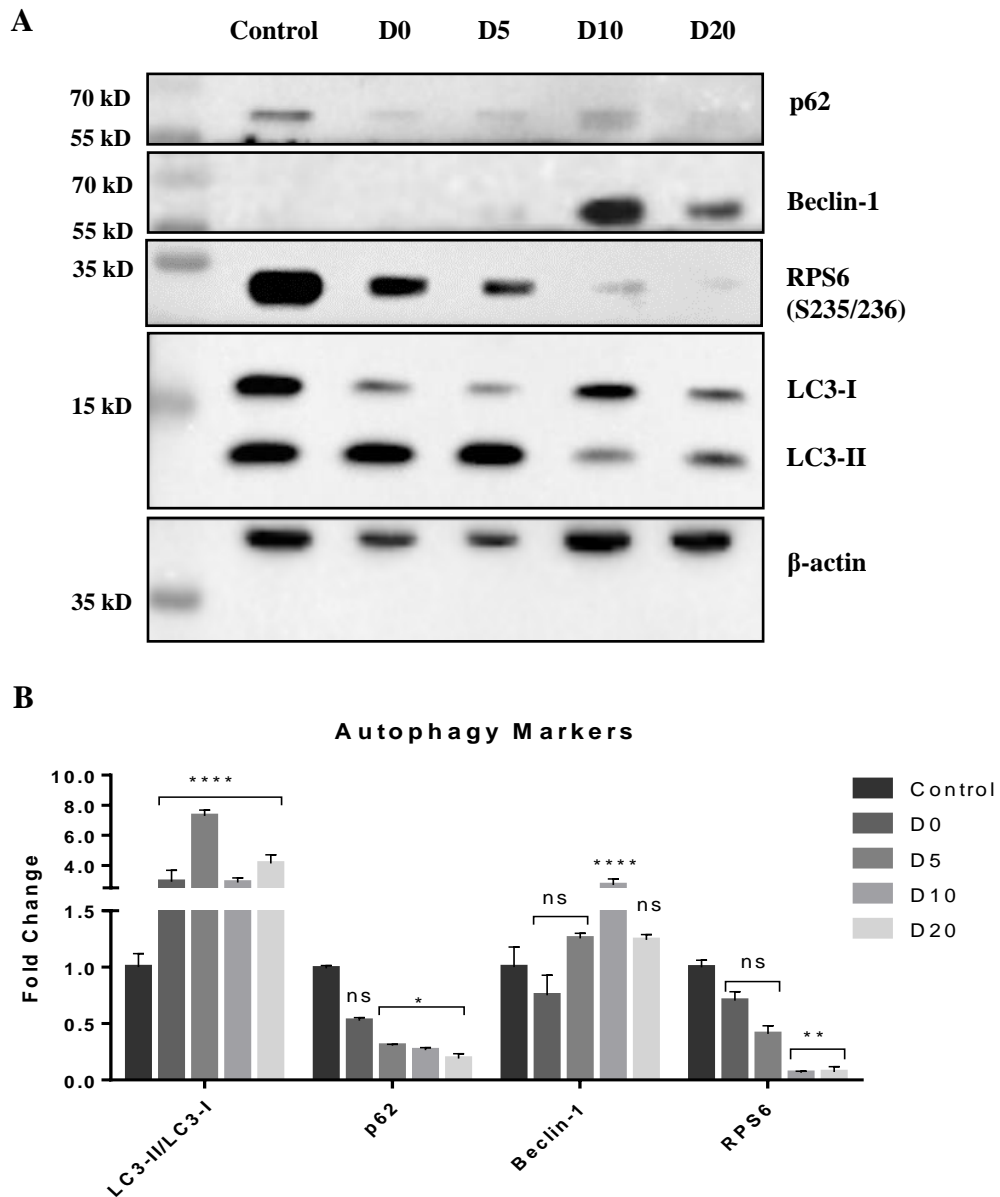
Figure 3.4 Induction of autophagy in spontaneously differentiating Caco-2 cells

The autophagy markers LC3, Beclin-1, p62 and RPS6 (S235/236) were examined by Western blot in spontaneously differentiating Caco-2 cells. Densitometry analysis was carried out with respect to control (undifferentiated) cells and normalized to loading control ß-actin. Figures are representative of 3 independent biological replicates. Bars represent mean ± SEM. *p<0.05, **p<0.01, ****p<0.0001, ANOVA ns: nonsignificant.

Our lab has previously shown that a dramatic increase in the secretory phenotype of differentiated cells, leading to the induction of endoplasmic reticulum stress and subsequently autophagy (Tunçer et al., 2020). I confirmed the induction of autophagy during the differentiation of Caco-2 cells, as evidenced by the increase in the Beclin-1 expression and increase in LC3II/I ratio. A robust increase in LC3-II (PE-conjugated, autophagosome-bound) was observed in the mid-stages of the differentiation process (D0-D5) followed by a decrease at later stages (D10-D20) in Caco-2 cells (Fig 3.4). This increase indicates an enhanced lipidation of LC3-I with phosphatidylethanolamine, giving rise to LC3II, which runs faster in the SDS-PAGE gel and appears as a lower band in a western blot. This increase in the conversion of LC3-I to LC3-II can be explained by either the high rate of autophagosome formation or a defective degradation machinery (i.e. the autophagosomes are formed but not cleared effectively).

 In order to understand this, monitoring the autophagic flux is of particular importance. The most common analysis of autophagic flux is via the protein level of the p62 adaptor, which interacts with LC3-II at the autophagosomes and is degraded along with its cargo protein (Parzych & Klionsky, 2014). Therefore, the decrease in p62 levels is an indicator of active autophagy machinery. During the course of differentiation of Caco-2 cells, p62 levels showed a decrease indicating the presence of functional autophagic flux. Moreover, the phosphorylation of ribosomal protein S6, which is phosphorylated upon the activation of mammalian target of Rapamycin (mTOR) decreased with the differentiation. Since the mTOR pathway is known to be inhibited in autophagy, the reduction in phosphorylation of S6 further confirms the induction of autophagy in the differentiated Caco-2 cells (Kim, Kundu, Viollet, & Guan, 2011).

3.3 Nutrient-Restriction Optimization Studies with Caco-2 Cell Line

Nutrient restriction is known to activate autophagy. In the literature, several modes of nutrient-restriction protocols are available which generally include complete or partial removal of energy sources from the growth media. In this study, we evaluated the effect of reduced glucose, L-glutamine and serum on Caco-2 cells and first confirmed whether the partial rather than complete removal of nutrients was sufficient to induce autophagy.

The conversion of LC3-I to LC3-II and the activation of AMP Kinase were used as markers for cellular response to nutrient restriction. AMPK is a primary nutrient sensor in the cells and one of the main pathways that is activated in response to starvation (Mihaylova & Shaw, 2011). The protein LC3 is incorporated into autophagosomal structures and is frequently used as a marker of the autophagic pathway (Yoshii & Mizushima, 2017).

We first evaluated the effect of decreasing the glucose and FBS amounts in the medium. For this, Caco-2 cells were treated with glucose-free DMEM, DMEM containing 0.1 g/L glucose and medium containing 5% FBS for 2 hours (Fig 3.5A) and 24 hours (Fig 3.5B). As controls, cells were cultured in both complete EMEM and DMEM media supplemented with 1 g/L glucose, 2 mM L-glutamine and 20% FBS (Fig 3.5A-B). The purpose of this control was to observe whether the expression of these markers was different in DMEM compared to EMEM, which is the recommended growth medium for Caco-2 cells.
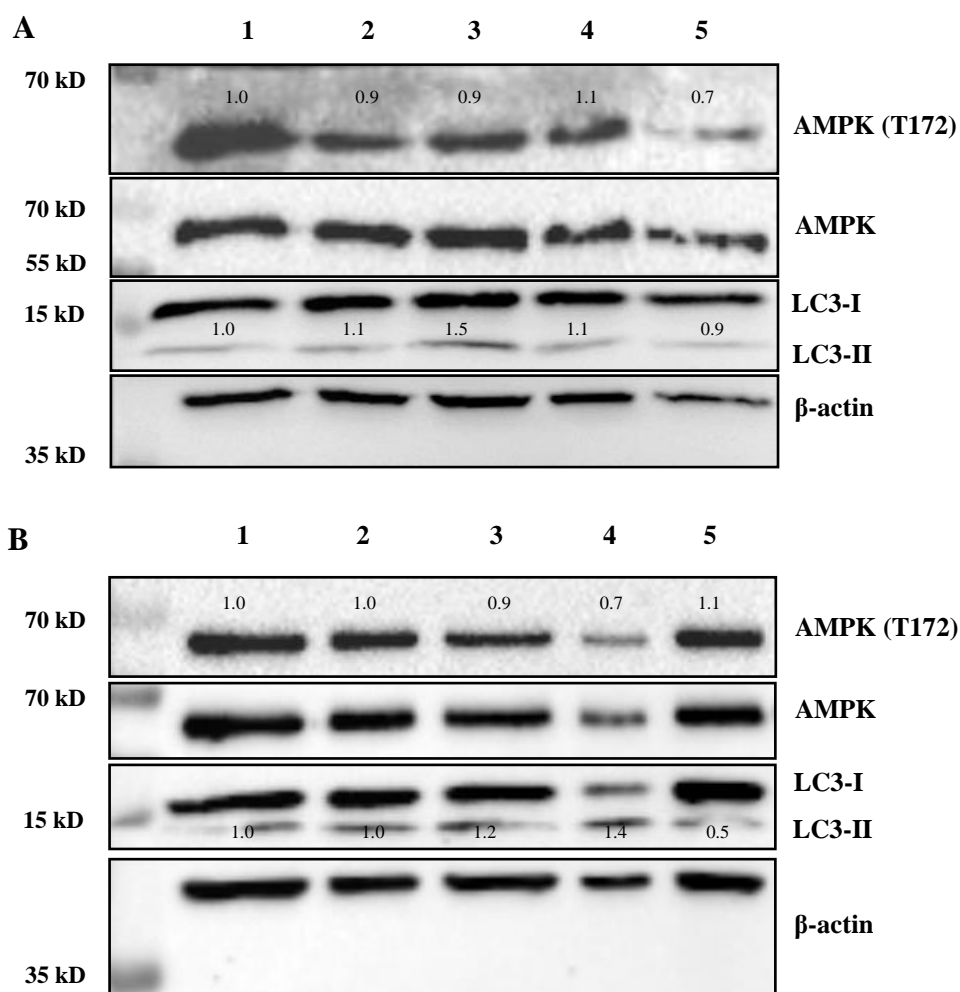
Figure 3.5 Treatment of Caco-2 cells with various media modifications for 2 hours and 24 hours

Caco-2 cells were treated with the indicated media modifications for 2 hours (A) and 24 hours (B). Densitometry analysis was performed with respect to complete growth medium (lane 1) and the respective ratios of LC3-II/LC3-I and AMPK phosphorylation (T172) are indicated on the figure. Representative figure of one replicate is shown. Lanes: 1- EMEM complete medium, 2- DMEM complete medium, 3- Glucose-free DMEM, 4- DMEM with 0.1 g/L glucose, 5- DMEM with 5% FBS.

We did not observe a significant difference in the expression of the markers in the cells cultured in EMEM or DMEM growth media (Fig 3.5, Lanes 1 and 2). Therefore,

42

for the subsequent experiments, cells cultured in complete EMEM was used as control, unless indicated otherwise.

As seen in Figure 3.5, no major change in the LC3-II/LC3-I ratio or the phosphorylation of AMPK at T172 was achieved in Caco-2 cells cultured in the absence of glucose or with low amount of FBS. Therefore, we decided to decrease the amount of FBS further and increase the treatment duration (Fig 3.6).
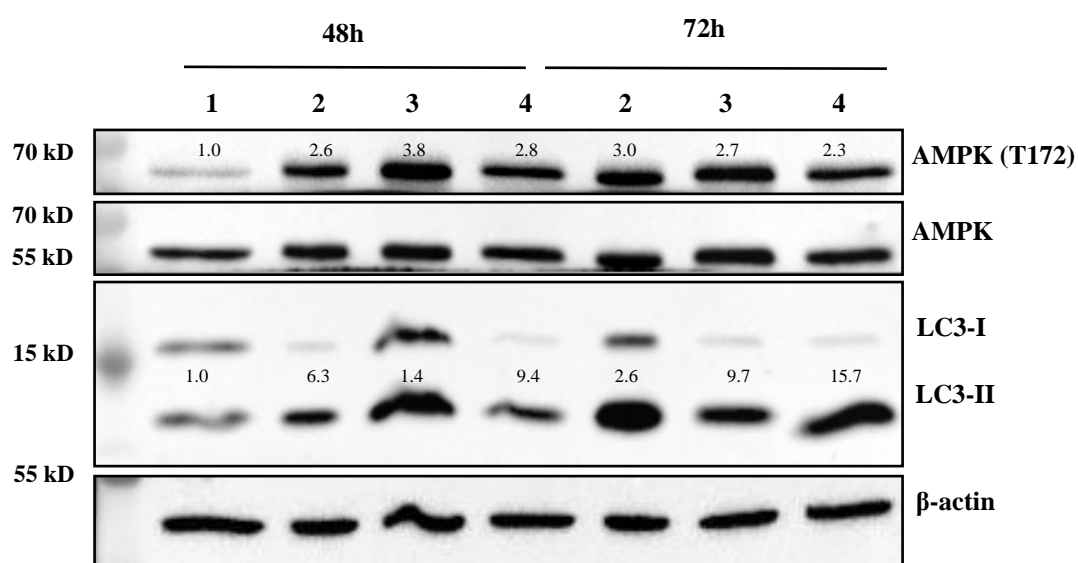
Figure 3.6 Treatment of Caco-2 cells with various media modifications for 48 hours and 72 hours

The response of cells to reduced glucose, FBS and their combination was evaluated. Densitometry analysis was performed with respect to complete growth medium (lane 1) and the respective ratios of LC3-II / LC3-I and change in phosphorylation of AMPK (T172) are indicated in the figure. Representative figure of one replicate is shown. Lanes: 1- EMEM complete medium, 2- DMEM with 0.1 g/L glucose, 3- DMEM with 1% FBS, 4- DMEM with 1% FBS and 0.1 g/L glucose.

We observed that the change in the expression of nutrient stress markers was time dependent. The increase in LC3II/I was higher after 72 hours of incubation compared to 48 hours, but a decrease in AMPK activation was observed at 72 hours (Fig 3.6).

Since we observed a better response with lower FBS and glucose amounts, we next withdrew non-essential amino acids (NEAA) and decreased the amount of glutamine in the culture medium from 2.0 to 0.2 mM (Fig 3.7). Both NEAA and glutamine and important sources of carbon and nitrogen in the cell and can contribute towards anaplerosis (Vaziri-Gohar et al., 2022). The treatments were carried out for 48 hours and 96 hours.
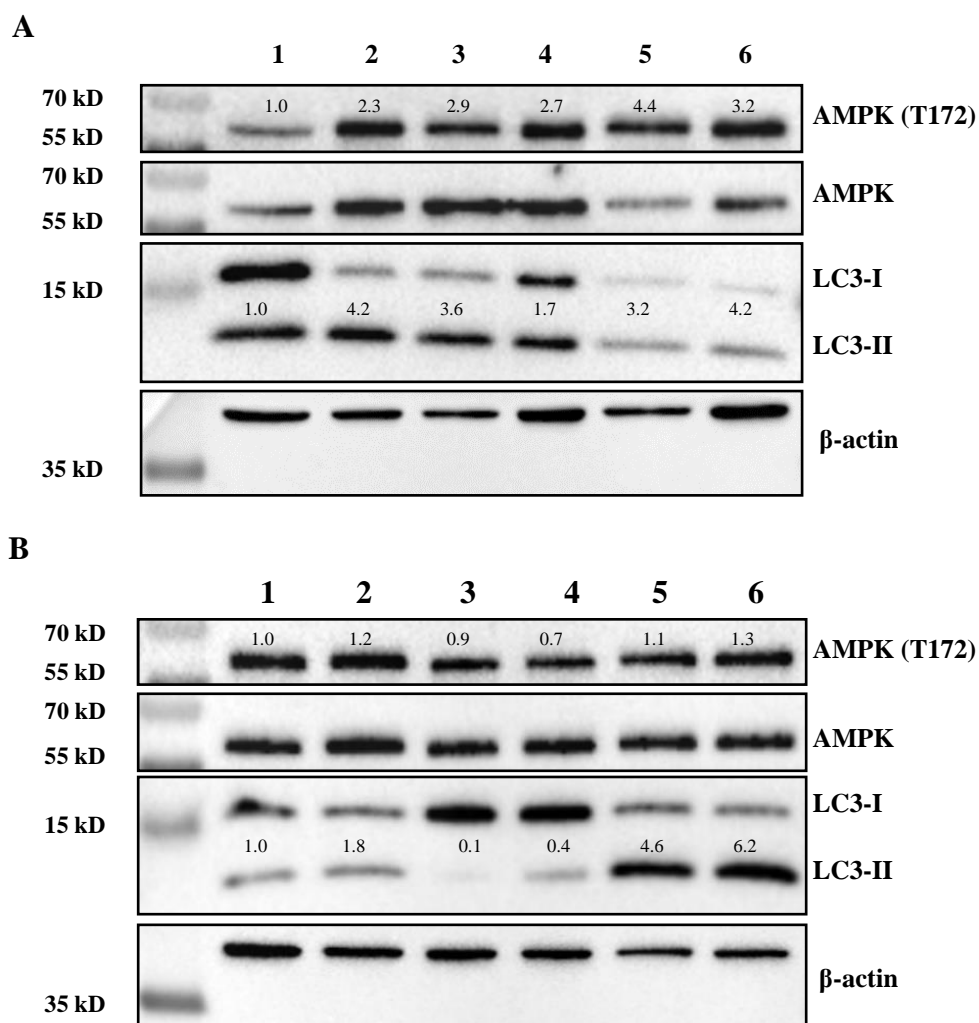
Figure 3.7 Treatment of Caco-2 cells with various media modifications for 48 hours and 96 hours

Figure 3.7 (cont'd) *Incubation of Caco-2 cells in medium containing low glucose, FBS, L-glutamine and their combination for 48 hours (A) and 96 hours (B) was evaluated. Densitometry analysis was performed with respect to complete growth medium (lane 1) and the respective ratios of LC3-II/LC3-I and AMPK phosphorylation (T172) are indicated in the figure. Representative figure of one replicate is shown. Lanes: 1- EMEM complete medium, 2- DMEM with 1% FBS and 0.1 g/L glucose, 3- DMEM with 0.2 mM L-glutamine, 4- DMEM with 0.2 mM L-glutamine without non-essential amino acids (NEAA), 5- DMEM with 1% FBS, 0.1 g/L glucose and 0.2 mM L-glutamine, 6- DMEM with 1% FBS, 0.1 g/L glucose and 0.2 mM L-glutamine without NEAA.*

When we examined the results for 48 h and 96 h, we observed that 48 h treatments showed a better response to nutrient restriction with a stronger activation of AMPK and LC3-II/LC3-I ratio. Among all trials, the base medium supplemented with 1% FBS, 0.1 g/L glucose and 0.2 mM L-glutamine applied for 48 h was selected as the optimal nutrient-restriction protocol.

3.4   Induction of Autophagy in Nutrient-Restricted Caco-2 Cells

The induction of autophagy in Caco-2 cells cultured in the optimized nutrient-restricted medium was examined by western blot. We evaluated the changes in the protein levels of autophagic and endo-lysosomal proteins; along with nutrient stress markers (Fig 3.8).
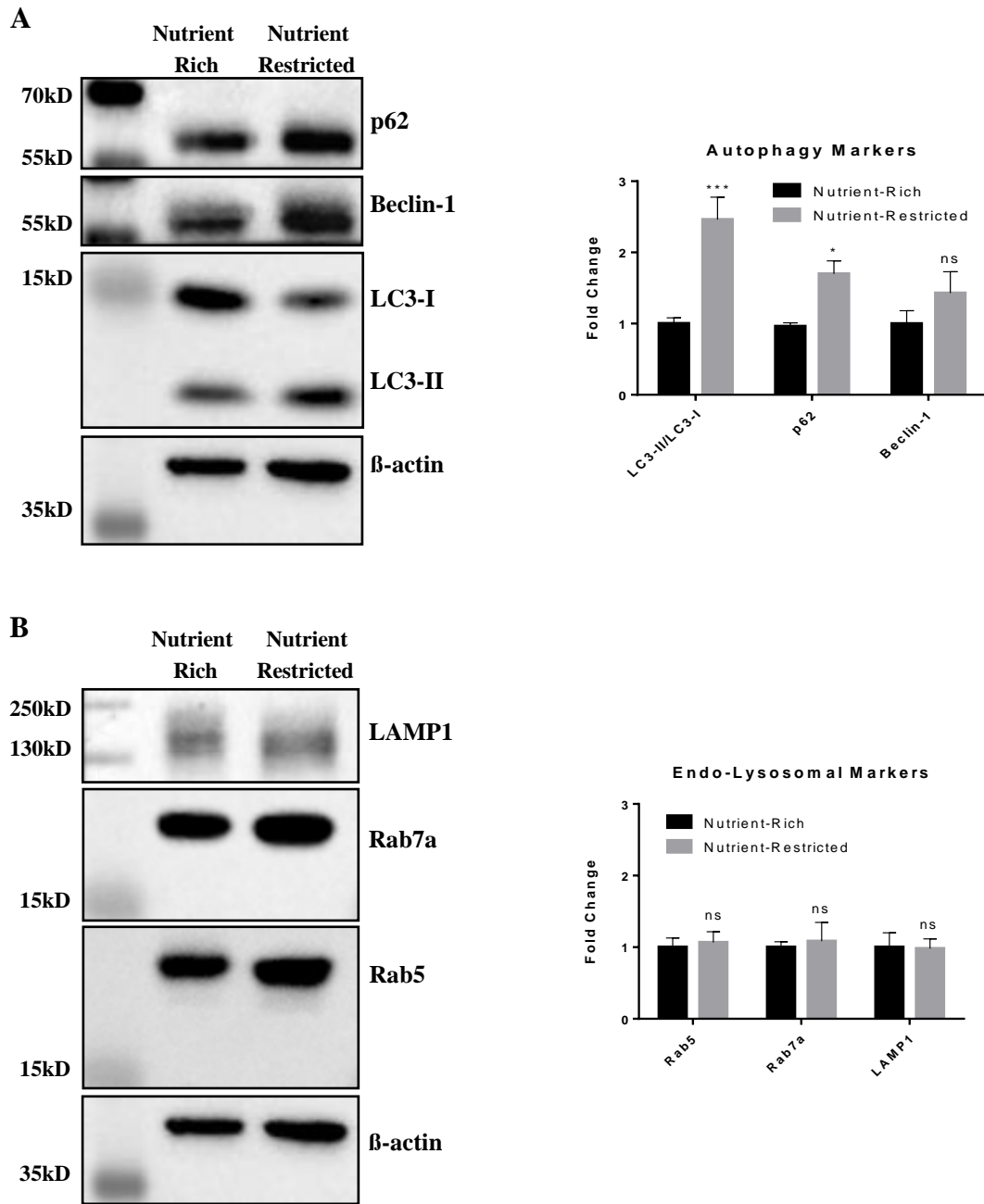
Figure 3.8 Evaluation of autophagy in nutrient-restricted Caco-2 cells

C

D
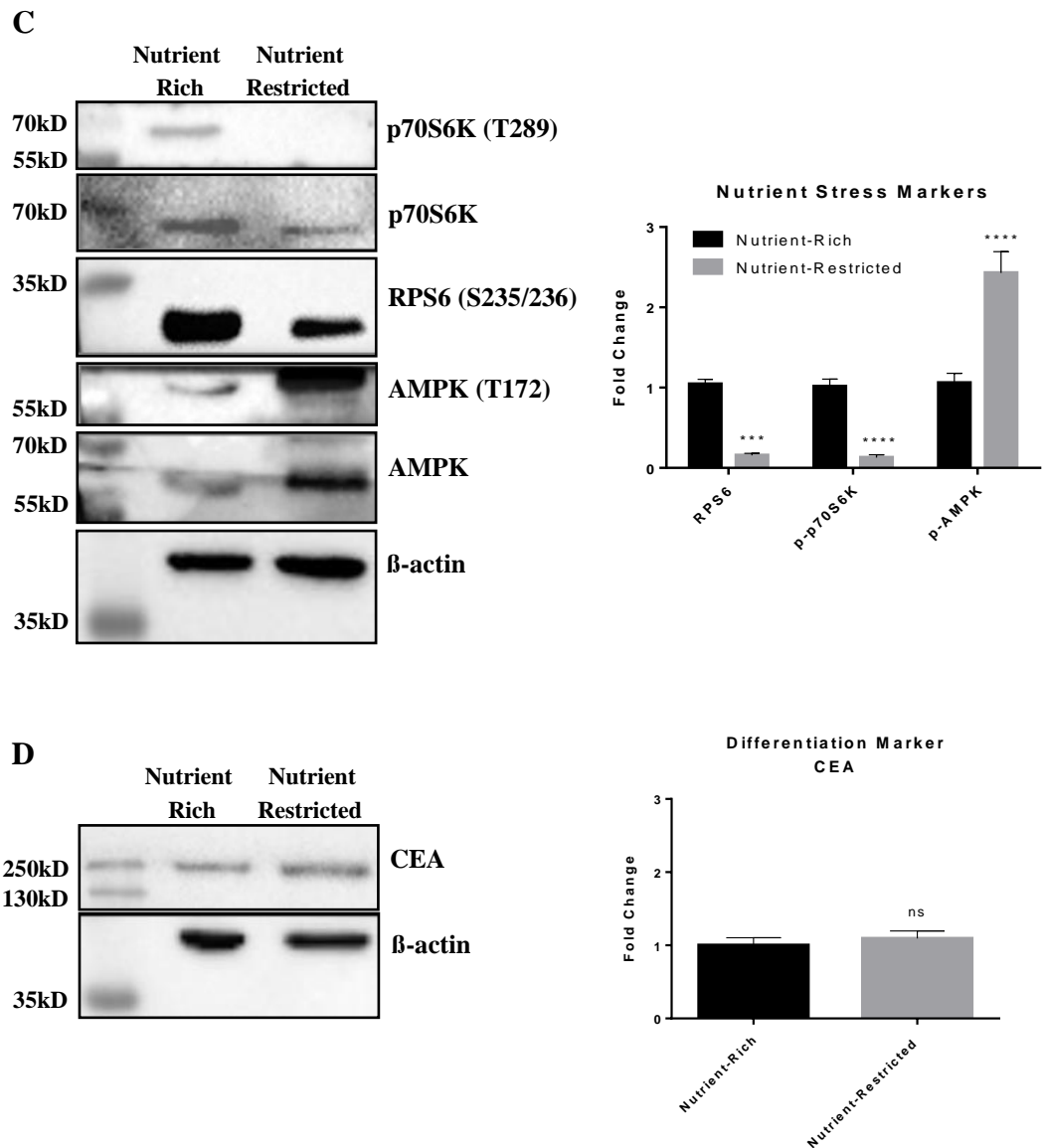
Figure 3.8 (cont'd) Evaluation of autophagy in nutrient-restricted Caco-2 cells

The autophagy markers LC3, p62 and Beclin-1 (A), endo-lysosomal markers Rab5, Rab7a and LAMP1 (B), nutrient stress markers RPS6, AMPK, p70S6K (C) and differentiation marker CEA (D) were examined by Western blot in nutrient-restricted Caco-2 cells. Densitometric analysis was carried out with respect to cells cultured in nutrient-rich medium (control cells) and normalized to the loading control ß-actin. Representative image of 4 biological replicates is shown. Bars represent mean ± SEM. *p<0.05, ***p<0.001, ****p<0.0001. ns: nonsignificant.

The induction of autophagy in response to nutrient restriction (NR) was evidenced by the trend in the increase in Beclin-1 levels (Fig 3.8A). The observed increase in LC3-II to LC3-I ratio also indicates the formation of autophagosomes in response to nutrient restriction. The activity of AMPK and mTOR pathways, which are the main energy sensors in the cells, was also analyzed. mTOR activity was determined with the phosphorylation of the downstream kinase p70S6K and RPS6 proteins. Increased AMPK phosphorylation, together with a decreased mTOR activity was observed in NR Caco-2 cells (Fig 3.8C).

The expression of endo-lysosomal proteins LAMP1, Rab5 and Rab7a did not show any difference with nutrient restriction (Fig 3.8B). In addition, the level of p62 cargo protein was increased. As mentioned earlier, p62 cargo protein that is degraded in autophagolysosomes together with its cargo. Therefore, a decrease in p62 levels is indicative of an active autophagic degradation machinery (as observed in the spontaneously differentiated Caco-2 cells, Figure 3.4). These observations might be indicative of impaired or slow autophagic flux in response to NR.

We next wanted to confirm that the increase in expression of autophagy markers in nutrient-restricted Caco-2 cells was not due to the induction of differentiation. For this, the differentiation marker CEA was examined by western blot (Fig 3.8D). We observed no change in the expression of CEA in the NR cells when compared to the control (nutrient-rich). This indicates the activation of autophagy in NR cells was due to nutrient deficiency-induced stress rather than differentiation.

3.5   Evaluation of Lysosomal Biogenesis and Function in Nutrient-Restriction

The induction of autophagy is associated with an increase in lysosomal activity and therefore is expected to increase endolysosomal signaling and expression of markers. Although we did not observe any change in the expression of LAMP1, Rab5 or Rab7A, we observed a robust decrease in mTOR activity. The mTORC1 complex

relies on its location on the lysosome for activity (Chung et al., 2019). We therefore wanted to examine whether the optimized NR medium could affect lysosomal biogenesis and activity. Lysosomal biogenesis is driven via the master transcription factor, TFEB (Szabo & Bala, 2018). Upon nutrient stress, mTORC1 activity is inhibited, which drives cytosolic TFEB protein to translocate to the nucleus to increase the expression of autophagosomal and lysosomal targets by direct binding to specific sites at their promoters (Palmieri et al., 2011). Therefore, to understand whether the optimized restriction medium results in nuclear translocation of TFEB, nuclear and cytoplasmic fractions of control and nutrient restricted Caco-2 cells were analyzed. A lysosomotrophic compound, Chloroquine (CHQ 100 µM, 3 h) was used as positive control since lysosomal sequestration of lysosomotrophic compounds results in a feedback response to drive lysosomal biogenesis through TFEB nuclear translocation (Zhitomirsky et al., 2018, Mauthe et al., 2018).

Contrary to our expectations, treatment with CHQ did not lead to an increase in nuclear translocation of TFEB in nutrient-rich cells. This may suggest a systemic resistance of Caco-2 cells to CHQ. We also did not observe any change in lysosomal acidity using Lysotracker (LTR) upon treatment with CHQ treatment (2h, 10 µM) (Please see Appendix A). LTR is a fluorescent dye that can track acidic compartments in cells. On the other hand, we observed a modest increase in nuclear TFEB in nutrient-restricted Caco-2 cells, and this increase was more pronounced when the cells were incubated with both CHQ and the NR medium (Fig 3.9A).

As a further evaluation of lysosomal biogenesis in nutrient restricted Caco-2 cells, the expression of several TFEB target genes was examined. All of the investigated target genes were upregulated with nutrient restriction (Fig 3.9B). All together, these data indicated that nuclear translocation of TFEB was stimulated in response to nutrient restriction which drove the expression of autophagosomal and lysosomal genes such as SQSTM1 (encoding the protein p62) in Caco-2 cells.

A
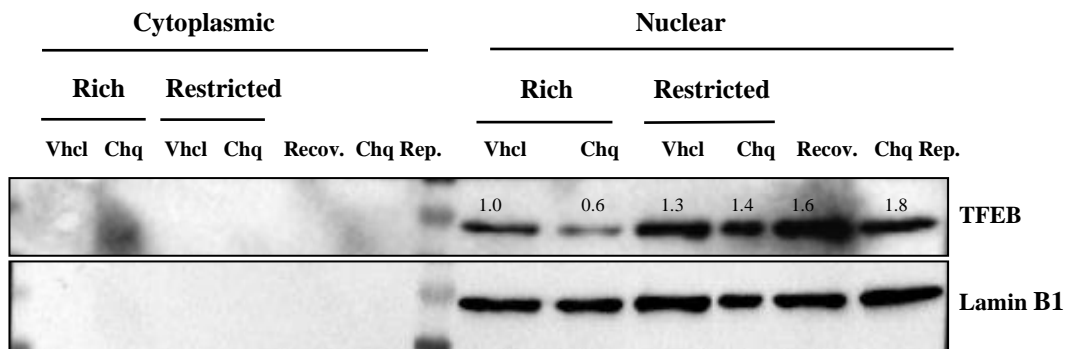
B
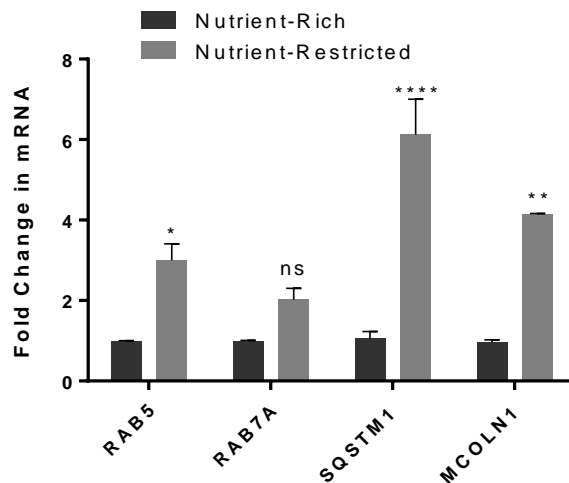
Figure 3.9 Evaluation of lysosomal biogenesis in nutrient restricted Caco-2 cells.

The changes in lysosome biogenesis in response to nutrient restriction was evaluated through TFEB nuclear translocation (A) and TFEB target expression (B). Cells treated with 100μM chloroquine (CHQ) for 3h served as a positive control. The western blot figure is the representative image of 2 biological replicates. Lamin B1 used for normalization of nuclear TFEB protein, and fold changes are written on the figure. Data in bar graph is representative of 3 biological replicates and is given as mean ± SEM. β-actin was used as normalization control. *p<0.05, **p<0.01. ****p<0.0001. ns: nonsignificant. Vhcl: Vehicle, Recov: Rocovery of NR, Chq Rep: Replacement of Chq.

Bafilomycin A1 (Baf) is a lysosomal V-ATPase inhibitor (Redmann et al., 2017). It prevents lysosomal acidification and autophagosome-lysosome fusion, thus impairing autophagic flux. Baf is frequently used as a late-stage autophagy inhibitor. Therefore, we evaluated lysosomal acidification in nutrient restricted cells with LTR using Baf as positive control (Fig 3.10C). A near complete loss in the LTR signal was observed in the Baf treated cells under both nutrient-rich and restricted conditions, suggesting a loss of lysosomal acidification, as expected. On the other hand, no change in LTR signal was observed in nutrient-restricted cells compared to the control (p>0.05). The level of LTR signal depends on lysosomal acidity as well as the lysosome numbers in cells. Our observation of no change in LAMP1 or Rab5 and Rab7A expression suggests that late endosome and lysosome numbers remained relatively steady in nutrient-restricted Caco-2 cells. Therefore, observing no change in LTR signal may represent a of lack of accumulation of lysosomes with nutrient-restriction in Caco-2 cells.

Next, we evaluated autophagic flux by treating nutrient rich and restricted Caco-2 cells with Baf, followed by withdrawal of Baf and replenishing the cells for 24h with either complete or nutrient-restriction media, respectively. As shown in Figure 3.10D, levels of autophagosomal proteins (LC3-II and p62) increased with Baf treatment in both nutrient rich and restricted conditions; however, this increase was not reversed to control levels when Baf was withdrawn. It is likely that the increase in the autophagy markers was observed due to the accumulation of autophagosomes, due to the inhibition of autophagic flux in Baf treated cells. This suggests that autophagic flux in nutrient-restricted cells was not inhibited; rather, the flux was slowed down and could be further inhibited with Baf.
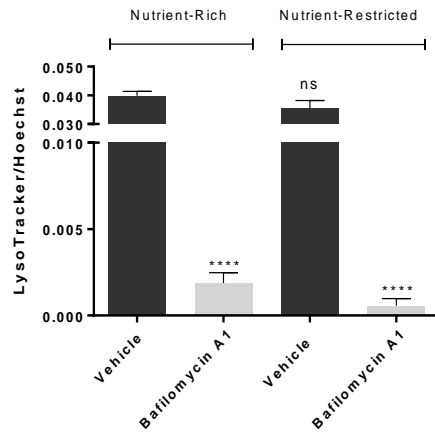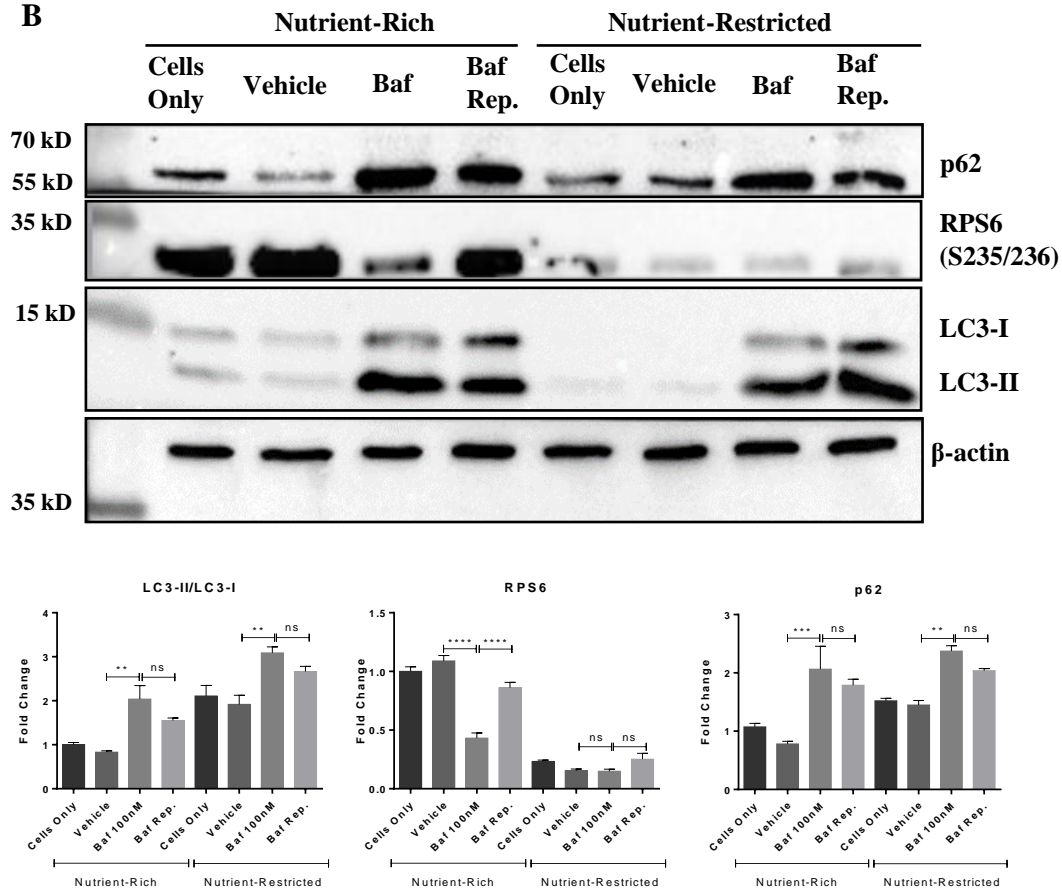
Figure 3.10 Evaluation of lysosomal function in nutrient restricted Caco-2 cells with Bafilomycin treatment

Figure 3.10 (cont'd) *The functionality of lysosomes and autophagic flux were analyzed with Lysotracker Red (LTR) Assay (A) and with western blot using Bafilomycin as lysosomal inhibitor (B). For LTR assay, Hoechst nuclear staining was performed to normalize the LTR signaling according to cell number. Data in bar graphs was represented as ± SEM. **p<0.01, ***p<0.001, ****p<0.0001. ns: nonsignificant. Data is representative of 3 biological replicates. Baf: Bafilomycin, Baf Rep: Replacement of Bafilomycin-containing medium with complete growth medium or nutrient restriction medium.*

The decrease in the phosphorylation of RPS6 in nutrient-restricted cells further supports the induction of autophagy due to inactivation of mTOR pathway. Of note, the phosphorylation of RPS6 was also decreased in Baf treated nutrient-replete cells. This indicates that the disruption of lysosomal pH through inhibition of v-ATPases with Bafilomycin A1 led to the inactivation of mTORC1 since the functionality of mTOR primarily depends on its localization on lysosomal surface through interaction with v-ATPases (Chung et al., 2019). The restoration of phosphorylation of RPS6 in the cells in which Bafilomycin was withdrawn indicates that 24h duration of replenishment after Bafilomycin withdrawal was enough for the re-activation of the mTOR pathway. However, the withdrawal of Bafilomycin and restart of autophagy did not lead to the activation of flux as shown by the high levels of p62 and LC3-II proteins in both nutrient rich and restricted cells (Fig 3.10D).

Overall, these data suggest that the NR medium led to the successful induction of autophagy in Caco-2 cells; however, the autophagic flux was rather slow.

3.6   Evaluation of Time-dependent Effects of Nutrient-Restriction

Recent studies have indicated that the prolonged starvation may result in inhibition of autophagic flux (Nwadike, Williamson, Gallagher, Guan, & Chan, 2018). We next evaluated whether the change in the expression of the autophagic and endo-lysosomal markers as well as nutrient sensors was altered at earlier time points of nutrient restriction (2h, 6h and 24h, Fig 3.11).
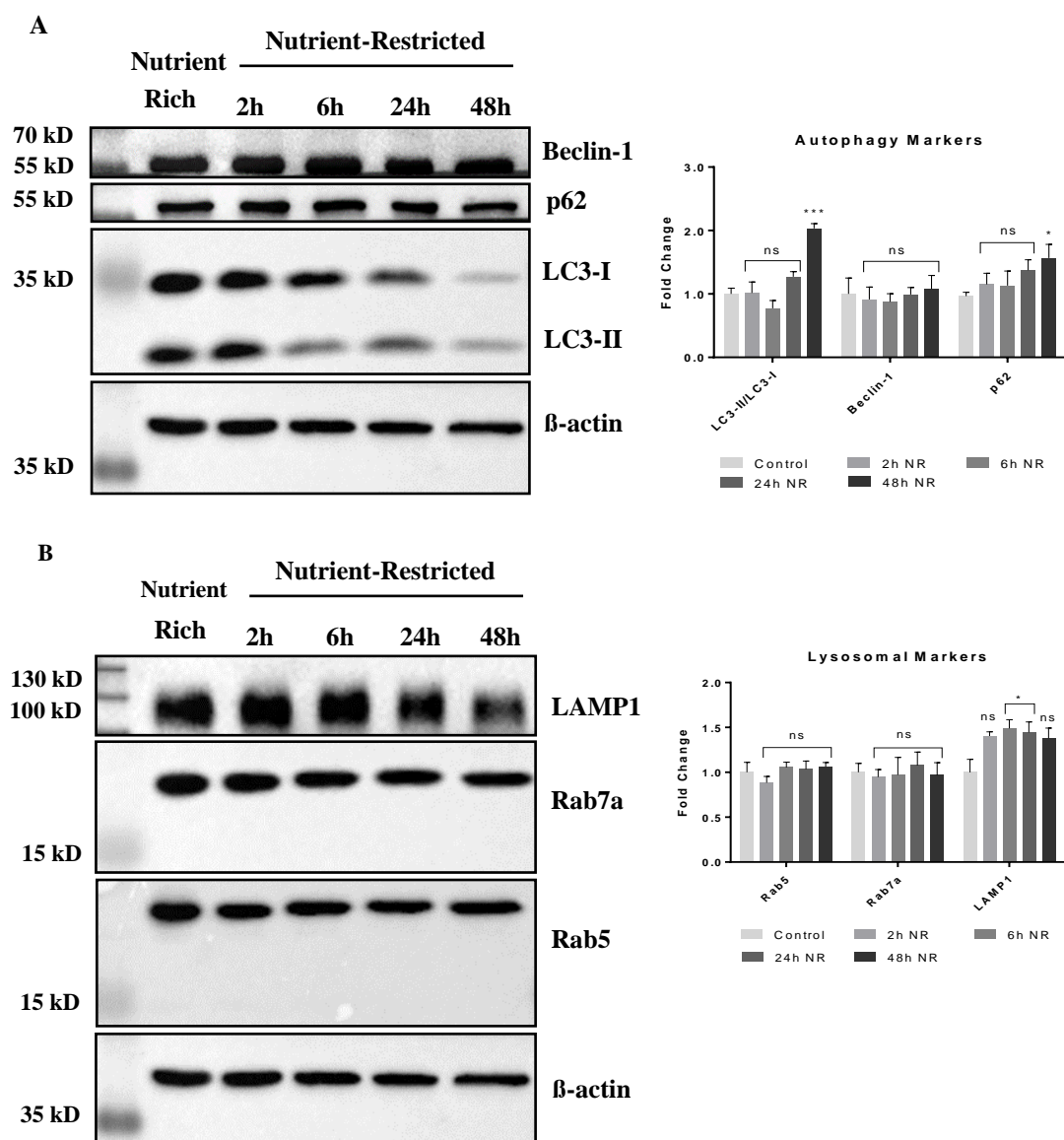
Figure 3.11 Analysis of autophagic and lysosomal markers in a time-course study of nutrient restriction.
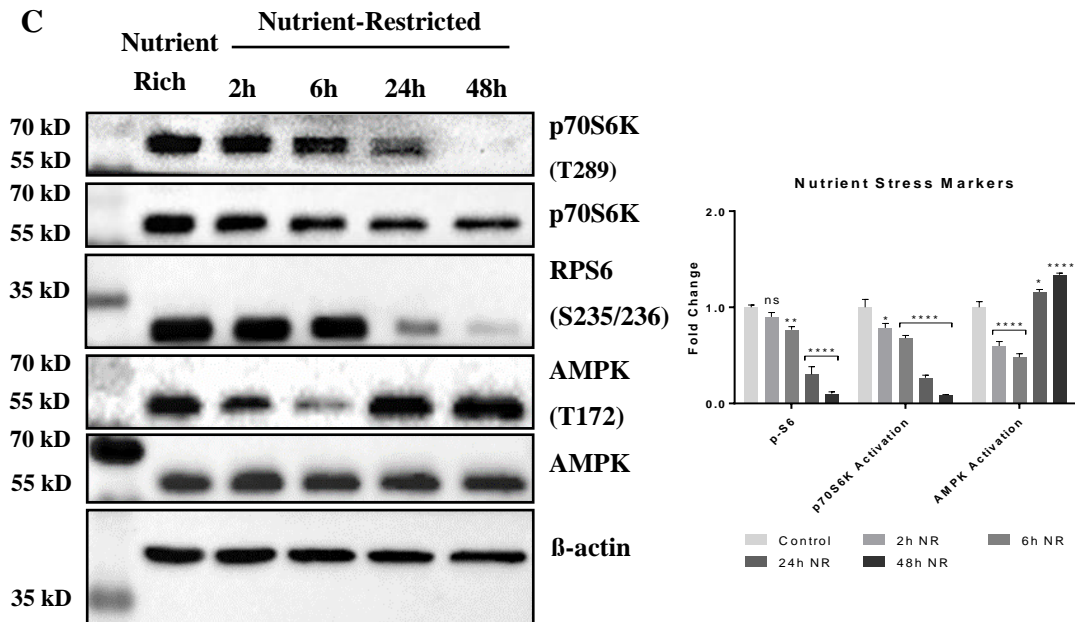
Figure 3.11 (cont'd) Analysis of autophagic and lysosomal markers in a time-course study of nutrient restriction.

Caco-2 cells were treated with restriction medium for 2h, 6h, 24h and 48h. The changes in the levels of autophagic (A) endo-lysosomal (B) and nutrient stress (C) markers were examined with western blotting. Densitometric analysis was performed with respect to nutrient-rich cells, and β-actin was used as a loading control. Data is representative of 3 biological replicates. *p<0.05, **p<0.01, ***<0.001, ****p<0.0001, ANOVA. ns: non-significant.

No significant change in any of the lysosomal markers (Rab5, Rab7a, LAMP1) as well as autophagic markers p62 and Beclin-1 was observed at any of the earlier time points (Fig 3.11). With nutrient-restriction, RPS6 levels showed a decrease in phosphorylation (S235/236) as expected, in a time-dependent manner starting from the 24h time point. The concurrent decrease in p-p70S6K also confirmed that the activation of autophagy was accompanied by a deactivation of the mTOR pathway. A decrease in the LC3-II levels was observed in a time dependent manner, which is most likely indicative of the degradation of autophagolysosomes, suggesting the presence of autophagic flux.

The levels of p-AMPK showed a decrease up to 6h and then an increase. The decreased p-AMPK levels coincided with the continuing activation of mTOR, suggesting that the cells were able to utilize the available nutrients and remain viable. After the 6h time point, the mTOR pathway showed an inhibition while the p-AMPK levels and autophagy markers showed an increase. These data also point towards the suitability of prolonged incubation of Caco-2 cells with the optimized nutrient restriction medium, to better evaluate the effects of prolonged starvation.

3.7   Evaluation of the Changes with Replenishment of Nutrients

In the optimized nutrient restriction medium, three important sources of carbon are limited: glucose, L-glutamine and FBS. We examined whether the addition of the missing nutrients could reverse autophagy induction and reactivate flux. For this, Caco-2 cells were starved for 48h in the nutrient restricted medium and then replenished with complete growth medium for 6h and 24h (Fig 3.12A). 24h Rapamycin (500nM) and Chloroquine (10nM) treated cells was used as a positive control. Rapamycin is an inhibitor of mTOR, which causes the induction of autophagy while chloroquine decreases the acidification of lysosomes, leading to the accumulation of the formed autophagolysosomes. The accumulation of autophagosomal and endolysosomal proteins in the positive control cells indicated the induction of autophagy followed by a flux inhibition, as expected (Fig 12A-B, 1st lane). Autophagy induction was reversed in the replenished cells as indicated with a decrease in LC3-II/LC3-I ratio within 6h of replenishment, which continued with longer duration (24h) of replenishment. The expression of LAMP1 and Rab7a were also decreased in the replenished cells compared to NR. Following the decrease in autophagy induction, the levels of p62 protein was also diminished which indicates that the active autophagic machinery was reversed with replenishment in complete medium.

56
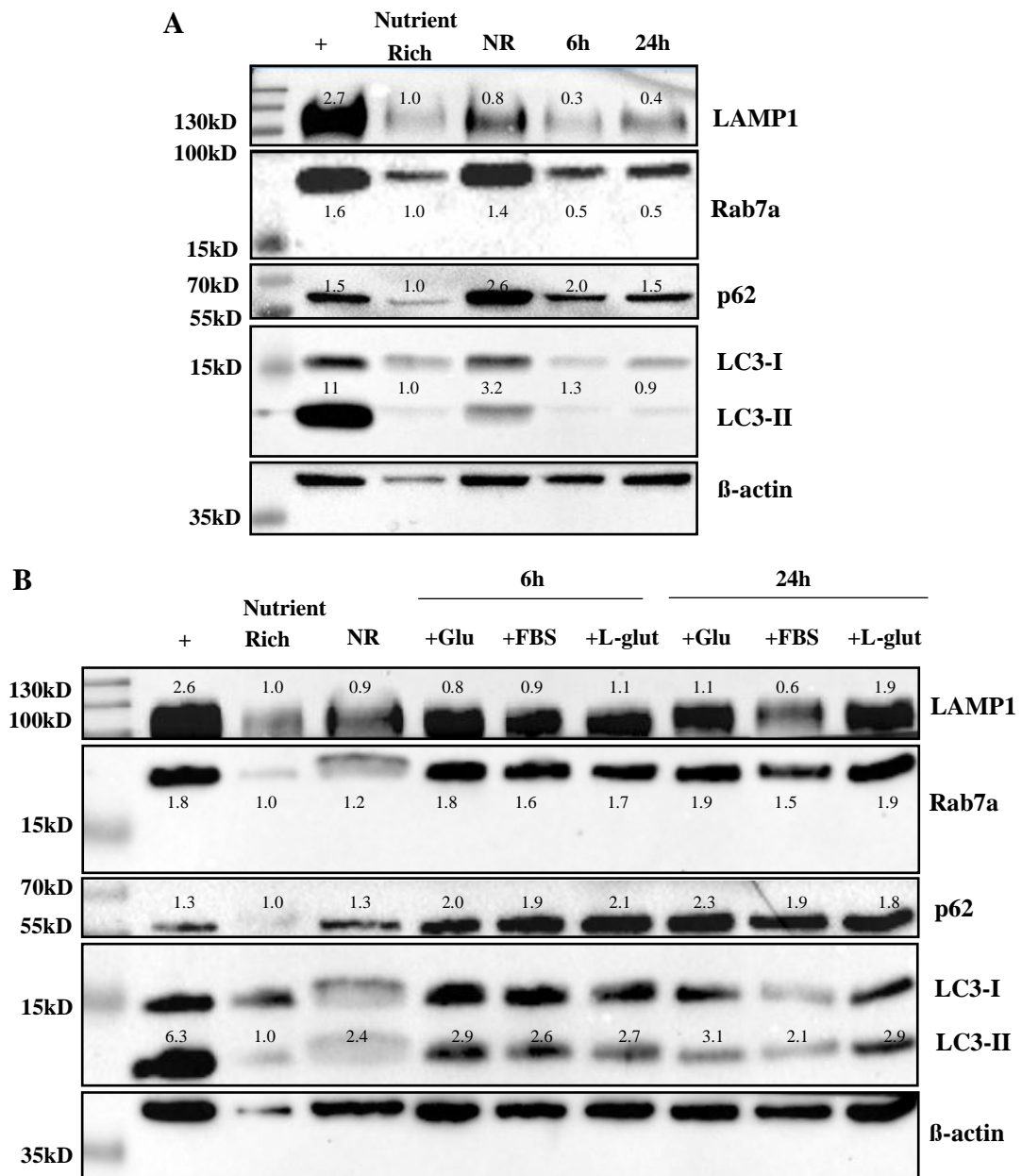
Figure 3.12 Replenishment of Caco-2 cells with complete growth medium for 6 hours and 24 hours after 48 hours starvation.

For the replenishment experiments, 48 h NR-cells were incubated either with the complete growth medium (A) or with the NR medium supplemented with Glucose (Glu), FBS or L-glutamine (L-glut) for 6 h and 24 h (B). As positive control (+) for autophagy induction and autophagic flux inhibition, cells were treated with 500 nM Rapamycin and 10 nM Chloroquine for 24 hours. Protein levels were normalized to ß-actin and fold changes with respect to nutrient-rich cells are shown on the figures. Representative blots from 2 biological replicates are shown.

In order to identify which nutrient was responsible for the reversal of autophagy observed in the replenished cells, the cells were replenished individually with glucose, FBS and L-glutamine for 6h and 24h after 48h starvation with the NR medium (Fig 3.12B). We observed that individual replenishment of the FBS, glutamine or glucose was not enough to restore autophagic flux in NR cells. These data suggest that for the reversal of autophagy induction, all three nutrient sources must be present in the medium.

3.8   Evaluation of Proliferation in Nutrient Restricted Caco-2 Cells

Metabolic activities of cancer cells can have an impact on their proliferative capacity. Cancer cells require a sufficient amount of nutrients to support growth and proliferation. Therefore, we examined proliferation and viability of Caco-2 cells incubated in nutrient restricted and nutrient rich media with the MTT assay, BrdU assay and the Muse Cell Count and Viability assay. Both nutrient-rich and nutrient-restricted cells were also treated with the chemotherapeutic reagent 5-Fluorouracil (5-FU) for 48h to evaluate any differential response as the function of nutrient availability to the drug. The MTT assay evaluates metabolically active cells, in part by the action of dehydrogenases that generate reducing equivalents such as NADH and NADPH (Rai et al., 2018). This assay was thus used as a marker for metabolic activity. The BrdU assay determines the incorporation of the thymidine analog bromodeoxyuridine (BrdU) during the S-phase of the cell cycle and is representative of cell cycle progression in cells proliferation (Crane & Bhattacharya, 2013). The Muse Cell Count and Viability assay differentiates between viable and non-viable cells through the incorporation of two DNA binding dyes. Non-viable cells are more likely to have permeable cell membranes that can incorporate the cell impermeable dye and stain the DNA. The total nucleated cell number is determined with a membrane permeable DNA binding dye and the percent viability is calculated.

We first determined whether autophagy inhibitors could affect the metabolic activity of cells. 3-MA is a class III PI3K inhibitor which inhibits the early stages of

autophagy by preventing the formation of the autophagy initiation complex (Y. T. Wu et al., 2010). Bafilomycin A1 is a late phase autophagy inhibitor that prevents the acidification of lysosomes and inhibits lysosome-autophagosome fusion (Newton, Vuppalapati, Bouderlique, & Chagin, 2015). Both nutrient-rich and nutrient-resticted cells were individually treated with 3-MA and Baf and metabolic activity was measured with the MTT assay (Fig 3.13A). We observed that the cells treated with 3-MA and Bafilomycin A1 responded differentially to drugs under nutrient-rich and nutrient-restricted conditions. Inhibition of autophagy at the early stages with 3-MA in both nutrient-rich and nutrient-restricted conditions caused a reduction in metabolic activity; however this decrease was more pronounced in nutrient-rich cells compared to the NR cells (Figure 3.13A). Interestingly, treatment Caco-2 cells grown under nutrient rich conditions with Baf did not lead to any change in metabolic activity, while nutrient restricted cells showed a decrease (Fig 3.13A). These data show that the induction of autophagy was necessary for the survival of Caco-2 cells, especially when the cells were growing in nutrient rich conditions, highlighting the importance of basal autophagy for cell survival. Late-stage autophagy was dispensable for survival under nutrient rich conditions but was necessary for survival under nutrient restriction.
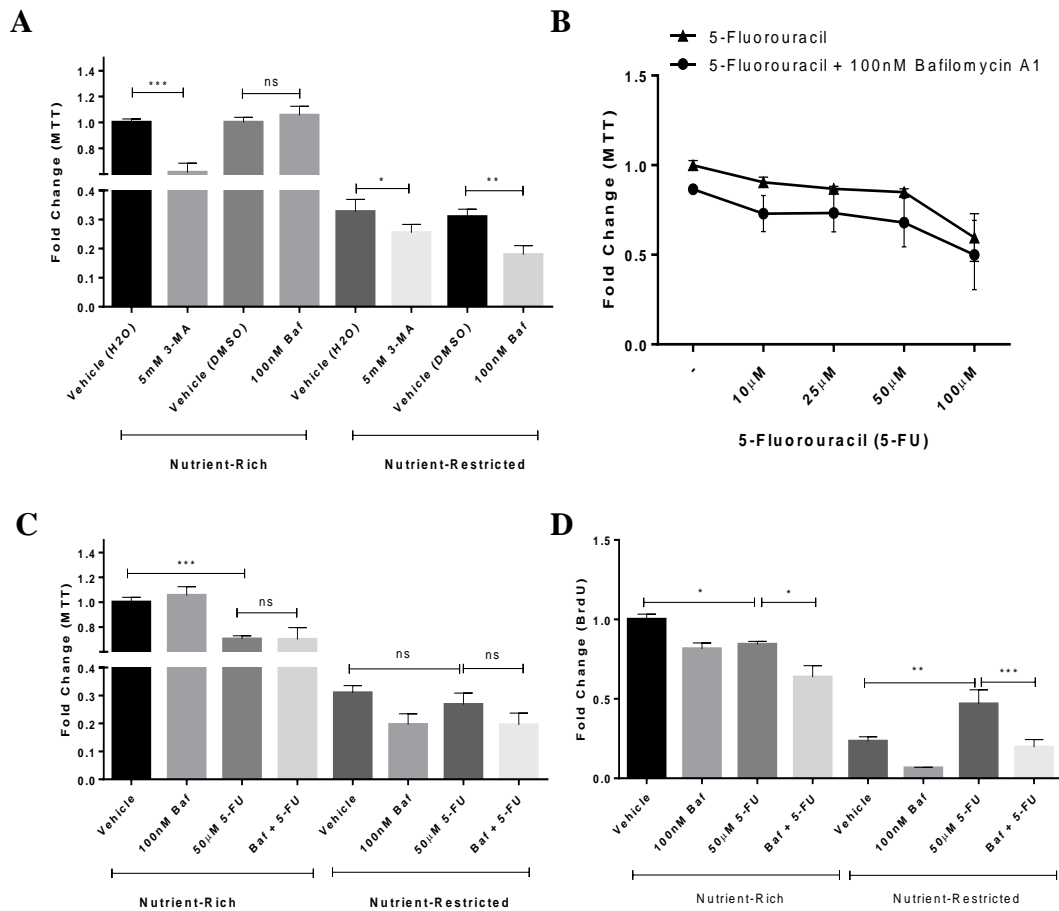
Figure 3.13 Evaluation of viability and proliferation in nutrient-restricted Caco-2 cells

The change in proliferation and viability of the Caco-2 cells in response nutrient restriction was evaluated with MTT (A-C) and BrDU assays (D). The effect of early and late stage autophagy inhibitors, 3-MA and Bafilomycin A1 was analyzed (A). The sensitivity of cells to 5-FU and the effect of autophagic flux inhibiton with Bafilomycin on the the drug sensitivity was evaluated in dose-response manner (B), with MTT (C) and BrDU (D) assays. Data represents 4 independent biological replicates for MTT and 3 biological replicates for BrDU assay. Analysis was performed with respect to vehicle-treated nutrient rich cells and the fold changes are expressed as mean ± SEM. *p<0.05, **p<0.01, ***p<0.001. ns: nonsignificant.

Next, we evaluated whether the inhibition of autophagy affected the proliferation of Caco-2 cells in the presence of the chemotherapy agent 5-FU. We observed that NR cells were mostly insensitive to 5-FU (Fig 3.12B). The NR cells were highly sensitive to lysosomal alkalinization with Baf. The MTT assay (C) and especially the BrdU assay (D) showed a decrease in signal after treatment with Baf alone to a higher extent than Baf treated nutrient-rich cells. Next, we determined whether the sensitivity of NR Caco-2 cells to 5-FU could be increased when combined with Baf. We observed that the sensitivity of NR cells to 5-FU remained the same when co-treated with Baf (Fig 3.12C), as seen with the MTT assay. The BrdU assay, which measures cell proliferation (Crane & Bhattacharya, 2013), showed a modest decrease when the NR cells were co-treated with Baf and 5-FU (Fig 3.13D). Based on the data presented, it can be speculated that the NR treatment decreased the proliferation rate of Caco-2 cells without decreasing the viability; and with Baf treatment (lysosomal alkalinization) this decrease became more prominent.

In the light of these observations, we next evaluated the change in viability in response to nutrient restriction in Caco-2 cells with the Muse Cell Count and Viability assay. As a control, another cell line, HCT-116, which is sensitive to 5-FU, was used. A remarkable decrease in the metabolic activity (determined by the MTT assay) was observed in both Caco-2 and HCT-116 subjected to the same nutrient restriction medium (Fig 3.14A and 3.14C). On the other hand, the viability of Caco-2 cells (Muse Cell Viability assay) was not affected with nutrient-restriction while HCT-116 cells showed a significant decrease in viability as well (Fig 3.14B and 3.14D).
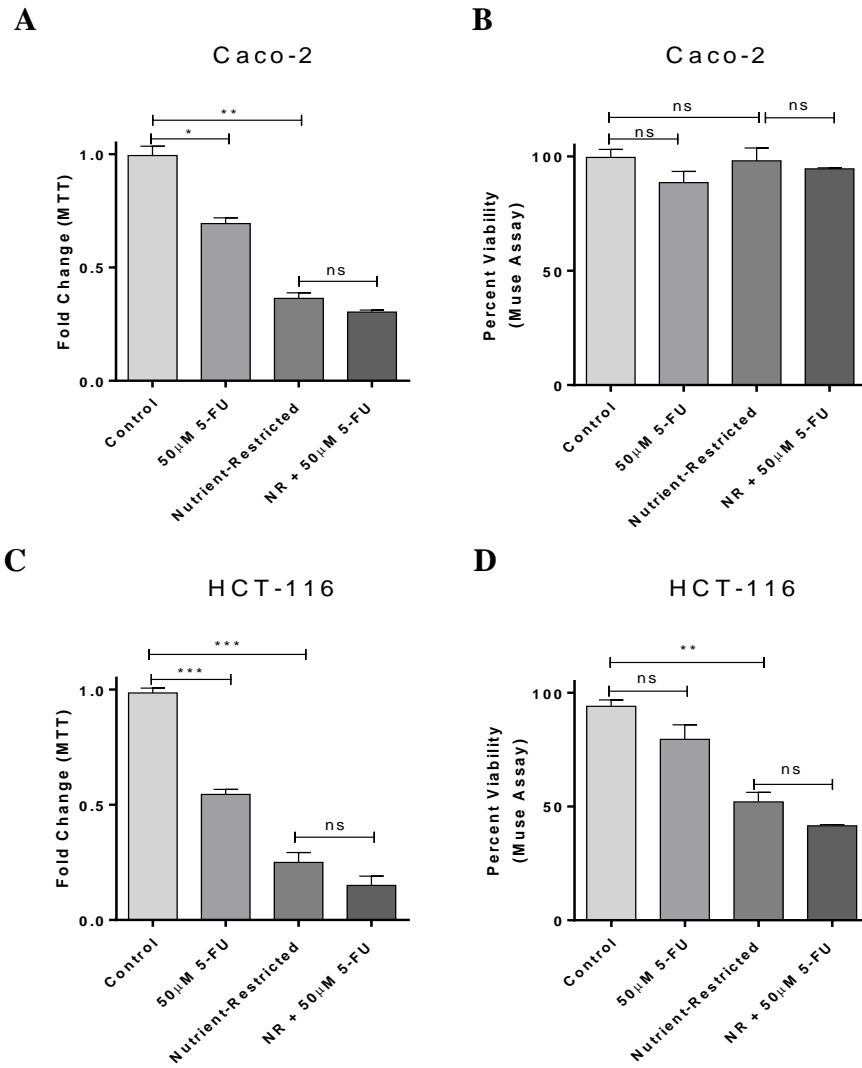
Figure 3.14 Analysis of cell viability in control and nutrient-restricted Caco-2 cells.

In order to analyze cell viability MTT (A,C) and Muse Cell Count and Viability (B,D) Assays were performed. With MTT assay, a decrease in metabolic activity with nutrient restriction in both Caco-2 (A) and HCT-116 (C) cells was observed. Muse cell viability assay (B) showed no significant change in cell viability in nutrient-restricted Caco-2 cells while the viability of HCT-116 was significantly decreased with nutrient restriction (D). 5-FU: 5-Flurouracil was used as positive control. Data represents the average of 3 biological replicates for the MTT assay and 2 biological replicates for the Muse Assay.

The decrease in the MTT signal in NR Caco-2 cells (Fig 3.13) was most likely due to decreased cell number rather than cell death. HCT-116 cells, on the other hand, were susceptible to death when cultured under nutrient restriction. Of note, treatment of Caco-2 and HCT-116 cells with 50μM and 20μM 5-FU, respectively, resulted in reduced cell numbers (Fig 3.14A, C, MTT assay). While this was reflected as reduced cell viability in nutrient restricted 5-FU treated HCT-116 cells (Fig 3.14D, Muse assay), no change in cell viability was seen in 5-FU treated Caco-2 cells under both nutrient rich or nutrient restricted growth (Fig 3.14B, Muse assay) suggesting the activation of resistance mechanisms in these cells.

3.9   Epithelial and Mesenchymal Properties of Nutrient-Restricted Caco-2 Cells

Various mechanisms may lead to drug resistance/insensitivity in cancer cells including activation of protective autophagy and epithelial-mesenchymal transition (EMT) along with other mechanisms such as decreased drug uptake, increased DNA damage repair and drug sequestration (Mansoori, Mohammadi, Davudian, Shirjang, & Baradaran, 2017; H. C. Zheng, 2017). The link between the nutrient-restriction and EMT has been demonstrated by several studies. Therefore, in order to understand the mechanism behind the insensitivity to 5-FU observed in Caco-2 cells we hypothesized the activation of EMT in nutrient-restricted cells.

For this, we analyzed the expression of well-established EMT markers (Hill & Wang, 2020) in control (nutrient rich) and nutrient-restricted Caco-2 and HCT-116 cells. Caco-2 cells incubated in nutrient-restricted medium underwent a hybrid/partial EMT as indicated by increased mRNA levels of both epithelial (E-cadherin, Occludin) and mesenchymal (Vimentin, Snai1) markers (Fig 3.15A). Although nutrient-restricted HCT-116 cells also showed minor changes in the expression of all markers, the difference did not reach statistical significance (except for an increase in SNAI1 expression); (Fig 3.15B). These data suggest that nutrient-restricted HCT-116 cells did not undergo changes in epithelial characteristics, while nutrient-

restricted Caco-2 cells became relatively more mesenchymal. This observation also supports the data presented in Figure 3.14, where nutrient restricted HCT-116 cells were more responsive to chemotherapeutic drugs compared to Caco-2 cells. Therefore, the partial EMT phenotype acquired by Caco-2 cells could explain the insensitivity of this cell line to 5-FU treatment when grown under NR.
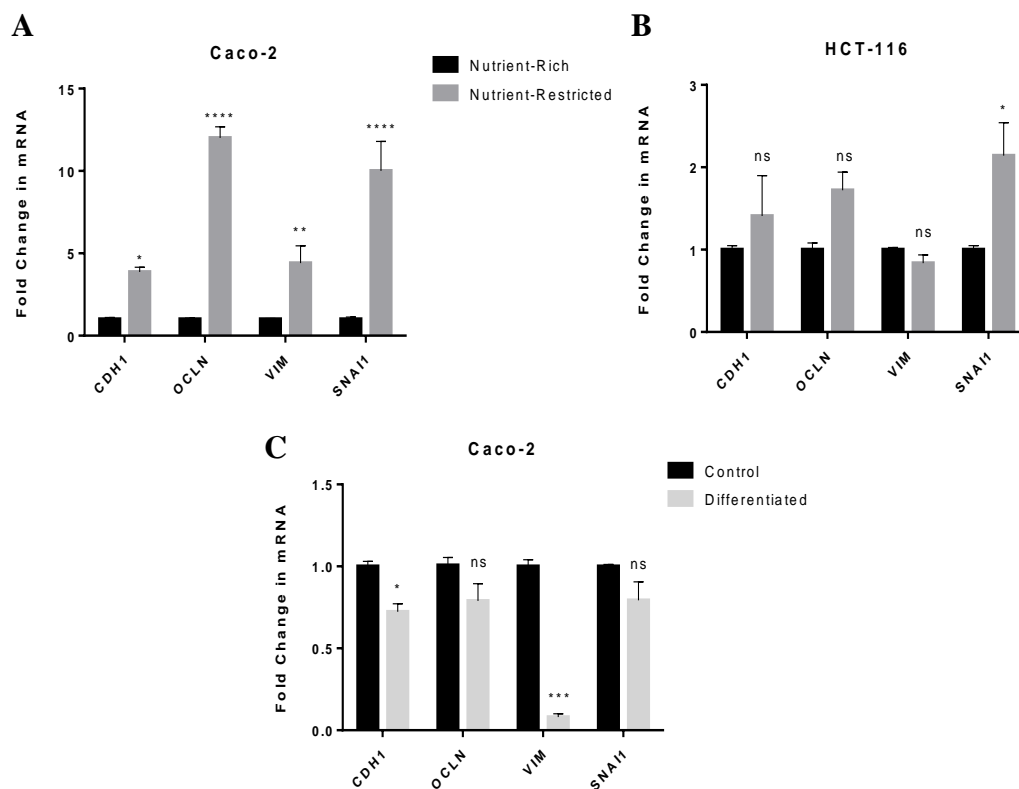
Figure 3.15 Change in epithelial and mesenchymal markers in nutrient restricted and differentiated Caco-2 cells.

*The change in both epithelial (E-cadherin, Occludin) and mesenchymal (Vimentin, Snai1) markers in nutrient-restricted Caco-2 (A) and HCT-116 (B) cells; and the differentiated Caco-2 (C) cells were analyzed with qRT-PCR. The fold change in markers was calculated in comparison to nutrient-rich/control cells and normalized to the geometric mean of reference genes ACTB and B2M. Bars represent mean ± SEM of 3 biological replicates. *p<0.05, **p<0.01, ***<0.001****p<0.0001. ns: nonsignificant. CDH1: E-cadherin, OCLN: Occludin, VIM: Vimentin, SNAI1: Snai1.*

The Caco-2 cells provide us with the opportunity to also evaluate the expression of EMT markers in cells that have undergone spontaneous differentiation. Previously, our lab has reported that spontaneously differentiated cells can undergo mesenchymal to epithelial transition (MET), via an increase in the expression of epithelial markers CDX2, Claudin-4 and E-cadherin, and a concomitant loss of mesenchymal markers Vimentin, Fibronectin-1 and Transgelin (Yilmaz-Ozcan et al., 2014). We also observed a decrease in the expression of Vimentin in differentiated Caco-2 cells; however, the expression of E-cadherin was also modestly but significantly reduced while no change was seen in the expression of the mesenchymal marker SNAI1 and the epithelial marker Occludin (Fig 3.15D). This suggests the activation of highly divergent signals for EMT and MET in the nutrient restricted and differentiated cells.

3.10 Epithelial And Mesenchymal Properties After Bafilomycin Treatment in Nutrient-Restricted Caco-2 Cells

Bafilomycin treatment led to a decrease in proliferation of NR Caco-2 cells but failed to enhance the sensitivity of the treated cells to 5-FU (Fig 3.13). We also observed that Caco-2 cells acquired a partial EMT phenotype after nutrient restriction (Fig 3.15) which was hypothesized to be the reason behind the insensitivity of these cells to 5-FU (Fig 3.13). Therefore, we wanted to evaluate whether the lysosomal alkalinization with Baf in NR Caco-2 cells abrogated the sensitivity of these cells to 5-FU via the activation of EMT.

Firstly, we analyzed the change in viability upon Baf treatment under both nutrient-rich and restricted conditions. We observed no change in the viability of cells using the Muse Cell Count and Viability assay (Fig 3.16). These data strongly suggest that despite a remarkable decrease in available nutrients, Caco-2 cells maintained their viability even when autophagic flux (lysosomal acidification) was inhibited.
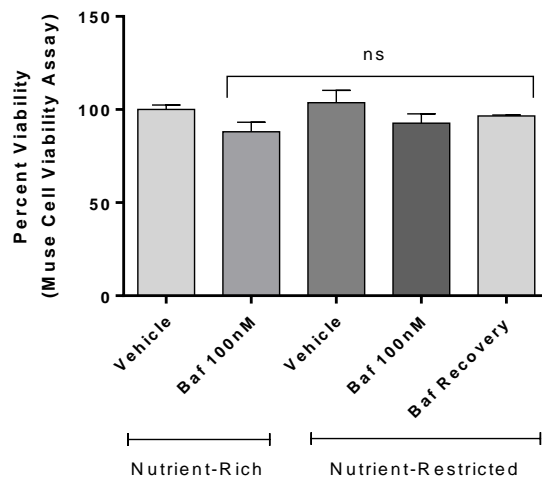
Figure 3.16 Analysis of cell viability in nutrient-restricted cells upon Bafilomycin treatment.

Caco-2 cells were treated with 100nM Bafilomycin for 48h in nutrient-rich and nutrient-restricted media. For the recovery, 48h NR+Bafilomycin treated cells were incubated in complete growth medium for 24h. The viability was measured with Muse Cell Count and Viability assay. Normalization was performed according to nutrient-rich cells. Data represents 2 biological replicates. Bars represent mean ± SEM. ns: nonsignificant

Next, we evaluated the morphology of NR Caco-2 cells treated with Baf. Epithelial cells undergoing EMT are known to alter their shape from cobblestone like shape to elongated fibroblast like shape. We observed a modest change in cellular morphology when Caco-2 cells underwent NR. However, a remarkable change in morphology was seen when NR Caco-2 cells were treated with Baf. Cells in NR+Baf medium gained spindle-like shape while the cells in nutrient-rich medium had the usual cobblestone-like morphology (Fig 3.17). Of note, the spindle-like shape after Baf treatment under NR was reverted to the cobblestone like shape after the recovery in complete medium suggesting that the process of EMT was highly reversible.
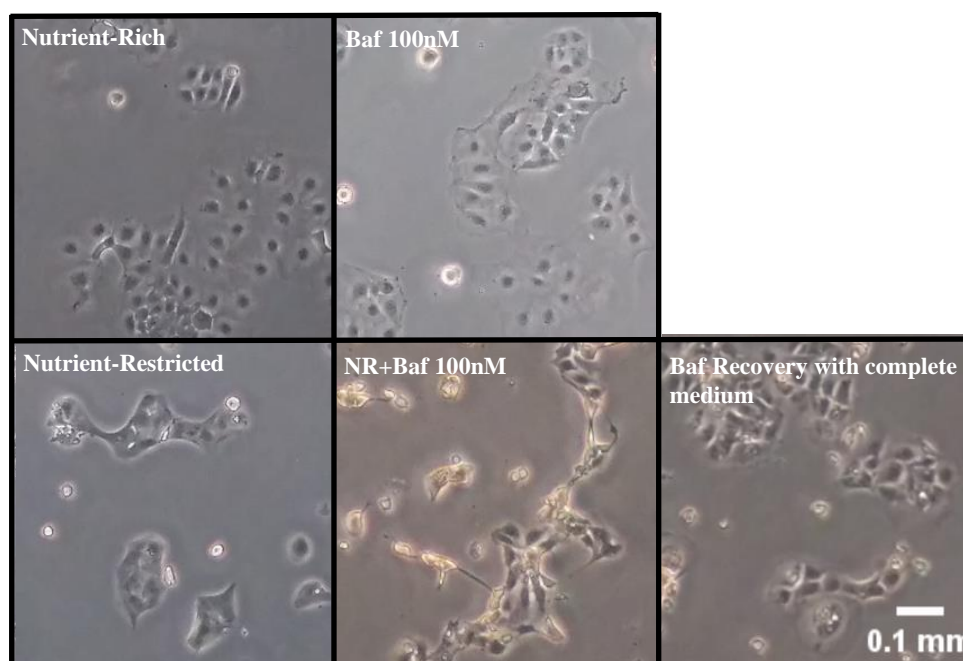
Figure 3.17 Analysis of cellular morphology in nutrient-restricted Caco-2 cells upon Bafilomycin treatment.

Caco-2 cells were treated with 100nM Bafilomycin for 48h in nutrient-rich and nutrient-restricted media. For the recovery, 48h NR+Bafilomycin treated cells were incubated in complete growth medium for 24h. Images were gathered with inverted light microscope at 20X magnification; and representative of 3 biological replicates.

Based on these dramatic and reversible change in the shape of the cells, we next evaluated the expression of epithelial and mesenchymal markers in Bafilomycin treated NR Caco-2 cells.

In Caco-2 cells, a significant increase in both epithelial and mesenchymal markers was observed with nutrient restriction, as also reported in Figure 3.18. NR+Baf co-treatment resulted in further increase in the mRNA expression of three out of four markers (except for E-cadherin, Fig 3.18). This increase was reversed with recovery in complete growth medium, with the expression of the markers decreasing more robustly than the replacement medium. This observation is also consistent with the observed reversion of the morphology of the NR+Baf treated cells to the cobblestone shape when replaced with complete medium (Fig 3.17).
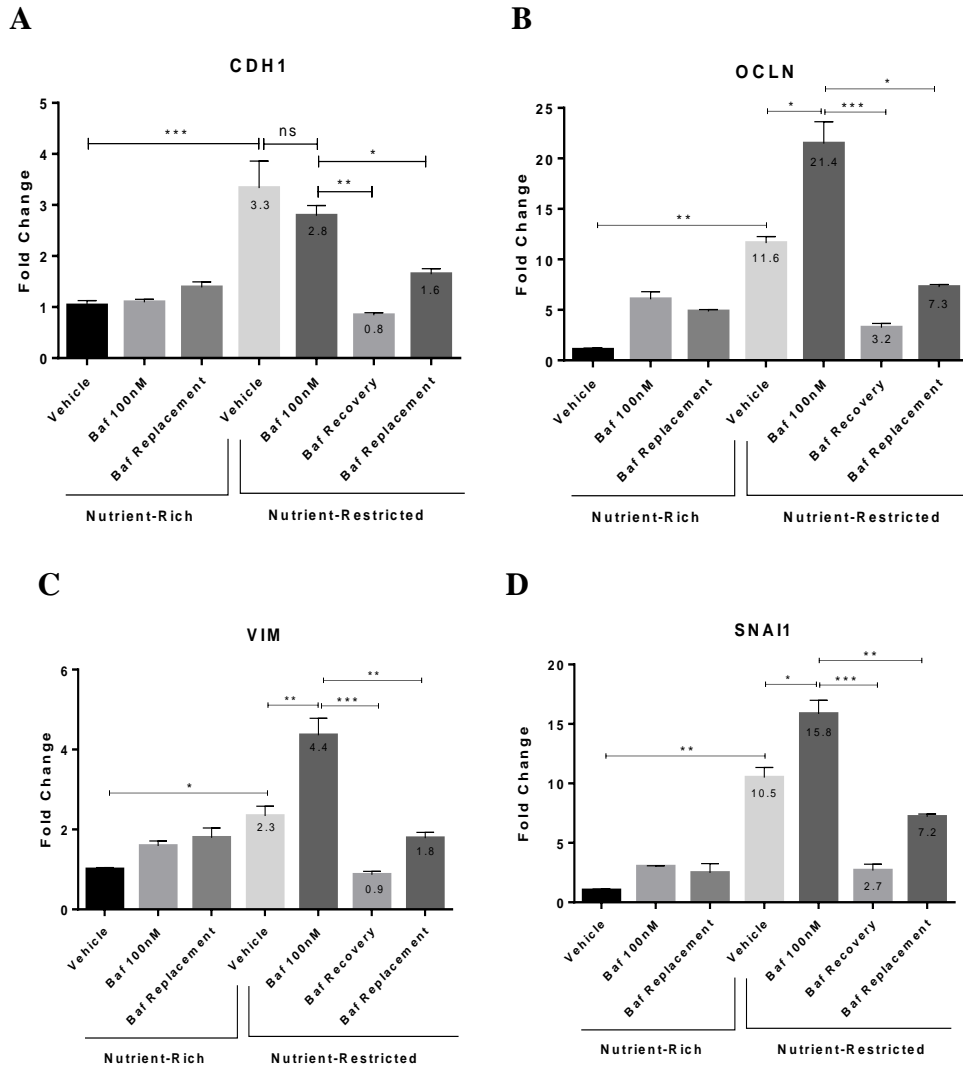
Figure 3.18 Change in epithelial and mesenchymal markers in nutrient restricted and Bafilomycin treated Caco-2 cells.

Expression of epithelial (E-cadherin, Occludin) and mesenchymal (Vimentin, Snai1) markers in nutrient-rich and restricted Caco-2 cells with or without Bafilomycin treatment was analyzed with qRT-PCR. Baf Replacement indicates the replacement of Bafilomycin containing medium with complete medium for nutrient-rich and starvation medium for restricted cells. Baf Recovery indicates the recovery of NR+Baf cells with complete medium. The fold change in markers was calculated compared to nutrient-rich cells and normalized to geometric mean of reference genes ß-actin and B2M. Bars represent mean ± SEM of 3 biological replicates. *p<0.05, **p<0.01, ***<0.001, ANOVA. ns: non-significant. CDH1: E-cadherin, OCLN: Occludin, VIM: Vimentin, SNAI1: Snai1

To further evaluate the phenotypic changes that might be indicative of an EMT phenotype, we analyzed cytoskeletal reorganization in response to NR+Baf treatment with Alexa Fluor 405-conjugated Phalloidin. In the absence of starvation or Bafilomycin treatment, Caco-2 cells grown in complete medium assumed a normal cobblestone-like morphology with cytoplasmic distribution of F-actin (Fig 3.19A). With nutrient restriction, cell morphology changed modestly with no obvious difference in F-actin expression or cellular distribution (Fig. 3.19B). In response to NR+Baf treatment, on the other hand, the cells acquired an elongated spindle-like shape with marked increase in F-actin staining (Fig 3.19C). This morphological change of enhanced polarity and actin rearrangement into cytosolic stress fibers are characteristic morphological changes of EMT (Das, Becker, Hoffmann, & Mertz, 2009). After recovery in complete medium, the actin stress fibers were lost (Fig 3.19D), and cells re-gained the cobblestone-like morphology as seen in control cells. Manual counting of the fibers indicated the presence of 0.5 fibers/cell in nutrient-rich, 2.1 fibers/cell in nutrient-restricted, 12.8 fibers/cell in NR+Baf and 3.2 fibers/cell in Bafilomycin recovery treatments.
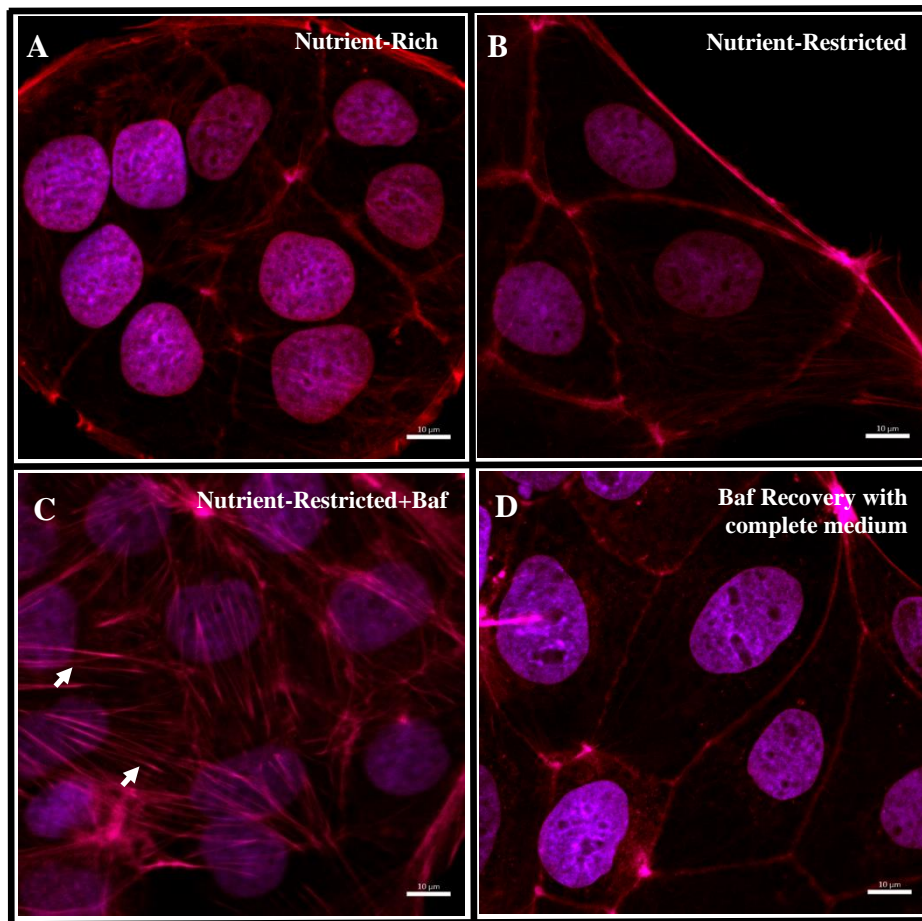
Figure 3.19 Evaluation of cytoskeletal reorganization after Bafilomycin treatment in nutrient restricted Caco-2 cells.

Bafilomycin treated and untreated Caco-2 cells were cultured on glass coverslips, stained with Alexa Fluor 405-conjugated phalloidin to detect F-actin, while DAPI was used to detect the nuclei. Images were taken with a Zeiss confocal microscope at 63× magnification. Scale bar is given at the bottom right corner. The stress fibers are indicated with white arrows.

The data so far suggest that lysosomal alkalinization in nutrient-restriction medium enables Caco-2 cells to undergo changes in gene expression and morphological reorganization reminiscent of the activation of a hybrid EMT program. Moreover, these changes could be completely reversed within 24 h of removal of Baf and

replenishment with complete medium. Next, we evaluated the time course for the reversal of this partial EMT phenotype. For this, 48 h NR+Baf treated cells were allowed to recover in complete medium and the changes in the expression EMT genes were analyzed in a time-dependent manner at 2, 6, 16 and 24 h (Fig 3.20).
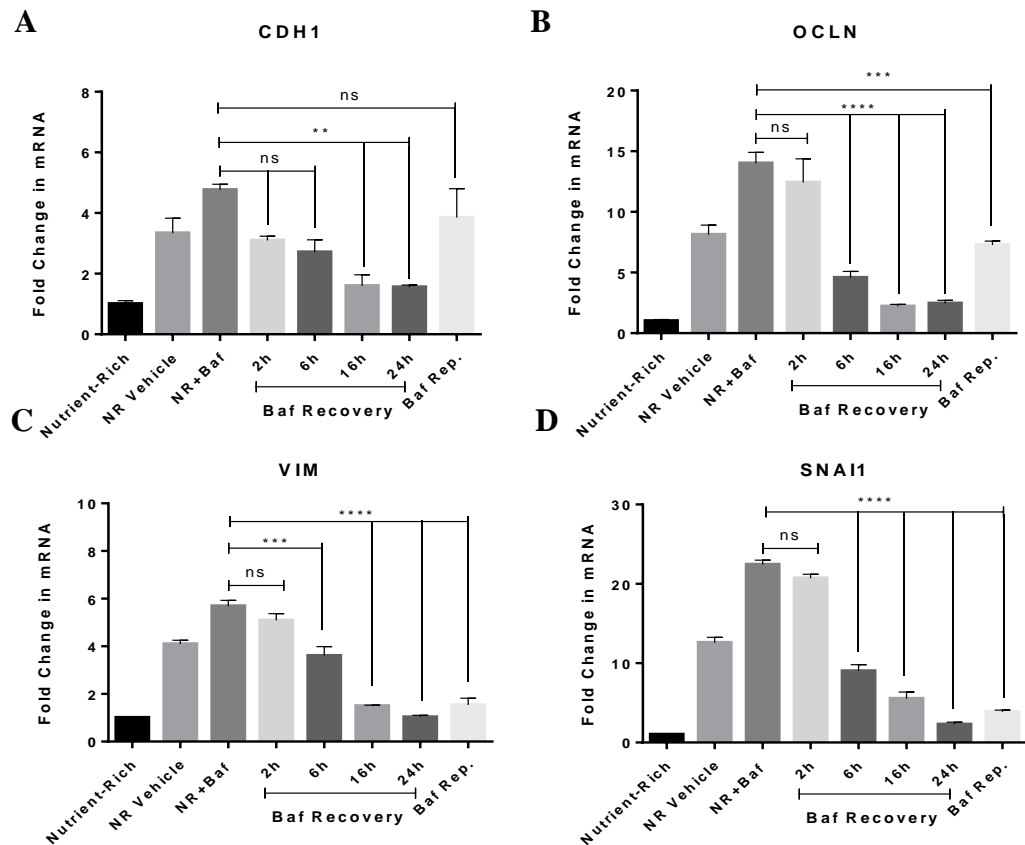
Figure 3.20 Evaluation of time-dependent change in the expression of epithelial and mesenchymal markers after recovery of nutrient restriction and Bafilomycin treatment with complete growth medium.

48 h NR+Baf treated Caco-2 cells were recovered in complete growth medium for 2h, 6 h, 16h and 24 h, with nutrient restriction medium for 24 h. The fold change in markers was calculated compared to nutrient-rich cells and normalized to geometric mean of reference genes ß-actin and B2M. Data is representative of 2 biological replicates. Bars represent mean ± SEM. *p<0.05, **p<0.01, ***<0.001, ****<0.0001, ns: nonsignificant. CDH1: E-cadherin, OCLN: Occludin, VIM: Vimentin, SNAI1: Snai1

We observed a quick recovery of partial EMT phenotype indicated with a statistically significant decrease in the expression of both epithelial and mesenchymal markers within 6 h recovery in complete medium, except for CDH1 which was recovered at 16 h (Fig 3.20). These changes in gene expression profile were also reflected in the cellular morphology, and the recovery of cell morphology was observed at around 6 h-16 h of recovery (Fig 3.21).
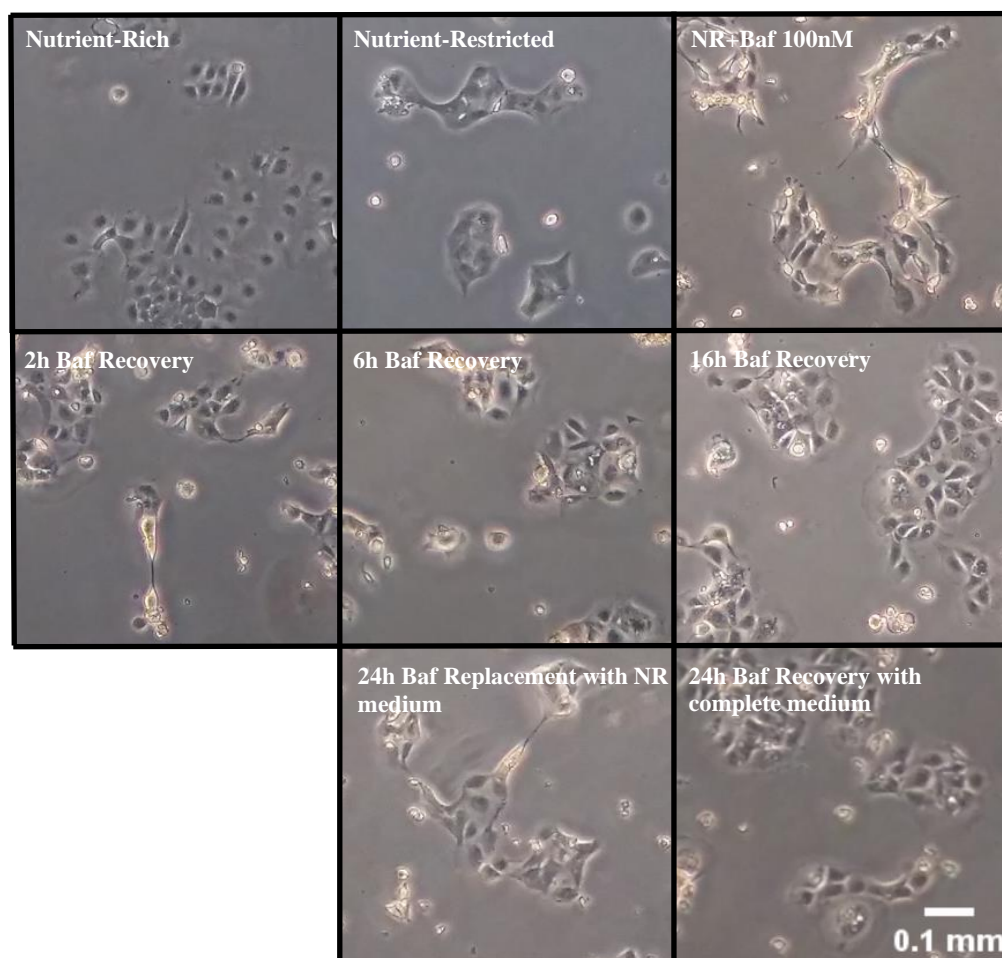
Figure 3.21 Evaluation of time-dependent change in cellular morphology after recovery of nutrient restriction and Bafilomycin treatment with complete growth medium.

48h NR+Baf treated Caco-2 cells were recovered in complete growth medium for 2h, 6h, 16h and 24h, with nutrient restriction medium for 24h. Images were gathered with an inverted light microscope at 20X magnification and representative of 3 biological replicates. Scale bar is given at the bottom right corner.

The data indicate that the changes associated with partial EMT phenotype acquired upon NR+Baf treatment were rapidly reversible within 6 h – 16 h of culture in complete medium (Fig 3.21).

3.11 The Effect of Nutrient-Restriction and Bafilomycin Treatment on Spheroid Formation Ability of Caco-2 Cells.

We observed very clear changes suggesting the acquisition of partial EMT in Caco-2 cells with nutrient restriction and Baf treatment in *in vitro* 2D culture. Therefore, we wanted to examine whether the EMT phenotype induced with NR+Baf treatment was also retained in 3D cell culture. For this, we generated Caco-2 spheroids in ultra-low attachment (ULA) 96-well plates in nutrient-rich and restricted medium with or without Bafilomycin and the capacity of spheroid forming abilities were analyzed. We observed that under nutrient-rich conditions, Caco-2 cells were able to form spheroids with relatively non-uniform edges (Fig 3.22A) compared to SW620 cells that can form very tight and uniform spheroids (not shown). The capacity of nutrient-rich cells to form spheroids was similar with Baf treatment. However, with nutrient-restriction, Caco-2 cells formed loose cell clusters rather than spheroids (Fig 3.22A). With Baf treatment and nutrient-restriction, the spheroid forming ability of Caco-2 cells was lost; rather, the cells formed multiple small clusters instead of single-large spheroids (Fig 3.22A).

We next examined the effect of passaging of the 3D cultured cells on the re-formation of spheroids. For this, the spheroids were collected, passed through a 26-gauge needle to disintegrate the spheroids, and separate the cells. These separated cells were immediately re-plated in ULA plates (Figure 3.22B) and left for 48 h to reform the spheroids. We observed that the Caco-2 cells grown in complete medium were able to reform the spheroids effectively, with no difference in the shape and tightness of the spheroids after passaging. Cells grown in complete medium and treated with Baf also showed reasonably good ability to reform spheroids, although the spheroids showed greater transparency after passaging, indicating some loss in

cell-cell interactions. The nutrient restricted cells underwent a complete loss in spheroid forming ability after passaging both in the presence and absence of Baf, suggesting that these cells are unable to maintain cell-cell contacts.

A   **No Passaging**
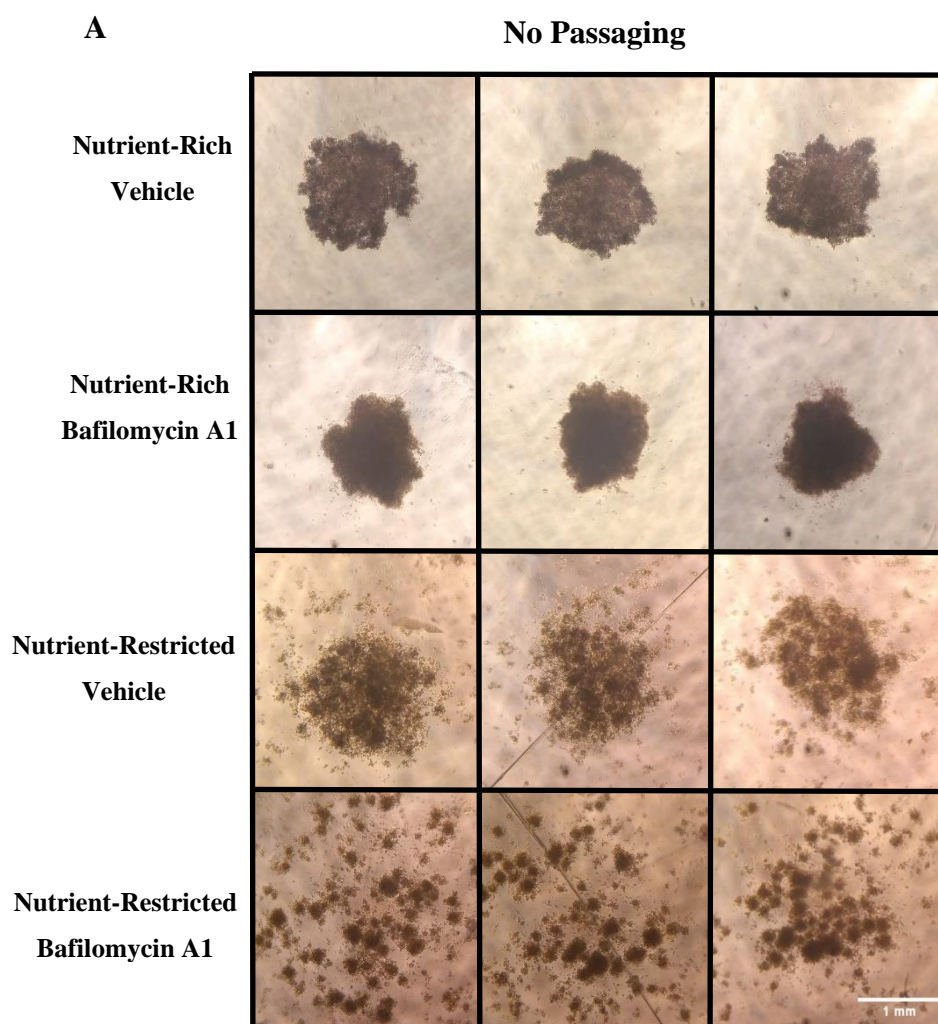
Figure 3.22 Effect of nutrient restriction and Bafilomycin treatment on spheroid formation ability of Caco-2 cells in 3D culture.

B

After Passaging

Nutrient-Rich Vehicle		
Nutrient-Rich Bafilomycin A1		
Nutrient-Restricted Vehicle		
Nutrient-Restricted Bafilomycin A1		
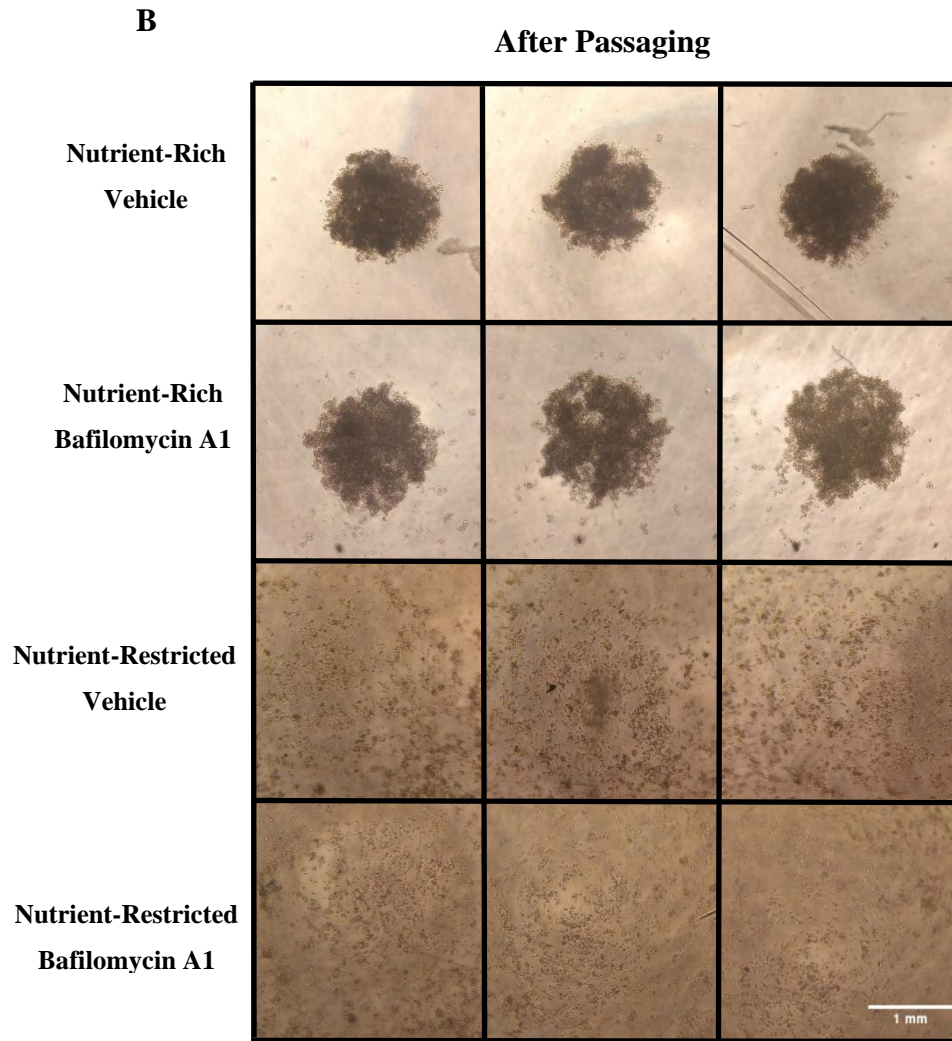
Figure 3.22 (cont'd) Effect of nutrient restriction and Bafilomycin treatment on spheroid formation ability of Caco-2 cells in 3D culture.

Nutrient-rich and restricted cells with or without Bafilomycin were plated at a density of 50,000 cells per well in an ultra-low attachment 96-well plate and allowed to form spheroids for 96h (A). In addition, cells were plated at a density of 50.000 cells/well with complete medium, allowed to form spheroids for 48 h, then collected and re-suspended in nutrient-rich and restricted medium with or without Bafilomycin and incubated for additional 48 h (B). Cells were imaged with as inverted light microscope at 4X magnification at the end of the incubation period. 3 technical replicates from each treatment were given. Figures are representative of 2 biological replicates.

To evaluate whether the loss of cell-cell interaction observed in the 3D cultured nutrient restricted cells after passaging, we collected the cells and isolated RNA for gene expression analysis (Fig 3.23). We observed that the 3D cultured and passaged nutrient-restricted Caco-2 cells showed higher expression of both epithelial and mesenchymal markers compared to the spheroids grown in complete medium; the expression of the markers was even higher when the NR cells were also treated with Baf. Thus, the partial EMT phenotype was activated in the NR cells when grown in 3D culture and this phenotype was more pronounced when Baf was added (Fig 3.23).
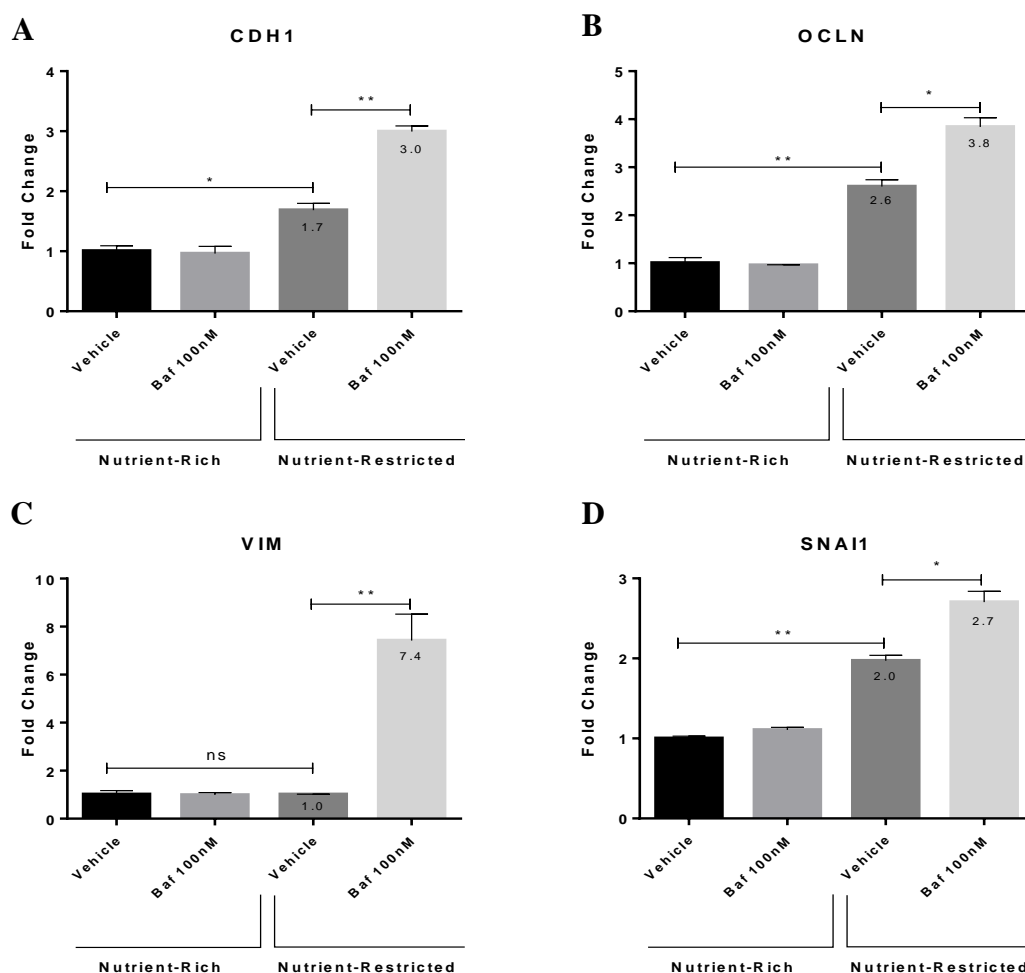
Figure 3.23 Change in epithelial and mesenchymal markers in nutrient restricted and Bafilomycin treated Caco-2 spheroids in 3D culture.

Fig 3.23 (cont'd) *The change in both epithelial (E-cadherin, Occludin) and mesenchymal (Vimentin, Snai1) markers after passaging spheroids incubated in nutrient-rich and restricted medium with or without Bafilomycin in 3D culture was analyzed with qRT-PCR. The fold change in the expression of the markers was calculated compared to nutrient-rich cells and normalized to geometric mean of reference genes ß-actin and B2M. Data is representative of 2 biological replicates. Bars represent mean ± SEM. *p<0.05, **p<0.01, ns: non-significant. CDH1: E-cadherin, OCLN: Occludin, VIM: Vimentin, SNAI1: Snai1*

The data with 3D culture further confirms the results obtained in 2D culture that Caco-2 cells were more epithelial under nutrient-rich conditions. The phenotype was shifted to more mesenchymal one through acquisition of partial EMT phenotype when cells were cultured under nutrient restriction and further exacerbated after NR+Baf treatment.

CHAPTER 4

DISCUSSION

The Caco-2 cell line has been widely used as a model for intestinal differentiation (Sambuy et al., 2005). These cells are able to undergo spontaneous differentiation in culture upon reaching 100% confluency. We have confirmed this finding and showed that when cultured for 20 days after confluency, Caco-2 cells acquired morphological (Fig 3.1) and functional (Fig 3.2) enterocyte-like features such as formation of tight junction-mediated dome structures, increased alkaline phosphatase activity, and increased expression of the differentiation markers sucrase isomaltase and CEA. Trans epithelial electrical impedance measurement in real time revealed the presence of tight junctions (TJ) in differentiated Caco-2 cells, as disruption with 6% EtOH lead to rapid and dramatic decrease in the impedance (Fig 3.3B). We did not observe such a dramatic change in impedance upon treatment with Ca^{2+} chelator EDTA although it affected the levels of adherens junction (AJ) protein E-cadherin (Fig 3.3C). Instead, EDTA treatment led to a delayed and mild decrease in impedance (Fig 3.3B). Although calcium ions do not directly regulate the function of TJ proteins, the formation of AJ is important for the assembly of TJ proteins on the surface (Hartsock & Nelson, 2008). In accordance with this observation, a study with differentiated T84 CRC cells showed that calcium depletion led to rapid internalization of AJ components, while TJ proteins were first disorganized and internalized at later time points (Ivanov, McCall, Parkos, & Nusrat, 2004). Therefore, considering the temporal effect of calcium depletion on TJ proteins, we can conclude that our assay confirmed the formation of TJs is differentiated Caco-2 cells (Fig 3.3).

Our lab has previously reported the induction of autophagy in spontaneously differentiating Caco-2 cells (Tunçer & Banerjee, 2019; Tunçer et al., 2020), and was corroborated in my thesis. Although autophagy can be activated through a number

of different stimuli and stresses, a basal level of autophagy is maintained in many cell types to regulate homeostasis (Ravanan et al., 2017). Autophagy is of particular importance during differentiation, in order to serve as a quality control mechanism for proteins and organelles that needs to be delicately regulated to implement the rapid changes in this process (Di Bartolomeo, Latella, Zarbalis, & Di Sano, 2021). We confirmed the induction of autophagy and the presence of a functional autophagic flux in spontaneously differentiated Caco-2 cells (Fig 3.4).

Cancer cells are often exposed to nutrient and oxygen deprivation, either due to their more "arid" location at the center of the tumor or when the vasculature is inadequate to ensure blood supply. Despite such shortcomings, cells in such "arid" regions continue to survive and proliferate (Liu & Ryan, 2012). One mechanism that may help the cells survive is autophagy (Degenhardt et al., 2006). Thus, in this study, using the Caco-2 colorectal cancer cell line as a model, the mechanisms of survival in the presence of reduced levels of the three main energy sources glucose, glutamine and serum were examined. The pathways evaluated were autophagy, along with cellular proliferation, sensitivity to chemotherapy drugs and acquisition of an EMT phenotype.

The starvation protocols in the literature generally depend on the complete or partial removal of nutrients including, glucose, serum, amino acids alone or in combinations. Induction of autophagy has previously been reported in a number CRC cell lines in response to serum, glucose or glutamine deprivation (Conacci-Sorrell et al., 2014; Sato et al., 2007). My study showed for the first time that culture of Caco-2 cells with limiting amounts of glucose, glutamine and serum could also activate autophagy (Fig 3.8). Such a medium restricts the availability of energy not only from glycolysis but also compromises the efficiency of the TCA cycle by preventing glutamine or serum induced anaplerosis (Dey, Kimmelman, & Depinho, 2021). The presence of low amounts of glucose, however, was likely to protect the cells from oxidative stress induced cell death (Endo, Owada, Inagaki, Shida, & Tatemichi, 2018).

The mTOR pathway acts as a sensor for nutrient availability in the cell, enabling protein translation and cell growth when appropriate nutrients are available. Upstream signaling to mTORC1 includes growth factor stimulation of cell surface receptor kinases and the activation of signaling pathways such as RAS/ERK and PI3K/AKT (Russell, Yuan, & Guan, 2014). ERK inhibition was shown to promote autophagy through AMPK activation and concomitant mTORC1 inhibition (Bryant et al., 2019). In addition to modulation of mTORC1 activity through inhibition of TSC1/2 complex, AKT also regulates autophagy through Beclin-1 activation (R. C. Wang et al., 2012). We demonstrated that the treatment of Caco-2 cells with the optimized nutrient restriction medium resulted in time-dependent activation of AMPK through phosphorylation at the Thr172 residue, and inhibition of mTORC1 activity (Fig 3.11). Under nutrient restriction, both signaling changes are necessary to activate autophagy (Laplante & Sabatini, 2012).

A time-course study of nutrient restriction showed that the level of autophagosome-associated lapidated LC3-II proteins increased, while the level of phosphorylated RPS6 (S235/236) was decreased in a temporal manner, again indicating the activation of autophagy. Of note, although autophagy was robustly induced with this nutrient restricted medium, the level of endo-lysosomal proteins remained steady and high through the duration of starvation (Fig 3.11). We also showed that replenishment of the starvation medium individually could not reverse these observations, suggesting that all three sources of carbon (glucose, glutamine and serum) were necessary to reverse the induction of autophagy (Fig 3.12).

Nutrient restriction is known to drive lysosomal biogenesis through the master transcription factor, TFEB (Szabo & Bala, 2018). TFEB is translocated to the nucleus upon nutrient stress and increases the expression of its autophagosomal and lysosomal targets mRNAs by direct binding to specific sites at their promoters. In starved cells, lysosome biogenesis helps to degrade macromolecules in autophagolysosomes and thereby promote cell survival (Sato et al., 2019). The presence of functional TFEB activity was observed after nutrient-restriction in Caco-2 cells along with an increase in the expression of its target genes (Fig 3.9).

Nevertheless, the completion of autophagic degradation with functional autophagic flux appeared to be slowed down in nutrient-restricted cells as indicated with high p62 levels (Fig 3.8 and 3.9) and lack of decrease in lysosomal acidity in the Lysotracker LTR assay (Fig 3.10). Of note, we observed a decrease in p62 levels in the differentiation model of Caco-2 cells indicating that this cell line does not have an impaired flux machinery (Fig 3.4).

The accumulation of autophagosome-associated LC3-II and p62 proteins might be indicative of either the enhanced autophagosome formation (robust induction of autophagy) or decreased clearance due to inhibited autophagic flux. Autophagic flux can be monitored with the use of lysosomal (autophagic flux) inhibitors (Yoshii & Mizushima, 2017). When we treated Caco-2 cells with 100 nM Bafilomycin A1 (lysosomal v-ATPase inhibitor) for 48 h, further accumulation of LC3 and p62 was observed, indicating that the flux was slowed down but not completely inhibited after nutrient-restriction. (Fig 3.10).

The metabolic rewiring in cancer cells render them vulnerable to the fluctuations in the microenvironment. Especially, nutrient availability has a great impact on the metabolism and survival of cancer cells and also influence response to chemotherapy (Muir & Vander Heiden, 2018). Autophagy, being a double-edged sword in cancer therapy, is activated in response to nutrient stress as a mechanism for survival and was reported the be involved both in the increased resistance and sensitivity to drugs (Conacci-Sorrell et al., 2014; L. Wang et al., 2018). In our study, we observed that nutrient-restricted Caco-2 cells were insensitive to chemotherapeutic drug 5-FU, compared to their nutrient-rich counterparts (Fig 3.13). Nutrient restriction (NR) resulted in slowed down metabolism (Fig 3.14A) and proliferation (Fig 3.13D), but did not decrease the viability of cells (Fig 3.14B). Even with prolonged starvation with restricted nutrients, Caco-2 cells maintained their viability; additionally, NR cells were remained viable even after 5-FU treatment (Fig 3.13D). Inhibition of lysosomal acidification with Bafilomycin A1 slowed down the metabolism (Fig 3.13C) and proliferation (Fig 3.13D), but did not reverse this insensitivity of NR cells to 5-FU (Fig 3.13A). Therefore, it can be suggested that the observed

insensitivity depends on proper lysosomal function rather than autophagy itself. The reliance of cancer cells on autophagy-independent lysosomal function has also been reported in metastatic bladder cancer cells (Morgan et al., 2018). In this study, increased sensitivity of metastatic cells to the lysosomal acidification inhibitors Chloroquine and Bafilomycin A1 was reported. On the other hand, these authors did not observe a differential sensitivity of metastatic cells to the depletion of early-stage autophagy regulators (Morgan et al., 2018). In addition, a study with various non-small cell lung cancer (NSCLC) cell lines reported the lack of correlation between the basal autophagy levels and autophagic flux inhibition and Chloroquine-mediated cytotoxicity (Van Roy & Berx, 2008). These examples emphasized function the autophagy-independent lysosomal activity in cancer cell survival.

Various mechanisms have been associated with drug resistance in cancer cells including activation of protective autophagy and epithelial-mesenchymal transition (EMT) along with other mechanisms such as decreased drug uptake, increased DNA damage repair and drug sequestration (Mansoori et al., 2017; H. C. Zheng, 2017). The link between the nutrient-restriction and EMT has been demonstrated by several studies. In order to address the underlying mechanism of how nutrient-restriction provides a survival advantage and resistance to 5-FU, we therefore have examined the activation of EMT. We observed that Caco-2 cells acquired characteristics of a partial EMT phenotype in response to nutrient-restriction via the activation of both epithelial and mesenchymal markers (Fig 3.15A). On the other hand, HCT-116 cells incubated with the same NR medium exhibited relatively epithelial phenotype (Fig 3.15B) which could explain the sensitivity of HCT-116 to 5-FU (Fig 3.14D). Of note, spontaneously differentiated Caco-2 cells showed an MET phenotype (Fig 3.15C), different from the nutrient-restricted cells. Although, both processes resulted in successful autophagy induction, they also differed in the way autophagic flux was conducted; thus, the levels of p62 decreased with differentiation (Fig 3.4) but increased with nutrient restriction (Fig 3.8). Therefore, we can speculate that the activation of reciprocal processes, EMT and MET, in those cells could be mediated through lysosome-dependent regulation.

Recent studies have shown that different degrees of EMT phenotype can occur in carcinomas including colorectal cancer (Sinha et al., 2020). Rather than the binary process of a complete transition from epithelial to a mesenchymal phenotype, these intermediate phenotypes co-express epithelial and mesenchymal markers (J. M. Lee, Dedhar, Kalluri, & Thompson, 2006). The cells with partial EMT phenotype are capable of collective migration and are generally associated with enhanced resistance to chemotherapy and poor prognosis (H. C. Zheng, 2017). Therefore, we hypothesized the activation of partial EMT as the reason behind the decreased cell viability and proliferative capacity, as well as the insensitivity to 5-FU in NR Caco-2 cells. Supporting our hypothesis, a partial EMT phenotype was observed in response to nutrient-restriction that was robustly augmented with lysosomal alkalinization with the use of Baf (Fig 3.18, NR+Baf). The NR+Baf treated cells expressed both functional and morphological characteristics of partial EMT. Thus, the expression of both epithelial and mesenchymal markers increased (Fig 3.18), and the cells gained a spindle-like morphology (Fig 3.17) with the formation of actin stress fibers (Fig 3.19). Moreover, these changes were rapidly reversible; the spindle like morphology and expression of EMT markers could be reversed within 6 h of culture in complete medium (Fig 3.20 and Fig 3.21). Of note, although single cell transcriptomic studies have revealed that partial EMT phenotype with the co-expression of epithelial and mesenchymal markers could be observable in single cell level (Puram, Parikh, & Tirosh, 2018), our current data is inadequate to establish whether each cell in the population is at the same stage of partial EMT, or whether a mixed population of cells exist, some with epithelial and some with mesenchymal characteristics.

Cancer cells undergoing autophagy and EMT are known to rewire their metabolism. The presence of a cross-talk between autophagy and EMT has been proposed (Singla & Bhattacharyya, 2017). EMT-associated proteins like Wnt, NF-κB, and TGFβ play major roles in autophagy. Moreover, an interaction between the cytoskeleton and mitochondria has been implicated in both EMT and autophagy (de Sousa Mesquita, de Araújo Lopes, Pernambuco Filho, Nader, & Lopes, 2017). However, the exact

relationship between autophagy and EMT remain undefined as treatment with the autophagy inhibitor chloroquine was shown to both activate and repress EMT (Singla & Bhattacharyya, 2017; Sinha et al., 2020). Considering the dual role of autophagy in cancer, acting both in a tumor suppressive and oncogenic manner, its effect on EMT is complex and likely dependent on the cellular context as well.

One important mechanism through which autophagy and lysosomal functioning can regulate EMT is via the selective degradation of key EMT proteins and transcription factors, mainly Twist1, Snail and ZEB1 (Gugnoni et al., 2016). These transcription factors are considered to be targets of p62. p62 is a selective autophagy-associated adaptor protein which also functions as a signaling hub for different pathways (Katsuragi et al., 2015). Through a ubiquitin-associated domain (UBA), p62 binds to polyubiquitinylated cargo and with LC3-interacting region (LIR) binding it is sequestered in autophagosomes and degraded with its cargo. Therefore, p62-mediated stabilization of EMT transcription factors has been considered as an important regulatory mechanism that can reflect the cross talk between lysosomal function and EMT.

Two recent studies showed that the autophagy inhibition induces EMT via p62-NFκB-related pathway through upregulation of EMT transcription factors ZEB1 and Snail2 (Hill et al., 2019; Y. Wang et al., 2019). In another study, the accumulation of p62 in response to growth factor-induced EMT was shown to result in the stabilization of Twist and TGF-β-Smad signaling coactivator Smad4 by attenuating their proteosomal degradation (Bertrand et al., 2015). p62-mediated stabilization and activation of Twist was shown to enhance the migratory and invasive properties of autophagy-deficient cancer cells through the activation of EMT (Qiang et al., 2014). p62 accumulation in patient specimens of intrahepatic cholangiocarcinoma (ICC) was reported to have a positive correlation with metastasis and poor prognosis (J. Chen et al., 2022). Increase in Snai1, Vimentin and N-cadherin levels and decrease in E-cadherin levels were also regulated via p62-mediated mechanism. In the same study, the involvement of dysregulated mitophagy (degradation of defective mitochondria) in this process and enhancement of EMT phenotype via p62 was also

demonstrated. Initiation of EMT in Bafilomycin treated cells that showed an accumulation of autophagosome has also been reported in noncancerous cells (G. Li et al., 2015). In podocytes, EMT was activated with introduction of lysosomal dysfunction in response to Bafilomycin, which was attributed to the accumulation of p62 and concomitant decrease in p62-phosphorylation levels via a CDK-1 dependent mechanism (G. Li et al., 2015).

On the other hand, the negative effect of lysosomal activity on the acquisition of the EMT phenotype has been supported with the observation that increased lysosomal activity and turnover contributes to increased TGF-β induced EMT (Kern, Wischnewski, Biniossek, Schilling, & Reinheckel, 2015). Use of lysosomal inhibitors resulted in a decrease in invasive properties in murine breast cancer cell lines. Taken together these observations demonstrate a complex interplay between autophagy, lysosomal function and EMT; which should be considered in a context-dependent manner. In our nutrient-restriction model with Caco-2 cells, for instance, p62 levels were increased and the levels of both epithelial and mesenchymal markers was also enhanced. On the other hand, with the differentiation model, we observed a decrease in p62 levels and an increase in the expression of epithelial but not mesenchymal markers. This may suggest the presence of shared regulators in two divergent processes, and an important association between p62 and the expression of mesenchymal markers in Caco-2 cells.

Since the data in *in vitro* two-dimensional (2D) culture strongly suggested the acquisition of partial EMT in Caco-2 cells with NR+ Baf treatment, we next evaluated whether EMT phenotype induced with NR+Baf treatment was also retained in 3D cell culture. 3D cancer models are used in cancer research since they better represent the gene expression profile, metabolic capacity, signaling mechanisms and proliferation of tumor cells *in vivo* (Stadler et al., 2016). When we cultured Caco-2 cells in anchorage-independent conditions in a 96 well ultra-low attachment (ULA) plate, we observed the formation of single spheroids with relatively non-uniform edges (Fig 3.22). In the literature, similar findings for Caco-2 cells have been reported. Stadler et al. showed that the morphology of Caco-2

spheroids resembled adenomatous cell clusters where the HCT-116 cells formed spheroids with smooth edges (Stadler et al., 2016). The effect of *TP53* mutational status on spheroid structure was also reported such that the cells having wild type *TP53* formed compact and rounded spheroids while the ones with mutant *TP53*, such as Caco-2 cells, formed spheroids that were smaller in size and with rough boundaries (Pomo, Taylor, & Gullapalli, 2016). We observed that the nutrient-rich cells could form spheroids irrespective of whether the cells were treated with Baf, suggesting that in the presence of nutrients, alkalinization of lysosomes did not affect the cell-cell interactions. However, when the cells were cultured under nutrient-restriction, the ability of Caco-2 cells to form compact spheroid structures was hindered (Fig 3.22A). Alkalinization of the lysosomes in the nutrient restricted cells resulted in a complete loss in the spheroid forming ability of Caco-2 cells; rather, the cells formed multiple small clusters instead of a single-large spheroid (Fig 3.22A). In the literature, spheroid formation assays with serum starvation have been reported. However, the culture media in such experiments are specifically designed to enrich stem cell populations (Boo et al., 2016; Goričan, Gole, & Potočnik, 2020; Herheliuk, Perepelytsina, Ugnivenko, Ostapchenko, & Sydorenko, 2019). Such stem cell enriched populations were able to form well-rounded and compact spheroids with enhanced stem cell characteristics and slower proliferation rates. Our protocol differs from these models since the medium we used was not designed to enrich the stem cell population; rather, we aimed to evaluate cell-cell interactions with the use of a nutrient restricted medium, in the presence or absence of Baf. We observed that whereas treatment of nutrient rich cells with Baf resulted in the formation of reasonably tight spheroids, the NR+Baf cells formed loose cell clusters (Fig 3.22A) most likely because of weak cell-cell adhesion.

The difference in spheroid formation between nutrient-rich and nutrient-restricted conditions was more prominent in the spheroids that were allowed to re-form after passaging. While Caco-2 cells grown in complete medium were able to reform the spheroids effectively, with no difference in the shape and tightness of the spheroids after passaging, cells grown in complete medium and treated with Baf reform

spheroids with greater transparency after passaging, indicating some loss in cell-cell interactions (Fig 3.22B). The nutrient restricted cells underwent a complete loss in spheroid forming ability after passaging both in the presence and absence of Baf, suggesting that these cells are unable to maintain cell-cell contacts. The adherence junction protein E-cadherin was suggested as the essential component in multicellular spheroid formation (Van Roy & Berx, 2008). The variations in the cell adhesion properties including E-cadherin levels have been associated with the alterations in the spheroid forming ability of various cancer cell lines causing the formation of either more compact or loose spheroids (Lin, Chou, Chien, & Chang, 2006; Pomo et al., 2016; Schmidt, Scholz, Polednik, & Roller, 2016; Shimazui et al., 2004).

Similar to the data we obtained with 2D culture, we observed that the 3D-cultured and passaged nutrient-restricted Caco-2 cells showed higher expression of both epithelial and mesenchymal markers compared to the spheroids grown in complete medium; and this phenotype became more pronounced when Baf was introduced (Fig 3.23). In accordance with our observations, a recent study with CRC cell lines demonstrated the importance of the cell-cell adhesion in spheroid formation (Stadler et al., 2018). These authors observed that all the tested cell lines formed spheroids; however, some of the single cells could be separated from compact structures. When these single cells were cultured separately, they expressed decreased levels of cell-cell adhesion protein. Moreover, enrichment of this non-spheroid forming single cell population resulted in complete loss of spheroid forming capacity and was associated with enhanced migratory and invasive properties (Stadler et al., 2018). Considering the data in the literature and our observation, the changes in the composition of cell-cell and cell-matrix adhesion proteins with NR+Baf treatment could be considered as the reason behind the loss in spheroid forming ability.

CHAPTER 5

CONCLUSION AND FUTURE STUDIES

The primary finding of this thesis study are as follows:

1- Caco-2 cells grown in a nutrient restricted (NR) medium containing 1% fetal bovine serum (FBS), 0.2 mM glutamine and 0.1 g/L glucose expressed several markers for autophagy. A time-dependent decrease in the phosphorylation of RPS6 and P70S6K levels indicated inactivation of the mTOR pathway and a concomitant activation of AMPK, along with an increase in LC3-II levels which are all indicative of nutrient stress (Kim et al., 2011). However, the autophagic flux appeared to be rather slow as the cells cultured under NR exhibited steady level of endo-lysosomal proteins, no alterations in lysosomal acidity was observed and an increase in the protein levels of the adaptor protein p62 was observed.

2- Our lab previously reported the induction of autophagy in spontaneously differentiating Caco-2 cells (Tunçer & Banerjee, 2019; Tunçer et al., 2020). In accordance with this observation, my data also confirmed the autophagy induction in spontaneously differentiated Caco-2 cells. Different from the stress response observed with NR, differentiated Caco-2 cells showed a robust activation of autophagic markers and a functional autophagic flux. In addition, spontaneously differentiated Caco-2 showed the presence of more epithelial rather than mesenchymal characteristics. It is therefore highly likely that complex and well-coordinated opposite signaling pathways are activated in cells undergoing nutrient restriction and differentiation.

3- Restriction of the main energy sources slowed down the metabolism of the Caco-2 cells and resulted in decreased proliferation. However, even with the prolonged starvation, Caco-2 cells sustained their viability and exhibited a systemic resistance to the chemotherapeutic drug 5-FU. Induction of partial

EMT phenotype was observed in Caco-2 cells grown under NR, which could explain this drug insensitivity. On the other hand, nutrient-restricted HCT-116 cells were more responsive to chemotherapeutic drugs, most likely because they did not undergo partial EMT. These data suggest that cells that are grown in more "arid" regions of tumors may be responsive to chemotherapy drugs if they do not undergo partial EMT, suggesting the presence of clinical relevance in our data.

4- The expression of partial EMT markers were further augmented and the formation of actin stress fibers were observed when lysosomal acidification was inhibited with Bafilomycin A1 (Mauvezin & Neufeld, 2015) in cells grown under NR. Cells in NR+Baf medium gained spindle-like shape while the cells in nutrient-rich medium had the usual cobblestone-like morphology. Moreover, the partial EMT phenotype acquired in response to NR+Baf treatment was highly dynamic and reversible within 6 h of replacement with complete medium as shown by decrease in the expression of partial EMT markers and the reversal of morphology. Caco-2 cells maintained their viability even when autophagic flux (lysosomal acidification) was inhibited with Baf. Moreover, NR+Baf cells still exhibited insensitivity to 5-FU. These observations suggest that rather than the autophagy induction itself, the inhibition of autophagic flux, perhaps via the accumulation of p62, could be implicated in the development of partial EMT and lower drug sensitivity in Caco-2 cells.

5- Culture of Caco-2 cells in 3D could further confirm the results obtained in 2D that Caco-2 cells were more epithelial under nutrient-rich conditions. The cell-cell adhesion properties and hence the spheroid forming capacity of the cells remained unchanged under nutrient rich conditions whether lysosomal alkalinization occurred or not; however, a loss of spheroid forming ability was seen in NR cells that was remarkably exacerbated with NR+Baf treatment. These observations suggest that the phenotype was shifted to more

mesenchymal one through acquisition of partial EMT phenotype upon lysosomal alkalinization with Bafilomycin in cells grown under NR.

Overall, this study showed for the first time that culture of Caco-2 cells with limiting amounts of glucose, glutamine and serum could activate partial EMT, which was further exacerbated when lysosomal acidification was perturbed. These data suggest that in addition to a critical role of the lysosome in the orchestration of nutrient sensing via the localization of the nutrient sensors mTOR and AMPK (Napolitano et al., 2018), it can also play a critical role in EMT, particularly in cells under nutrient stress. The induction of partial EMT in cells grown under nutrient restriction and lysosomal alkalinization could also be implicated in reduced sensitivity of the cells to 5-FU, suggesting the presence of clinical relevance in our observations.

Although our findings are of interest, several unanswered questions remain that need to be addressed. Future experiments that can be conducted to better substantiate the findings of this thesis are as follows:

1- In order to further characterize the functional consequences of partial EMT phenotype, migratory and invasive properties of NR+Baf treated Caco-2 cells could be evaluated.

2- The effect of Bafilomycin can be analyzed in spontaneously differentiated Caco-2 cells which exhibit a functional autophagy flux, in order to better elaborate the role of lysosomal alkalinization in acquisition of partial EMT phenotype.

3- Increasing evidence suggest that p62-mediated stabilization of key EMT transcription factors and EMT proteins could be the mechanism behind the lysosomal-alkalinization-induced EMT (Bertrand et al., 2015; Kern et al., 2015; G. Li et al., 2015). In order to better understand whether an increase in p62 the mechanism by which Caco-2 cells was gained partial EMT

phenotype in response to NR+Baf, the levels of EMT markers could be analyzed after the silencing of p62 in these cells.

REFERENCES

Ahmadiankia, N. (2020). In vitro and in vivo studies of cancer cell behavior under nutrient deprivation. *Cell Biology International*, *44*(8), 1588–1597. https://doi.org/10.1002/cbin.11368

Ahmed, D., Eide, P. W., Eilertsen, I. A., Danielsen, S. A., Eknæs, M., Hektoen, M., … Lothe, R. A. (2013). Epigenetic and genetic features of 24 colon cancer cell lines. *Oncogenesis*, *2*(2). https://doi.org/10.1038/oncsis.2013.35

Akkoc, Y., & Gozuacik, D. (2020). MicroRNAs as major regulators of the autophagy pathway. *Biochimica et Biophysica Acta - Molecular Cell Research*, Vol. 1867. https://doi.org/10.1016/j.bbamcr.2020.118662

Amaravadi, R. K., Kimmelman, A. C., & Debnath, J. (2019). Targeting autophagy in cancer: Recent advances and future directions. *Cancer Discovery*, Vol. 9, pp. 1167–1181. https://doi.org/10.1158/2159-8290.CD-19-0292

Astarci, E., Sade, A., Çimen, I., Savaş, B., & Banerjee, S. (2012). The NF-κB target genes ICAM-1 and VCAM-1 are differentially regulated during spontaneous differentiation of Caco-2 cells. *FEBS Journal*, *279*(16), 2966–2986. https://doi.org/10.1111/j.1742-4658.2012.08677.x

Baghban, R., Roshangar, L., Jahanban-Esfahlan, R., Seidi, K., Ebrahimi-Kalan, A., Jaymand, M., … Zare, P. (2020, April 7). Tumor microenvironment complexity and therapeutic implications at a glance. *Cell Communication and Signaling*, Vol. 18, pp. 1–19. https://doi.org/10.1186/s12964-020-0530-4

Bertrand, M., Petit, V., Jain, A., Amsellem, R., Johansen, T., Larue, L., … Beau, I. (2015). SQSTM1/p62 regulates the expression of junctional proteins through epithelialmesenchymal transition factors. *Cell Cycle*, *14*(3), 364–374. https://doi.org/10.4161/15384101.2014.987619

Boo, L., Ho, W. Y., Ali, N. M., Yeap, S. K., Ky, H., Chan, K. G., … Cheong, S. K.

(2016). MiRNA transcriptome profiling of spheroid-enriched cells with cancer stem cell properties in human breast MCF-7 cell line. *International Journal of Biological Sciences*, *12*(4), 427–445. https://doi.org/10.7150/ijbs.12777

Bose, S., Allen, A. E., & Locasale, J. W. (2020). The Molecular Link from Diet to Cancer Cell Metabolism. *Molecular Cell*, *78*(6), 1034–1044. https://doi.org/10.1016/j.molcel.2020.05.018

Brattain MG, Fine WD, Khaled FM, Thompson J, B. D. (1981). Heterogeneity of malignant cells from a human colonic carcinoma. *Cancer Research*, *41*(5), 1751–1756.

Bryant, K. L., Stalnecker, C. A., Zeitouni, D., Klomp, J. E., Peng, S., Tikunov, A. P., … Der, C. J. (2019). Combination of ERK and autophagy inhibition as a treatment approach for pancreatic cancer. *Nature Medicine*, *25*(4), 628–640. https://doi.org/10.1038/s41591-019-0368-8

Chakraborty, A., Bodipati, N., Demonacos, M. K., Peddinti, R., Ghosh, K., & Roy, P. (2012). Long term induction by pterostilbene results in autophagy and cellular differentiation in MCF-7 cells via ROS dependent pathway. *Molecular and Cellular Endocrinology*, *355*(1), 25–40. https://doi.org/10.1016/j.mce.2012.01.009

Chen, J., Gao, Z., Li, X., Shi, Y., Tang, Z., Liu, W., … Ding, Z. (2022). SQSTM1/p62 in intrahepatic cholangiocarcinoma promotes tumor progression via epithelial-mesenchymal transition and mitochondrial function maintenance. *Cancer Medicine*. https://doi.org/10.1002/CAM4.4908

Chen, Y., Zhang, J., Lin, Y., Lei, Q., Guan, K. L., Zhao, S., & Xiong, Y. (2011). Tumour suppressor SIRT3 deacetylates and activates manganese superoxide dismutase to scavenge ROS. *EMBO Reports*, *12*(6), 534. https://doi.org/10.1038/EMBOR.2011.65

Chung, C. Y. S., Shin, H. R., Berdan, C. A., Ford, B., Ward, C. C., Olzmann, J. A., … Nomura, D. K. (2019). Covalent targeting of the vacuolar H+-ATPase

activates autophagy via mTORC1 inhibition. *Nature Chemical Biology*, *15*(8), 776–785. https://doi.org/10.1038/s41589-019-0308-4

Comito, G., Ippolito, L., Chiarugi, P., & Cirri, P. (2020, March 24). Nutritional Exchanges Within Tumor Microenvironment: Impact for Cancer Aggressiveness. *Frontiers in Oncology*, Vol. 10, p. 396. https://doi.org/10.3389/fonc.2020.00396

Conacci-Sorrell, M., Ngouenet, C., Anderson, S., Brabletz, T., & Eisenman, R. N. (2014). Stress-induced cleavage of Myc promotes cancer cell survival. *Genes and Development*, *28*(7), 689–707. https://doi.org/10.1101/gad.231894.113

Crane, A. M., & Bhattacharya, S. K. (2013). The use of bromodeoxyuridine incorporation assays to assess corneal stem cell proliferation. *Methods in Molecular Biology*, *1014*, 65–70. https://doi.org/10.1007/978-1-62703-432-6_4

Das, S., Becker, B. N., Hoffmann, F. M., & Mertz, J. E. (2009). Complete reversal of epithelial to mesenchymal transition requires inhibition of both ZEB expression and the Rho pathway. *BMC Cell Biology*, *10*(1), 1–18. https://doi.org/10.1186/1471-2121-10-94

De Both, N. J., Vermey, M., Dinjens, W. N., & Bosman, F. T. (1999). A comparative evaluation of various invasion assays testing colon carcinoma cell lines. *British Journal of Cancer*, *81*(6), 934–941. https://doi.org/10.1038/sj.bjc.6690790

de Sousa Mesquita, A. P., de Araújo Lopes, S., Pernambuco Filho, P. C. A., Nader, H. B., & Lopes, C. C. (2017). Acquisition of anoikis resistance promotes alterations in the Ras/ERK and PI3K/Akt signaling pathways and matrix remodeling in endothelial cells. *Apoptosis*, *22*(9), 1116–1137. https://doi.org/10.1007/s10495-017-1392-0

Degenhardt, K., Mathew, R., Beaudoin, B., Bray, K., Anderson, D., Chen, G., … White, E. (2006). Autophagy promotes tumor cell survival and restricts

necrosis, inflammation, and tumorigenesis. *Cancer Cell*, *10*(1), 51–64. https://doi.org/10.1016/j.ccr.2006.06.001

Devriese, S., Van den Bossche, L., Van Welden, S., Holvoet, T., Pinheiro, I., Hindryckx, P., … Laukens, D. (2017). T84 monolayers are superior to Caco-2 as a model system of colonocytes. *Histochemistry and Cell Biology*, *148*(1), 85–93. https://doi.org/10.1007/s00418-017-1539-7

Dey, P., Kimmelman, A. C., & Depinho, R. A. (2021). Metabolic codependencies in the tumor microenvironment. *Cancer Discovery*, *11*(5), 1067–1081. https://doi.org/10.1158/2159-8290.CD-20-1211

Di Bartolomeo, S., Latella, L., Zarbalis, K., & Di Sano, F. (2021). Editorial: Autophagy in Mammalian Development and Differentiation. *Frontiers in Cell and Developmental Biology*, Vol. 9, p. 722821. https://doi.org/10.3389/fcell.2021.722821

Ding, Q. M., Ko, T. C., & Mark Evers, B. (1998). Caco-2 intestinal cell differentiation is associated with G1 arrest and suppression of CDK2 and CDK4. *The American Journal of Physiology*, *275*(5). https://doi.org/10.1152/AJPCELL.1998.275.5.C1193

Endo, H., Owada, S., Inagaki, Y., Shida, Y., & Tatemichi, M. (2018). Glucose starvation induces LKB1-AMPK-mediated MMP-9 expression in cancer cells. *Scientific Reports*, *8*(1), 1–16. https://doi.org/10.1038/s41598-018-28074-w

Fantini, J., Abadie, B., & Tirard, A. (1986). Spontaneous and induced dome formation by two clonal cell populations derived from a human adenocarcinoma cell line, HT29. *Journal of Cell Science*, *VOL. 83*, 235–249. https://doi.org/10.1242/jcs.83.1.235

Gehart, H., & Clevers, H. (2019, January 1). Tales from the crypt: new insights into intestinal stem cells. *Nature Reviews Gastroenterology and Hepatology*, Vol. 16, pp. 19–34. https://doi.org/10.1038/s41575-018-0081-y

González, A., Hall, M. N., Lin, S. C., & Hardie, D. G. (2020, March 3). AMPK and TOR: The Yin and Yang of Cellular Nutrient Sensing and Growth Control. *Cell Metabolism*, Vol. 31, pp. 472–492. https://doi.org/10.1016/j.cmet.2020.01.015

Goričan, L., Gole, B., & Potočnik, U. (2020). Head and Neck Cancer Stem Cell-Enriched Spheroid Model for Anticancer Compound Screening. *Cells*, *9*(7). https://doi.org/10.3390/cells9071707

Gozuacik, D., Akkoc, Y., Ozturk, D. G., & Kocak, M. (2017). Autophagy-Regulating microRNAs and Cancer. *Frontiers in Oncology*, *7*, 1. https://doi.org/10.3389/fonc.2017.00065

Gugnoni, M., Sancisi, V., Manzotti, G., Gandolfi, G., & Ciarrocchi, A. (2016). Autophagy and epithelial–mesenchymal transition: An intricate interplay in cancer. *Cell Death and Disease*, Vol. 7. https://doi.org/10.1038/cddis.2016.415

Gwinn, D. M., Shackelford, D. B., Egan, D. F., Mihaylova, M. M., Mery, A., Vasquez, D. S., … Shaw, R. J. (2008). AMPK Phosphorylation of Raptor Mediates a Metabolic Checkpoint. *Molecular Cell*, *30*(2), 214–226. https://doi.org/10.1016/j.molcel.2008.03.003

Harris, A. R., Daeden, A., & Charras, G. T. (2014). Formation of adherens junctions leads to the emergence of a tissue-level tension in epithelial monolayers. *Journal of Cell Science*, *127*(11), 2507–2517. https://doi.org/10.1242/jcs.142349

Hartsock, A., & Nelson, W. J. (2008). Adherens and tight junctions: Structure, function and connections to the actin cytoskeleton. *Biochimica et Biophysica Acta - Biomembranes*, Vol. 1778, pp. 660–669. https://doi.org/10.1016/j.bbamem.2007.07.012

Hensley, C. T., Wasti, A. T., & DeBerardinis, R. J. (2013). Glutamine and cancer: Cell biology, physiology, and clinical opportunities. *Journal of Clinical*

Investigation, Vol. 123, pp. 3678–3684. https://doi.org/10.1172/JCI69600

Herheliuk, T., Perepelytsina, O., Ugnivenko, A., Ostapchenko, L., & Sydorenko, M. (2019). Investigation of multicellular tumor spheroids enriched for a cancer stem cell phenotype. *Stem Cell Investigation*, *6*(August). https://doi.org/10.21037/sci.2019.06.07

Hettmer, S., Schinzel, A. C., Tchessalova, D., Schneider, M., Parker, C. L., Bronson, R. T., … Wagers, A. J. (2015). Functional genomic screening reveals asparagine dependence as a metabolic vulnerability in sarcoma. *ELife*, *4*(OCTOBER2015). https://doi.org/10.7554/eLife.09436

Hill, C., Li, J., Liu, D., Conforti, F., Brereton, C. J., Yao, L., … Wang, Y. (2019). Autophagy inhibition-mediated epithelial–mesenchymal transition augments local myofibroblast differentiation in pulmonary fibrosis. *Cell Death and Disease*, *10*(8), 1–11. https://doi.org/10.1038/s41419-019-1820-x

Hill, C., & Wang, Y. (2020). The importance of epithelial-mesenchymal transition and autophagy in cancer drug resistance. *Cancer Drug Resistance*, *3*(1), 38–47. https://doi.org/10.20517/cdr.2019.75

Hofmann, C., Obermeier, F., Artinger, M., Hausmann, M., Falk, W., Schoelmerich, J., … Grossmann, J. (2007). Cell-Cell Contacts Prevent Anoikis in Primary Human Colonic Epithelial Cells. *Gastroenterology*, *132*(2), 587–600. https://doi.org/10.1053/j.gastro.2006.11.017

Hu, Y. L., Yin, Y., Liu, H. Y., Feng, Y. Y., Bian, Z. H., Zhou, L. Y., … Huang, Z. H. (2016). Glucose deprivation induces chemoresistance in colorectal cancer cells by increasing ATF4 expression. *World Journal of Gastroenterology*, *22*(27), 6235–6245. https://doi.org/10.3748/wjg.v22.i27.6235

Huang, Y., Fu, Z., Dong, W., Zhang, Z., Mu, J., & Zhang, J. (2018). Serum starvation-induces down-regulation of Bcl-2/Bax confers apoptosis in tongue coating-related cells in vitro. *Molecular Medicine Reports*, *17*(4), 5057–5064. https://doi.org/10.3892/mmr.2018.8512

Inoki, K., Zhu, T., & Guan, K.-L. (2003). TSC2 mediates cellular energy response to control cell growth and survival. *Cell*, *115*(5), 577–590. https://doi.org/10.1016/s0092-8674(03)00929-2

Ivanov, A. I., McCall, I. C., Parkos, C. A., & Nusrat, A. (2004). Role for Actin Filament Turnover and a Myosin II Motor in Cytoskeleton-driven Disassembly of the Epithelial Apical Junctional Complex. *Molecular Biology of the Cell*, *15*(6), 2639. https://doi.org/10.1091/MBC.E04-02-0163

Jin, K., Ewton, D. Z., Park, S., Hu, J., & Friedman, E. (2009). Mirk regulates the exit of colon cancer cells from quiescence. *Journal of Biological Chemistry*, *284*(34), 22916–22925. https://doi.org/10.1074/jbc.M109.035519

Kanarek, N., Petrova, B., & Sabatini, D. M. (2020). Dietary modifications for enhanced cancer therapy. *Nature*, *579*(7800), 507–517. https://doi.org/10.1038/s41586-020-2124-0

Katsuragi, Y., Ichimura, Y., & Komatsu, M. (2015). P62/SQSTM1 functions as a signaling hub and an autophagy adaptor. *FEBS Journal*, *282*(24), 4672–4678. https://doi.org/10.1111/febs.13540

Kenific, C. M., & Debnath, J. (2015). Cellular and metabolic functions for autophagy in cancer cells. *Trends in Cell Biology*, *25*(1), 37–45. https://doi.org/10.1016/J.TCB.2014.09.001

Kern, U., Wischnewski, V., Biniossek, M. L., Schilling, O., & Reinheckel, T. (2015). Lysosomal protein turnover contributes to the acquisition of TGFβ-1 induced invasive properties of mammary cancer cells. *Molecular Cancer*, *14*(1), 1–17. https://doi.org/10.1186/s12943-015-0313-5

Kim, J., Kundu, M., Viollet, B., & Guan, K.-L. (2011). AMPK and mTOR regulate autophagy through direct phosphorylation of Ulk1. *Nature Cell Biology*, *13*(2), 132–141. https://doi.org/10.1038/ncb2152

Knott, S. R. V., Wagenblast, E., Khan, S., Kim, S. Y., Soto, M., Wagner, M., …

Hannon, G. J. (2018). Asparagine bioavailability governs metastasis in a model of breast cancer. *Nature*, *554*(7692), 378–381. https://doi.org/10.1038/nature25465

Kocaturk, N. M., Akkoc, Y., Kig, C., Bayraktar, O., Gozuacik, D., & Kutlu, O. (2019). Autophagy as a molecular target for cancer treatment. *European Journal of Pharmaceutical Sciences*, *134*(September 2018), 116–137. https://doi.org/10.1016/j.ejps.2019.04.011

Langan, T. J., Rodgers, K. R., & Chou, R. C. (2016). Synchronization of mammalian cell cultures by serum deprivation. In *Methods in Molecular Biology* (Vol. 1524, pp. 97–105). https://doi.org/10.1007/978-1-4939-6603-5_6

Lee, J. M., Dedhar, S., Kalluri, R., & Thompson, E. W. (2006, March 3). The epithelial-mesenchymal transition: New insights in signaling, development, and disease. *Journal of Cell Biology*, Vol. 172, pp. 973–981. https://doi.org/10.1083/jcb.200601018

Lee, S. H., Jung, Y. S., Chung, J. Y., Oh, A. Y., Lee, S. J., Choi, D. H., … Park, B. J. (2011). Novel tumor suppressive function of Smad4 in serum starvation-induced cell death through PAK1-PUMA pathway. *Cell Death and Disease*, *2*(12). https://doi.org/10.1038/cddis.2011.116

Levin, V. A., Panchabhai, S. C., Shen, L., Kornblau, S. M., Qiu, Y., & Baggerly, K. A. (2010). Different Changes in Protein and Phosphoprotein Levels Result from Serum Starvation of High-Grade Glioma and Adenocarcinoma Cell Lines NIH Public Access. *J Proteome Res*, *9*(1), 179–191. https://doi.org/10.1021/pr900392b

Levine, B., & Kroemer, G. (2019). Biological Functions of Autophagy Genes: A Disease Perspective. *Cell*, *176*(1–2), 11–42. https://doi.org/10.1016/J.CELL.2018.09.048

Levine, B., Mizushima, N., & Virgin, H. W. (2011, January 20). Autophagy in

immunity and inflammation. *Nature*, Vol. 469, pp. 323–335.
https://doi.org/10.1038/nature09782

Li, C., Jung, S., Lee, S., Jeong, D., Yang, Y., Kim, K. Il, … Lee, M. S. (2015).
Nutrient/serum starvation derived TRIP-Br3 down-regulation accelerates
apoptosis by destabilizing XIAP. *Oncotarget*, *6*(10), 7522–7535.
https://doi.org/10.18632/oncotarget.3112

Li, G., Li, C. X., Xia, M., Ritter, J. K., Gehr, T. W. B., Boini, K., & Li, P. L.
(2015). Enhanced epithelial-to-mesenchymal transition associated with
lysosome dysfunction in podocytes: Role of p62/sequestosome 1 as a
signaling hub. *Cellular Physiology and Biochemistry*, *35*(5), 1773–1786.
https://doi.org/10.1159/000373989

Li, Jiaqi, Eu, J. Q., Kong, L. R., Wang, L., Lim, Y. C., Goh, B. C., & Wong, A. L.
A. (2020). Targeting metabolism in cancer cells and the tumour
microenvironment for cancer therapy. *Molecules*, Vol. 25.
https://doi.org/10.3390/molecules25204831

Li, Jun, Yang, B., Zhou, Q., Wu, Y., Shang, D., Guo, Y., … Xiong, J. (2013).
Autophagy promotes hepatocellular carcinoma cell invasion through
activation of epithelial-mesenchymal transition. *Carcinogenesis*, *34*(6), 1343–
1351. https://doi.org/10.1093/carcin/bgt063

Liberti, M. V., & Locasale, J. W. (2016). The Warburg Effect: How Does it Benefit
Cancer Cells? *Trends in Biochemical Sciences*, *41*(3), 211–218.
https://doi.org/10.1016/J.TIBS.2015.12.001

Lin, R. Z., Chou, L. F., Chien, C. C. M., & Chang, H. Y. (2006). Dynamic analysis
of hepatoma spheroid formation: Roles of E-cadherin and β1-integrin. *Cell
and Tissue Research*, *324*(3), 411–422. https://doi.org/10.1007/s00441-005-
0148-2

Liu, E. Y., & Ryan, K. M. (2012). Autophagy and cancer - issues we need to
digest. *Journal of Cell Science*, *125*(10), 2349–2358.

https://doi.org/10.1242/jcs.093708

Maddocks, O. D. K., Athineos, D., Cheung, E. C., Lee, P., Zhang, T., Van Den Broek, N. J. F., … Vousden, K. H. (2017). Modulating the therapeutic response of tumours to dietary serine and glycine starvation. *Nature*, *544*(7650), 372–376. https://doi.org/10.1038/nature22056

Mansoori, B., Mohammadi, A., Davudian, S., Shirjang, S., & Baradaran, B. (2017). The Different Mechanisms of Cancer Drug Resistance: A Brief Review. *Advanced Pharmaceutical Bulletin*, *7*(3), 339. https://doi.org/10.15171/APB.2017.041

Mauvezin, C., & Neufeld, T. P. (2015). Bafilomycin A1 disrupts autophagic flux by inhibiting both V-ATPase-dependent acidification and Ca-P60A/SERCA-dependent autophagosome-lysosome fusion. *Autophagy*, *11*(8), 1437–1438. https://doi.org/10.1080/15548627.2015.1066957

McKay, L. K., & White, J. P. (2021). The ampk/p27kip1 pathway as a novel target to promote autophagy and resilience in aged cells. *Cells*, Vol. 10. https://doi.org/10.3390/cells10061430

Mihaylova, M. M., & Shaw, R. J. (2011, September). The AMPK signalling pathway coordinates cell growth, autophagy and metabolism. *Nature Cell Biology*, Vol. 13, pp. 1016–1023. https://doi.org/10.1038/ncb2329

Miyo, M., Konno, M., Nishida, N., Sueda, T., Noguchi, K., Matsui, H., … Ishii, H. (2016). Metabolic Adaptation to Nutritional Stress in Human Colorectal Cancer. *Scientific Reports*, *6*(1), 1–13. https://doi.org/10.1038/srep38415

Morgan, M. J., Fitzwalter, B. E., Owens, C. R., Powers, R. K., Sottnik, J. L., Gamez, G., … Thorburn, A. (2018). Metastatic cells are preferentially vulnerable to lysosomal inhibition. *Proceedings of the National Academy of Sciences of the United States of America*, Vol. 115, pp. E8479–E8488. https://doi.org/10.1073/pnas.1706526115

Muir, A., & Vander Heiden, M. G. (2018). The nutrient environment affects therapy Nutrient availability affects cancer cell metabolism and therapeutic responses. *Science*, *360*(6392), 962–963. https://doi.org/10.1126/science.aar5986

Napolitano, G., Esposito, A., Choi, H., Matarese, M., Benedetti, V., Di Malta, C., … Ballabio, A. (2018). mTOR-dependent phosphorylation controls TFEB nuclear export. *Nature Communications*, *9*(1). https://doi.org/10.1038/s41467-018-05862-6

Naveed, S., Aslam, M., & Ahmad, A. (2014). Starvation based differential chemotherapy: A novel approach for cancer treatment. *Oman Medical Journal*, *29*(6), 391–398. https://doi.org/10.5001/omj.2014.107

Newton, P. T., Vuppalapati, K. K., Bouderlique, T., & Chagin, A. S. (2015). Pharmacological inhibition of lysosomes activates the MTORC1 signaling pathway in chondrocytes in an autophagy-independent manner. *Autophagy*, *11*(9), 1594–1607. https://doi.org/10.1080/15548627.2015.1068489

Ni, Y., Ji, C., Wang, B., Qiu, J., Wang, J., & Guo, X. (2013). A Novel pro-adipogenesis factor abundant in adipose tissues and over-expressed in obesity acts upstream of PPARγ and C/EBPα. *Journal of Bioenergetics and Biomembranes*, *45*(3), 219–228. https://doi.org/10.1007/s10863-012-9492-6

Nwadike, C., Williamson, L. E., Gallagher, L. E., Guan, J.-L., & Chan, E. Y. W. (2018). AMPK Inhibits ULK1-Dependent Autophagosome Formation and Lysosomal Acidification via Distinct Mechanisms. In *Molecular and Cellular Biology* (Vol. 38). https://doi.org/10.1128/mcb.00023-18

Ohshima, K., & Morii, E. (2021, January 1). Metabolic reprogramming of cancer cells during tumor progression and metastasis. *Metabolites*, Vol. 11, pp. 1–23. https://doi.org/10.3390/metabo11010028

Palm, W., & Thompson, C. B. (2017). Nutrient acquisition strategies of mammalian cells. *Nature*, *546*(7657), 234–242.

https://doi.org/10.1038/nature22379

Palmieri, M., Impey, S., Kang, H., di Ronza, A., Pelz, C., Sardiello, M., & Ballabio, A. (2011). Characterization of the CLEAR network reveals an integrated control of cellular clearance pathways. *Human Molecular Genetics*, *20*(19), 3852–3866. https://doi.org/10.1093/hmg/ddr306

Pandey, S., Lopez, C., & Jammu, A. (2003). Oxidative stress and activation of proteasome protease during serum deprivation-induced apoptosis in rat hepatoma cells; inhibition of cell death by melatonin. *Apoptosis*, *8*(5), 497–508. https://doi.org/10.1023/A:1025542424986

Parzych, K. R., & Klionsky, D. J. (2014). An overview of autophagy: Morphology, mechanism, and regulation. *Antioxidants and Redox Signaling*, Vol. 20, pp. 460–473. https://doi.org/10.1089/ars.2013.5371

Pastushenko, I., & Blanpain, C. (2019). EMT Transition States during Tumor Progression and Metastasis. *Trends in Cell Biology*, *29*(3), 212–226. https://doi.org/10.1016/j.tcb.2018.12.001

Pattingre, S., Tassa, A., Qu, X., Garuti, R., Xiao, H. L., Mizushima, N., … Levine, B. (2005). Bcl-2 antiapoptotic proteins inhibit Beclin 1-dependent autophagy. *Cell*, *122*(6), 927–939. https://doi.org/10.1016/J.CELL.2005.07.002

Pavlova, N. N., Hui, S., Ghergurovich, J. M., Fan, J., Intlekofer, A. M., White, R. M., … Zhang, J. (2018). As Extracellular Glutamine Levels Decline, Asparagine Becomes an Essential Amino Acid. *Cell Metabolism*, *27*(2), 428-438.e5. https://doi.org/10.1016/j.cmet.2017.12.006

Pavlova, N. N., & Thompson, C. B. (2016). The Emerging Hallmarks of Cancer Metabolism. *Cell Metabolism*, *23*(1), 27–47. https://doi.org/10.1016/j.cmet.2015.12.006

Pomo, J. M., Taylor, R. M., & Gullapalli, R. R. (2016). Influence of TP53 and CDH1 genes in hepatocellular cancer spheroid formation and culture: A

model system to understand cancer cell growth mechanics. *Cancer Cell International*, *16*(1), 44. https://doi.org/10.1186/s12935-016-0318-1

Puram, S. V., Parikh, A. S., & Tirosh, I. (2018). Single cell RNA-seq highlights a role for a partial EMT in head and neck cancer. *Molecular and Cellular Oncology*, *5*(3). https://doi.org/10.1080/23723556.2018.1448244

Qiang, L., Zhao, B., Ming, M., Wang, N., He, T. C., Hwang, S., … He, Y. Y. (2014). Regulation of cell proliferation and migration by p62 through stabilization of Twist1. *Proceedings of the National Academy of Sciences of the United States of America*, *111*(25), 9241–9246. https://doi.org/10.1073/pnas.1322913111

Rai, Y., Pathak, R., Kumari, N., Sah, D. K., Pandey, S., Kalra, N., … Bhatt, A. N. (2018). Mitochondrial biogenesis and metabolic hyperactivation limits the application of MTT assay in the estimation of radiation induced growth inhibition. *Scientific Reports*, *8*(1), 1–15. https://doi.org/10.1038/s41598-018-19930-w

Rasool, R. U., Nayak, D., Chakraborty, S., Jamwal, V. L., Mahajan, V., Katoch, A., … Goswami, A. (2017). Differential regulation of NM23-H1 under hypoxic and serum starvation conditions in metastatic cancer cells and its implication in EMT. *European Journal of Cell Biology*, *96*(2), 164–171. https://doi.org/10.1016/j.ejcb.2017.01.008

Ravanan, P., Srikumar, I. F., & Talwar, P. (2017, November 1). Autophagy: The spotlight for cellular stress responses. *Life Sciences*, Vol. 188, pp. 53–67. https://doi.org/10.1016/j.lfs.2017.08.029

Ravanidis, S., Grundler, F., de Toledo, F. W., Dimitriou, E., Tekos, F., Skaperda, Z., … Doxakis, E. (2021). Fasting-mediated metabolic and toxicity reprogramming impacts circulating microRNA levels in humans. *Food and Chemical Toxicology*, *152*. https://doi.org/10.1016/j.fct.2021.112187

Redmann, M., Benavides, G. A., Berryhill, T. F., Wani, W. Y., Ouyang, X.,

Johnson, M. S., … Zhang, J. (2017). Inhibition of autophagy with bafilomycin and chloroquine decreases mitochondrial quality and bioenergetic function in primary neurons. *Redox Biology*, *11*, 73–81. https://doi.org/10.1016/j.redox.2016.11.004

Rodrigues, J. P., David, L., Almeida, R., Barros, R., Freitas, T., Silva, J., … Carvalho, J. (2018, June 1). Mechanisms of regulation of normal and metaplastic intestinal differentiation. *Histology and Histopathology*, Vol. 33, pp. 523–532. https://doi.org/10.14670/HH-11-938

Rousset, M. (1986, September 1). The human colon carcinoma cell lines HT-29 and Caco-2: Two in vitro models for the study of intestinal differentiation. *Biochimie*, Vol. 68, pp. 1035–1040. https://doi.org/10.1016/S0300-9084(86)80177-8

Russell, R. C., Yuan, H. X., & Guan, K. L. (2014). Autophagy regulation by nutrient signaling. *Cell Research*, *24*(1), 42–57. https://doi.org/10.1038/cr.2013.166

Saitoh, M. (2018). Involvement of partial EMT in cancer progression. *Journal of Biochemistry*, *164*(4), 257–264. https://doi.org/10.1093/jb/mvy047

Sambuy, Y., De Angelis, I., Ranaldi, G., Scarino, M. L., Stammati, A., & Zucco, F. (2005). The Caco-2 cell line as a model of the intestinal barrier: in£uence of cell and culture-related factors on Caco-2 cell functional characteristics. In *Cell Biology and Toxicology* (Vol. 21). Springer.

Sato, K., Tsuchihara, K., Fujii, S., Sugiyama, M., Goya, T., Atomi, Y., … Botelho, R. J. (2019). Autophagosome maturation: An epic journey from the ER to lysosomes. *Journal of Cell Science*, *288*(7), 1–16. https://doi.org/10.1016/j.physbeh.2017.03.040

Sato, K., Tsuchihara, K., Fujii, S., Sugiyama, M., Goya, T., Atomi, Y., … Esumi, H. (2007). Autophagy is activated in colorectal cancer cells and contributes to the tolerance to nutrient deprivation. *Cancer Research*, *67*(20), 9677–9684.

https://doi.org/10.1158/0008-5472.CAN-07-1462

Schmidt, M., Scholz, C. J., Polednik, C., & Roller, J. (2016). Spheroid-based 3-dimensional culture models: Gene expression and functionality in head and neck cancer. *Oncology Reports*, *35*(4), 2431–2440. https://doi.org/10.3892/or.2016.4581

Shi, Y., Felley-Bosco, E., Marti, T. M., Orlowski, K., Pruschy, M., & Stahel, R. A. (2012). Starvation-induced activation of ATM/Chk2/p53 signaling sensitizes cancer cells to cisplatin. *BMC Cancer*, *12*(1), 1–10. https://doi.org/10.1186/1471-2407-12-571

Shibata-Seki, T., Nagaoka, M., Goto, M., Kobatake, E., & Akaike, T. (2020). Direct visualization of the extracellular binding structure of E-cadherins in liquid. *Scientific Reports 2020 10:1*, *10*(1), 1–10. https://doi.org/10.1038/s41598-020-72517-2

Shimazui, T., Schalken, J. A., Kawai, K., Kawamoto, R., Van Bockhoven, A., Oosterwijk, E., & Akaza, H. (2004). Role of complex cadherins in cell-cell adhesion evaluated by spheroid formation in renal cell carcinoma cell lines. *Oncology Reports*, *11*(2), 357–360. https://doi.org/10.3892/or.11.2.357

Singla, M., & Bhattacharyya, S. (2017). Autophagy as a potential therapeutic target during epithelial to mesenchymal transition in renal cell carcinoma: An in vitro study. *Biomedicine and Pharmacotherapy*, *94*, 332–340. https://doi.org/10.1016/j.biopha.2017.07.070

Sinha, D., Saha, P., Samanta, A., & Bishayee, A. (2020). Emerging concepts of hybrid epithelial-to-mesenchymal transition in cancer progression. *Biomolecules*, Vol. 10, pp. 1–22. https://doi.org/10.3390/biom10111561

Solanas, G., Porta-de-la-Riva, M., Agusti, C., Casagolda, D., Sánchez-Aguilera, F., Larriba, M. J., … Baulida, J. (2008). E-cadherin controls β-catenin and NF-κB transcriptional activity in mesenchymal gene expression. *Journal of Cell Science*, *121*(13), 2224–2234. https://doi.org/10.1242/jcs.021667

Spill, F., Reynolds, D. S., Kamm, R. D., & Zaman, M. H. (2016, August 1). Impact of the physical microenvironment on tumor progression and metastasis. *Current Opinion in Biotechnology*, Vol. 40, pp. 41–48. https://doi.org/10.1016/j.copbio.2016.02.007

Spitz, D., Simons, A., Mattson, D., & Dornfeld, K. (2009). Glucose deprivation-induced metabolic oxidative stress and cancer therapy. *Journal of Cancer Research and Therapeutics*, *5*(9), 2. https://doi.org/10.4103/0973-1482.55133

Stadler, M., Dolznig, H., Pudelko, K., Unger, C., Kenner, L., Kramer, N., … Walter, S. (2016). Comparison of cancer cells in 2D vs 3D culture reveals differences in AKT-mTOR-S6K signaling and drug response. *Journal of Cell Science*, *130*(1), 203–218. https://doi.org/10.1242/jcs.188102

Stadler, M., Scherzer, M., Walter, S., Holzner, S., Pudelko, K., Riedl, A., … Dolznig, H. (2018). Exclusion from spheroid formation identifies loss of essential cell-cell adhesion molecules in colon cancer cells. *Scientific Reports*, *8*(1), 1–16. https://doi.org/10.1038/s41598-018-19384-0

Sullivan, M. R., Mattaini, K. R., Dennstedt, E. A., Nguyen, A. A., Sivanand, S., Reilly, M. F., … Vander Heiden, M. G. (2019). Increased Serine Synthesis Provides an Advantage for Tumors Arising in Tissues Where Serine Levels Are Limiting. *Cell Metabolism*, *29*(6), 1410-1421.e4. https://doi.org/10.1016/j.cmet.2019.02.015

Sun, M., Fu, H., Cheng, H., Cao, Q., Zhao, Y., Mou, X., … Ke, Y. (2012). A dynamic real-time method for monitoring epithelial barrier function in vitro. *Analytical Biochemistry*, *425*(2), 96–103. https://doi.org/10.1016/j.ab.2012.03.010

Szabo, G., & Bala, S. (2018). TFEB, a master regulator of lysosome biogenesis and autophagy, is a new player in alcoholic liver disease. *Physiology & Behavior*, *176*(1), 139–148. https://doi.org/10.1016/j.physbeh.2017.03.040

Tanida, I., Ueno, T., & Kominami, E. (2004, December). LC3 conjugation system

in mammalian autophagy. *International Journal of Biochemistry and Cell Biology*, Vol. 36, pp. 2503–2518. https://doi.org/10.1016/j.biocel.2004.05.009

Tavaluc, T. T., Hart, L. T., Dicker, D. T., & El-Deiry, W. S. (2007). Effects of low confluency, serum starvation and hypoxia on the side population of cancer cell lines. *Cell Cycle*, *6*(20), 2554–2562. https://doi.org/10.4161/cc.6.20.4911

Thomas, M., Davis, T., Nell, T., Sishi, B., & Engelbrecht, A. M. (2020). Amino Acid Starvation Sensitizes Resistant Breast Cancer to Doxorubicin-Induced Cell Death. *Frontiers in Cell and Developmental Biology*, *8*, 1071. https://doi.org/10.3389/fcell.2020.565915

Tong, H., Yin, H., Hossain, M. A., Wang, Y., Wu, F., Dong, X., … He, W. (2019). Starvation-induced autophagy promotes the invasion and migration of human bladder cancer cells via TGF-β1/Smad3-mediated epithelial-mesenchymal transition activation. *Journal of Cellular Biochemistry*, *120*(4), 5118–5127. https://doi.org/10.1002/jcb.27788

Tong, J., Sun, D., Yang, C., Wang, Y., Sun, S., Li, Q., … Liu, Y. (2016). Serum starvation and thymidine double blocking achieved efficient cell cycle synchronization and altered the expression of p27, p53, bcl-2 in canine breast cancer cells. *Research in Veterinary Science*, *105*, 10–14. https://doi.org/10.1016/j.rvsc.2016.01.008

Tunçer, S., & Banerjee, S. (2019). Determination of autophagy in the caco-2 spontaneously differentiating model of intestinal epithelial cells. In *Methods in Molecular Biology* (Vol. 1854, pp. 55–70). https://doi.org/10.1007/7651_2017_66

Tunçer, S., Sade-Memişoğlu, A., Keşküş, A. G., Sheraj, I., Güner, G., Akyol, A., & Banerjee, S. (2020). Enhanced expression of HNF4α during intestinal epithelial differentiation is involved in the activation of ER stress. *FEBS Journal*, *287*(12), 2504–2523. https://doi.org/10.1111/febs.15152

Van Roy, F., & Berx, G. (2008, November). The cell-cell adhesion molecule E-

cadherin. *Cellular and Molecular Life Sciences*, Vol. 65, pp. 3756–3788. https://doi.org/10.1007/s00018-008-8281-1

Vaziri-Gohar, A., Cassel, J., Mohammed, F. S., Zarei, M., Hue, J. J., Hajihassani, O., … Winter, J. M. (2022). Limited nutrient availability in the tumor microenvironment renders pancreatic tumors sensitive to allosteric IDH1 inhibitors. *Nature Cancer*. https://doi.org/10.1038/s43018-022-00393-y

Wang, L., Shang, Z., Zhou, Y., Hu, X., Chen, Y., Fan, Y., … Gao, Z. (2018). Autophagy mediates glucose starvation-induced glioblastoma cell quiescence and chemoresistance through coordinating cell metabolism, cell cycle, and survival. *Cell Death and Disease*, *9*(2). https://doi.org/10.1038/s41419-017-0242-x

Wang, R. C., Wei, Y., An, Z., Zou, Z., Xiao, G., Bhagat, G., … Levine, B. (2012). Akt-mediated regulation of autophagy and tumorigenesis through Beclin 1 phosphorylation. *Science*, *338*(6109), 956–959. https://doi.org/10.1126/science.1225967

Wang, Y., Xiong, H., Liu, D., Hill, C., Ertay, A., Li, J., … Lu, X. (2019). Autophagy inhibition specifically promotes epithelial-mesenchymal transition and invasion in RAS-mutated cancer cells. *Autophagy*, *15*(5), 886–899. https://doi.org/10.1080/15548627.2019.1569912

Ward, P. S., & Thompson, C. B. (2012). Signaling in control of cell growth and metabolism. *Cold Spring Harbor Perspectives in Biology*. https://doi.org/10.1101/cshperspect.a006783

Wu, C. A., Chao, Y., Shiah, S. G., & Lin, W. W. (2013). Nutrient deprivation induces the Warburg effect through ROS/AMPK-dependent activation of pyruvate dehydrogenase kinase. *Biochimica et Biophysica Acta (BBA) - Molecular Cell Research*, *1833*(5), 1147–1156. https://doi.org/10.1016/J.BBAMCR.2013.01.025

Wu, Y. T., Tan, H. L., Shui, G., Bauvy, C., Huang, Q., Wenk, M. R., … Shen, H.

M. (2010). Dual role of 3-methyladenine in modulation of autophagy via different temporal patterns of inhibition on class I and III phosphoinositide 3-kinase. *Journal of Biological Chemistry*, *285*(14), 10850–10861. https://doi.org/10.1074/jbc.M109.080796

Xu, J., Huang, G., Zhang, Z., Zhao, J., Zhang, M., Wang, Y., … Lu, J. (2015). Up-Regulation of Glioma-Associated Oncogene Homolog 1 Expression by Serum Starvation Promotes Cell Survival in ER-Positive Breast Cancer Cells. *Cellular Physiology and Biochemistry*, *36*(5), 1862–1876. https://doi.org/10.1159/000430156

Yakisich, J. S., Venkatadri, R., Azad, N., & Iyer, A. K. V. (2017). Chemoresistance of Lung and Breast Cancer Cells Growing Under Prolonged Periods of Serum Starvation. *Journal of Cellular Physiology*, *232*(8), 2033–2043. https://doi.org/10.1002/jcp.25514

Yang, J., Antin, P., Berx, G., Blanpain, C., Brabletz, T., Bronner, M., … Sheng, G. (2020, June). Guidelines and definitions for research on epithelial–mesenchymal transition. *Nature Reviews Molecular Cell Biology*, Vol. 21, pp. 341–352. https://doi.org/10.1038/s41580-020-0237-9

Yeung, T. M., Gandhi, S. C., Wilding, J. L., Muschel, R., & Bodmer, W. F. (2010). Cancer stem cells from colorectal cancer-derived cell lines. *Proceedings of the National Academy of Sciences of the United States of America*, *107*(8), 3722–3727. https://doi.org/10.1073/pnas.0915135107

Yilmaz-Ozcan, S., Sade, A., Kucukkaraduman, B., Kaygusuz, Y., Senses, K. M., Banerjee, S., & Gure, A. O. (2014). Epigenetic mechanisms underlying the dynamic expression of cancer-testis genes, PAGE2,-2B and SPANX-B, during mesenchymal-to-epithelial transition. *PLoS ONE*, *9*(9). https://doi.org/10.1371/journal.pone.0107905

Ying, W., Jing, T., Bing, C., Baifang, W., Dai, Z., & Bingyuan, W. (2014). Effects of alcohol on intestinal epithelial barrier permeability and expression of tight

junction-associated proteins. *Molecular Medicine Reports*, *9*(6), 2352–2356. https://doi.org/10.3892/mmr.2014.2126

Yoshii, S. R., & Mizushima, N. (2017). Monitoring and measuring autophagy. *International Journal of Molecular Sciences*, *18*(9), 1–13. https://doi.org/10.3390/ijms18091865

Zheng, H. C. (2017). The molecular mechanisms of chemoresistance in cancers. *Oncotarget*, Vol. 8, pp. 59950–59964. https://doi.org/10.18632/oncotarget.19048

Zheng, N., Wang, K., He, J., Qiu, Y., Xie, G., Su, M., … Li, H. (2016). Effects of ADMA on gene expression and metabolism in serum-starved LoVo cells. *Scientific Reports*, *6*(1), 1–12. https://doi.org/10.1038/srep25892

Zhuge, J., & Cederbaum, A. I. (2006). Serum deprivation-induced HepG2 cell death is potentiated by CYP2E1. *Free Radical Biology and Medicine*, *40*(1), 63–74. https://doi.org/10.1016/j.freeradbiomed.2005.08.012
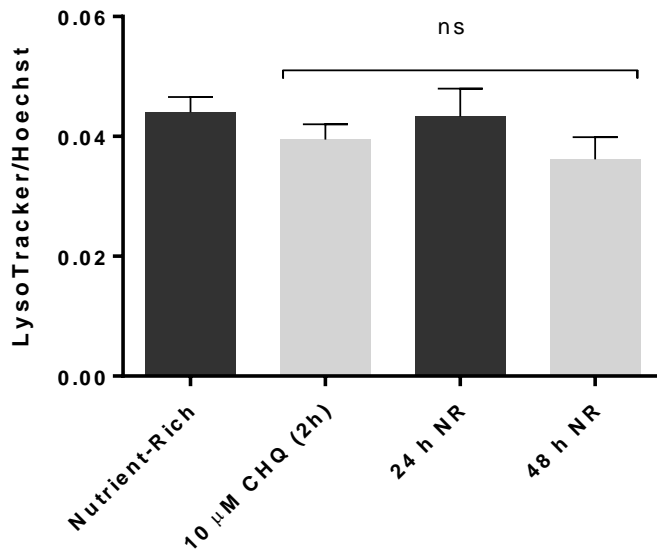
A. Lysotracker Red Assay with Chloroquine

Figure A.1 Analysis of lysosomal acidity with Chloroquine in LTR assay
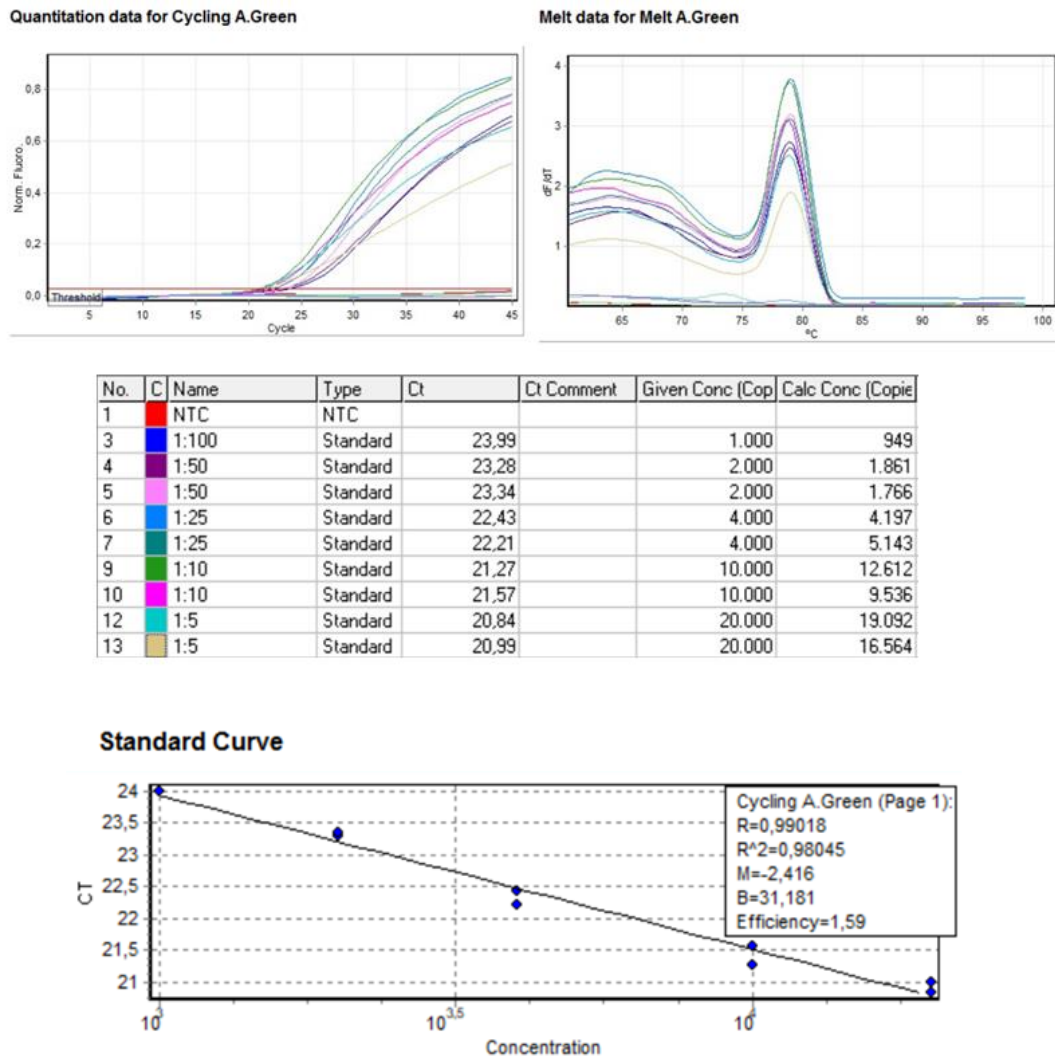
B. qRT-PCR Standard Curves

Quantitation data for Cycling A.Green

Melt data for Melt A.Green

No.	C	Name	Type	Ct	Ct Comment	Given Conc (Cop	Calc Conc (Copie
1		NTC	NTC				
3		1:100	Standard	23,99		1.000	949
4		1:50	Standard	23,28		2.000	1.861
5		1:50	Standard	23,34		2.000	1.766
6		1:25	Standard	22,43		4.000	4.197
7		1:25	Standard	22,21		4.000	5.143
9		1:10	Standard	21,27		10.000	12.612
10		1:10	Standard	21,57		10.000	9.536
12		1:5	Standard	20,84		20.000	19.092
13		1:5	Standard	20,99		20.000	16.564

Standard Curve

Cycling A.Green (Page 1):
R=0,99018
R^2=0,98045
M=-2,416
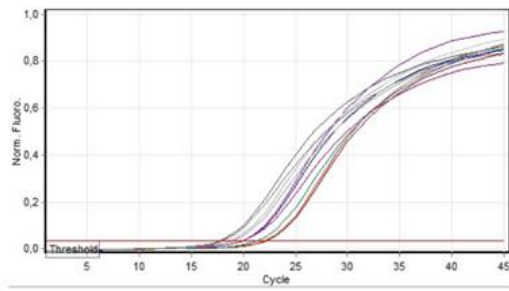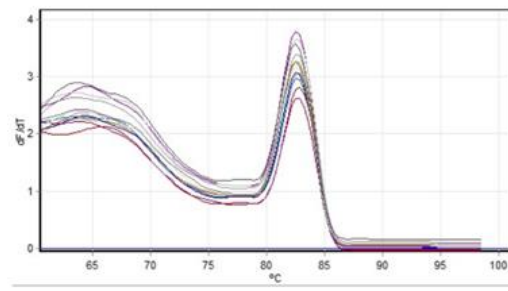B=31,181
Efficiency=1,59

Figure B.1 Standard and melt curves used for RAB5 qRT-PCR primers

114

Quantitation data for Cycling A.Green

Melt data for Melt A.Green

No.	C	Name	Type	Ct	Ct Comment	Given Conc (Cop	Calc Conc (Copie
19		1:100	Standard	22,18		1.000	1.052
20		1:100	Standard	22,30		1.000	972
21		1:100	Standard	22,20		1.000	1.037
22		1:50	Standard	21,32		2.000	1.933
23		1:50	Standard	21,46		2.000	1.745
24		1:50	Standard	21,48		2.000	1.730
25		1:25	Standard	20,13		4.000	4.441
26		1:25	Standard	20,07		4.000	4.649
27		1:25	Standard	20,14		4.000	4.428
28		1:10	Standard	19,01		10.000	9.772
29		1:10	Standard	18,81		10.000	11.242
30		1:10	Standard	19,15		10.000	8.834
31		1:5	Standard	18,14		20.000	18.064
32		1:5	Standard	17,94		20.000	20.668

Standard Curve

Cycling A.Green (Page 1):
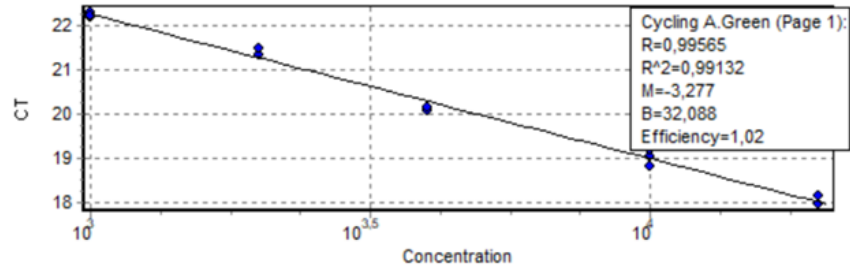R=0,99565
R^2=0,99132
M=-3,277
B=32,088
Efficiency=1,02
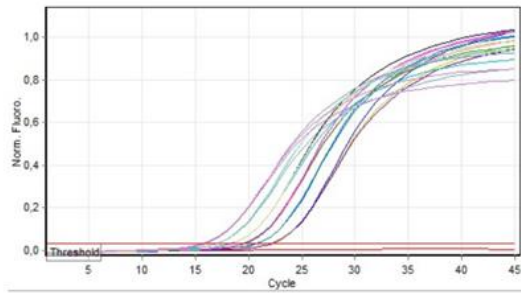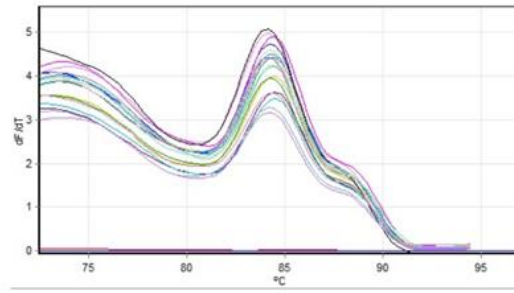
Figure B.2 Standard and melt curves used for RAB7A qRT-PCR primers

Quantitation data for Cycling A.Green

Melt data for Melt A.Green

No.	C	Name	Type	Ct	Ct Comment	Given Conc (Cop	Calc Conc (Copie
1		NTC	NTC				
2		1:250	Standard	22,30		10.000	10.036
3		1:250	Standard	22,25		10.000	10.377
4		1:250	Standard	22,26		10.000	10.311
5		1:100	Standard	20,88		25.000	24.000
6		1:100	Standard	20,83		25.000	24.769
7		1:100	Standard	20,88		25.000	23.995
8		1:50	Standard	19,74		50.000	48.353
9		1:50	Standard	19,59		50.000	52.810
10		1:50	Standard	19,74		50.000	48.432
11		1:25	Standard	18,56		100.000	99.812
12		1:25	Standard	18,47		100.000	105.131
13		1:25	Standard	18,55		100.000	100.059
14		1:10	Standard	17,07		250.000	248.625
15		1:10	Standard	17,12		250.000	241.656
16		1:10	Standard	17,14		250.000	238.688
17		1:5	Standard	16,08		500.000	456.550
18		1:5	Standard	15,74		500.000	560.766
19		1:5	Standard	15,86		500.000	522.400

Standard Curve

Cycling A.Green (Page 1):
R=0,99937
R^2=0,99874
M=-3,752
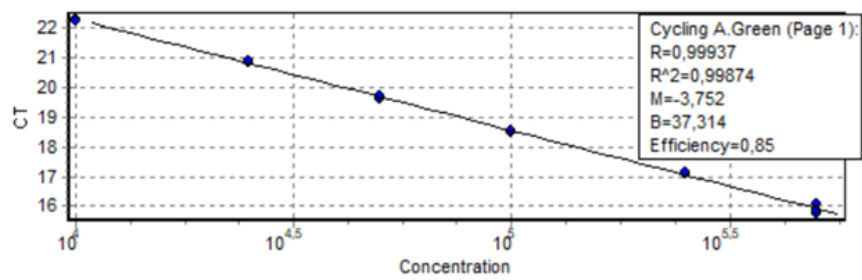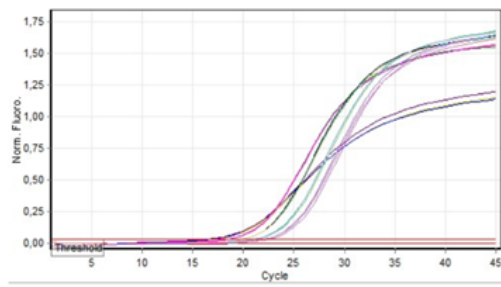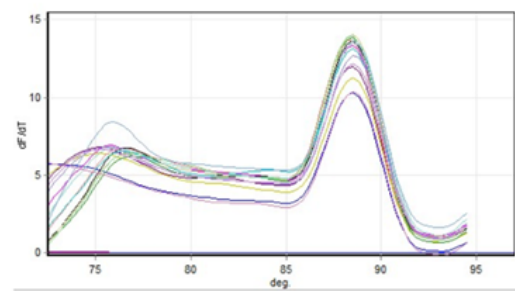B=37,314
Efficiency=0,85

Figure B.3 Standard and melt curves used for SQSTM1 qRT-PCR primers

Quantitation data for Cycling A.Green

Melt data for Melt A.Green

No.	C	Name	Type	Ct	Ct Comment	Given Conc (Cop	Calc Conc (Copie
1		NTC	NTC				
2		1:1	Standard	16,56		5.000	4.005
3		1:1	Standard	16,58		5.000	3.966
4		1:1	Standard	16,08		5.000	5.550
8		1:5	Standard	18,16		1.000	1.358
9		1:5	Standard	18,19		1.000	1.327
10		1:5	Standard	18,24		1.000	1.289
11		1:10	Standard	19,82		500	441
12		1:10	Standard	19,76		500	460
13		1:10	Standard	19,84		500	436
14		1:25	Standard	21,01		200	198
15		1:25	Standard	20,91		200	211
16		1:25	Standard	21,09		200	187
17		1:50	Standard	22,00		100	101
18		1:50	Standard	22,17		100	90
19		1:50	Standard	22,05		100	98

Standard Curve

Cycling A.Green (Page 1):
R=0,99257
R^2=0,98519
M=-3,402
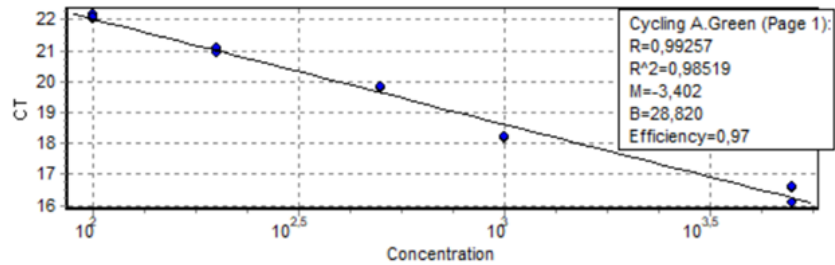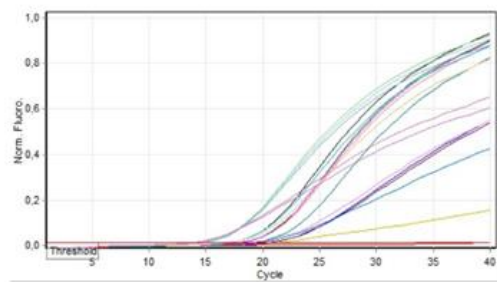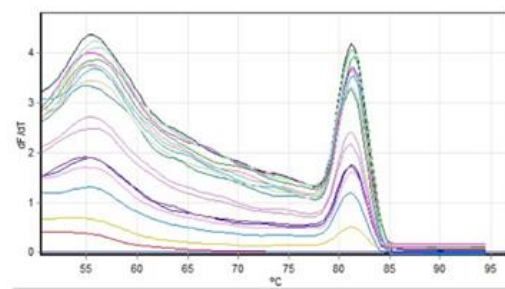B=28,820
Efficiency=0,97

Figure B.4 Standard and melt curves used for MCOLN1 qRT-PCR primers

Quantitation data for Cycling A.Green

Melt data for Melt A.Green

No.	C	Name	Type	Ct	Ct Comment	Given Conc (Cop	Calc Conc (Copie
1		NTC	NTC				
2		1.500	Standard	20,77		1.000	785
3		1.500	Standard	20,44		1.000	978
4		1.500	Standard	20,27		1.000	1.095
5		1.250	Standard	19,51		2.000	1.814
6		1.250	Standard	19,26		2.000	2.150
7		1.250	Standard	19,14		2.000	2.324
8		1.100	Standard	17,95		5.000	5.152
9		1.100	Standard	17,92		5.000	5.263
10		1.100	Standard	17,90		5.000	5.314
11		1.50	Standard	16,94		10.000	10.144
12		1.50	Standard	17,04		10.000	9.482
13		1.50	Standard	17,05		10.000	9.399
14		1.10	Standard	14,28		50.000	59.685
15		1.10	Standard	14,48		50.000	52.311
16		1.10	Standard	14,63		50.000	47.404
18		1.5	Standard	13,56		100.000	96.741
19		1.5	Standard	13,70		100.000	87.945

Standard Curve

Cycling A.Green (Page 1):
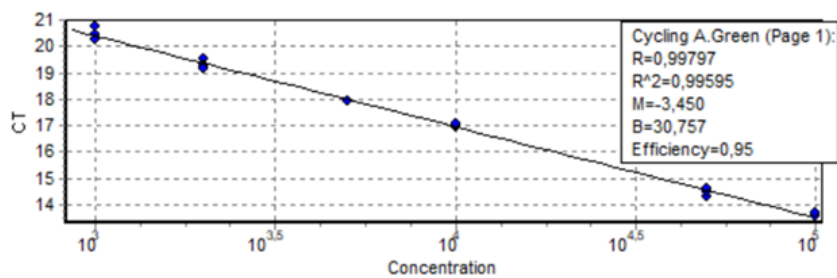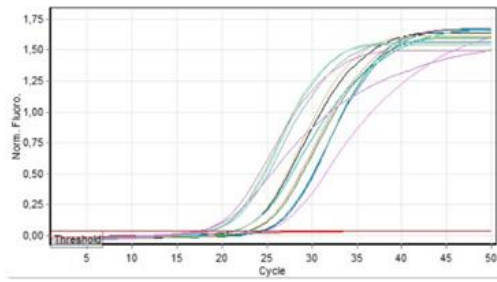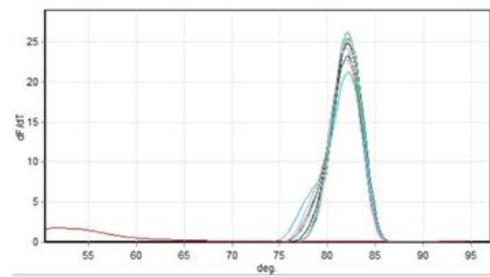R=0,99797
R^2=0,99595
M=-3,450
B=30,757
Efficiency=0,95

Figure B.5 Standard and melt curves used for CDH1 qRT-PCR primers

Quantitation data for Cycling A.Green

Melt data for Melt A.Green

No.	C	Name	Type	Ct	Ct Comment	Given Conc [Cop	Calc Conc [Copie
1		NTC	NTC				
5		1:250	Standard	24,72		2,0000000E+00	1,8764901E+00
6		1:250	Standard	24,39		2,0000000E+00	2,2702328E+00
7		1:250	Standard	24,70		2,0000000E+00	1,8935493E+00
8		1:100	Standard	23,24		5,0000000E+00	4,3952599E+00
9		1:100	Standard	23,23		5,0000000E+00	4,4142421E+00
11		1:50	Standard	21,72		1,0000000E+01	1,0560031E+01
12		1:50	Standard	21,51		1,0000000E+01	1,1924603E+01
13		1:50	Standard	21,76		1,0000000E+01	1,0308235E+01
14		1:10	Standard	18,77		5,0000000E+01	5,7760591E+01
15		1:10	Standard	19,02		5,0000000E+01	5,0082053E+01
16		1:10	Standard	18,96		5,0000000E+01	5,1849956E+01
18		1:5	Standard	17,89		1,0000000E+02	9,6232332E+01
19		1:5	Standard	18,10		1,0000000E+02	8,5256881E+01

Standard Curve

Cycling A.Green (Page 1):
R=0,99454
R^2=0,98910
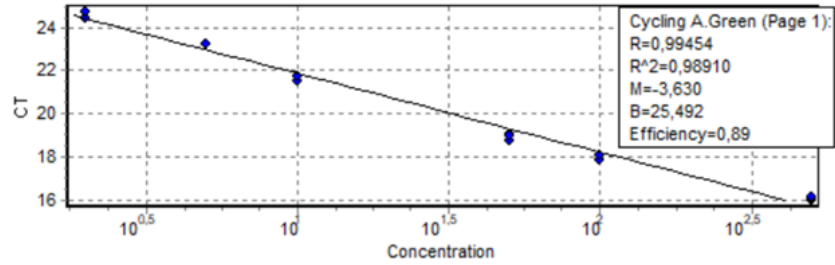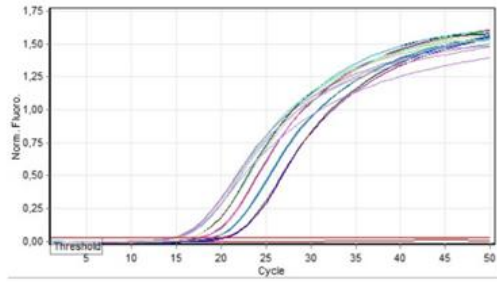M=-3,630
B=25,492
Efficiency=0,89

Figure B.6 Standard and melt curves used for OCLN qRT-PCR primers

Quantitation data for Cycling A.Green

Melt data for Melt A.Green
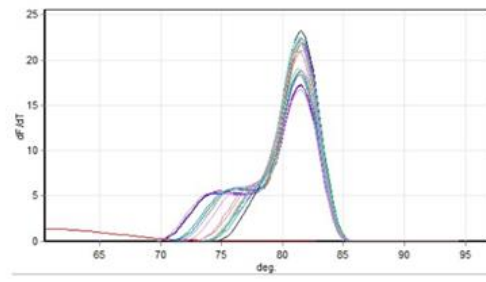
No.	C	Name	Type	Ct	Ct Comment	Given Conc (cop	Calc Conc (copie
1		NTC	NTC				
2		1:250	Standard	20,16		10.000	10.727
3		1:250	Standard	20,47		10.000	8.813
4		1:250	Standard	20,08		10.000	11.268
5		1:100	Standard	18,91		25.000	23.784
6		1:100	Standard	19,11		25.000	20.910
7		1:100	Standard	19,06		25.000	21.620
8		1:50	Standard	17,87		50.000	46.271
9		1:50	Standard	17,68		50.000	52.194
10		1:50	Standard	17,62		50.000	54.109
11		1:25	Standard	16,47		100.000	113.292
12		1:25	Standard	16,61		100.000	103.130
13		1:25	Standard	16,56		100.000	106.759
14		1:10	Standard	14,94		250.000	299.248
15		1:10	Standard	14,79		250.000	329.207
16		1:10	Standard	15,00		250.000	288.455
17		1:5	Standard	14,38		500.000	430.230
18		1:5	Standard	14,42		500.000	417.293
19		1:5	Standard	14,49		500.000	400.519

Standard Curve

Cycling A.Green (Page 1):
R=0,99439
R^2=0,98881
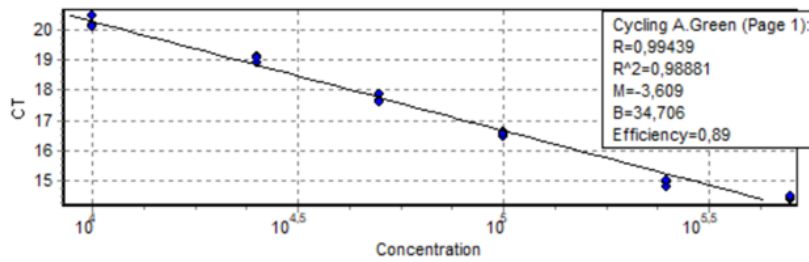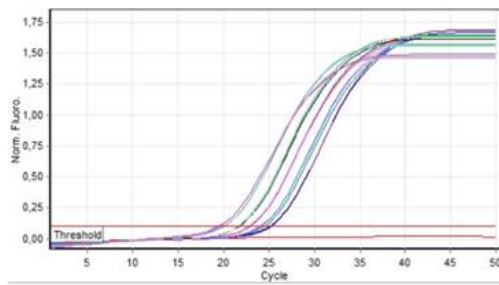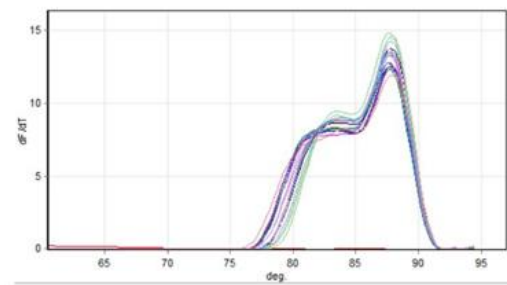M=-3,609
B=34,706
Efficiency=0,89

Figure B.7 Standard and melt curves used for VIM qRT-PCR primers

Quantitation data for Cycling A.Green

Melt data for Melt A.Green

No.	C	Name	Type	Ct	Ct Comment	Given Conc (Cop	Calc Conc (Copie
1		NTC	NTC				
3		1:250	Standard	25,03		10.000	12.030
4		1:250	Standard	25,21		10.000	10.700
5		1:100	Standard	24,01		25.000	23.362
6		1:100	Standard	24,12		25.000	21.861
7		1:100	Standard	24,47		25.000	17.400
8		1:50	Standard	22,83		50.000	50.671
9		1:50	Standard	22,88		50.000	48.978
10		1:50	Standard	22,90		50.000	48.249
11		1:25	Standard	21,73		100.000	103.635
12		1:25	Standard	21,72		100.000	104.268
13		1:25	Standard	21,57		100.000	114.595
14		1:10	Standard	20,06		250.000	307.515
15		1:10	Standard	20,02		250.000	315.794
16		1:10	Standard	20,04		250.000	311.399
17		1:5	Standard	19,66		500.000	400.397
18		1:5	Standard	19,61		500.000	411.928
19		1:5	Standard	19,47		500.000	450.907

Standard Curve

Cycling A.Green (Page 1):
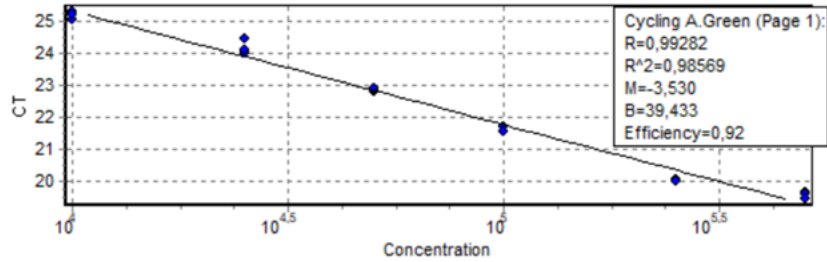R=0,99282
R^2=0,98569
M=-3,530
B=39,433
Efficiency=0,92

Figure B.8 Standard and melt curves used for SNAI1 qRT-PCR primers

121

C. Compositions of Buffers Used in this Study

Table C.1 Compositions of buffers in western blot experiment

CYTOPLASMIC AND NUCLEAR PROTEIN ISOLATION BUFFERS	
HYPOTONIC BUFFER	**NUCLEAR EXTRACTION BUFFER**
10 mM HEPES, pH 7	10 mM HEPES, pH 7.9
4 mM sodium fluoride,	1.5 mM MgCl2
10 µM sodium molybdate	420 mM NaCl
0.1 mM EDTA	0.1 mM EDTA
1X protease and phosphatase inhibitors	1X protease and phosphatase inhibitors
	10% glycerol
4% SDS-PAGE STACKING GEL	**12% SDS-PAGE SEPERATING GEL**
3.1 mL dH2O	3.4 mL dH2O
1.25 mL Stacking Buffer (10% SDS, 1.5M Tris, pH 6.8)	2.5 mL 4X Separating Buffer (10% SDS, 1.5M Tris, pH 8.8)
650 µL Acrylamide/Bis Solution (SERVA, Germany)	4 mL Acrylamide/Bis Solution (SERVA, Germany)
50 µL 10% APS	100 µL 10% APS
5 µL TEMED	10 µL TEMED
6X SDS-PAGE SAMPLE LOADING DYE	
12% SDS	
30% β-Mercaptoethanol	
30% Glycerol	
0.012% Bromophenol Blue	
0.375 M Tris-HCl pH 6.8	

Table C.1 (cont'd)

10X SDS-PAGE RUNNING BUFFER	1X SDS-PAGE RUNNING BUFFER
25 mM Tris	100 mL 10X Running Buffer
192 mM Glycine	900 mL dH_2O
0.1% SDS	
10X TRANSFER BUFFER	**1X TRANSFER BUFFER**
0.25 M Tris	100 mL 10X Transfer Buffer
1.92 M Glycine	200 mL Methanol
pH 8.3 in 1 L dH_2O	Fill up to 1L with dH_2O
20X TBS	**1X TBS-T**
50 mM Tris	50 mL 20X TBS
300 mM NaCl	950 mL dH_2O
4mM KCl	1 mL Tween 20
pH 7.4 in 1 L dH_2O	
MILD STRIPPING BUFFER	
15 g Glycine	
1 g SDS	
10 mL Tween-20	
pH 2.2 in 1L dH2O	

CURRICULUM VITAE

Surname, Name: Hüsnügil, Hepşen Hazal

EDUCATION

Degree	Institution	Year of Graduation
MS	METU Biochemistry	2016
BS	METU Molecular Biology and Genetics	2014
High School	Eskişehir Anadolu High School, Eskişehir	2009

FOREIGN LANGUAGES

Advanced English, Intermediate German, Elementary Japanese

PUBLICATIONS

1. Peptidomic characterization and bioactivity of Protoiurus kraepelini (Scorpiones: Iuridae venom). 2018. Somay Dogan T., Igci N., Biber A., Gerekci S., Husnugil H.H., Izbirak A., Özen C. Turkish Journal of Biology, 42 (6) , 490-498.

2. Anti-cancer effect of clofazimine as a single agent and in combination with cisplatin on U266 multiple myeloma cell line. 2017. Durusu İ.Z., Husnugil H.H., Atas H., Biber A., Gerekci S., EA Gulec A.E., Özen C. Leukemia Research, 55, 33-40.

CONFERENCE PAPERS

1. Pastorino G., Sheraj I., Hampel C., Hohmann P., Kunze P., Hartmann A., Huebner K., Husnugil H.H., Gulec A.E., Oral G., Erlenbach-Wuensch, K., Banerjee S., Schneider-Stock R. "Identification of a unique gene signature for partial epithelial-mesenchymal transition in colorectal cancer cells", COST Action no. CA17118, Torino, Italy, 2022.

2. Investigation of the effects of nutrient restriction on endolysosomal signaling in colorectal cancer (CRC) cells. 2021. Husnugil H.H., Gulec A.E., Oral G., Sheraj I., Banerjee S. Cancer Research, 81 (13).

3. Husnugil H.H., Güleç AE., Sheraj I., Erson Bensan A.E., Banerjee S., "Analysis of a potential microRNA network that co-regulates autophagy and epithelial to mesenchymal transition under nutrient restriction", HIBIT 2020, İstanbul, Turkey, 22 - 23 October 2020.

4. Husnugil H.H. & Gulec A.E., Banerjee S. (2019). "Nutrient Restriction Induced CeLL Death in Caco-2 Colon cancer Cells", 7th International Congress of the Molecular Biology Association of Turkey, İstanbul, Turkey, 2019.

5. Husnugil H.H., Yener C., Igci N., Banerjee S., Ozen C. "Cytotoxic Effect of Kv1.3 Blocker Clofazimine on HCT-116 Colon Cancer Cell Line", 3rd EACR-Sponsored Anticancer Agent Development Congress. Dokuz Eylül University. 18-19 May 2015.

6. Husnugil H.H., Erdes E., Agyuz U., Biber A., Ozen C., "Discovery of Novel Potassium Ion Channel Blocking Peptides from Scorpion Venom", 3rd International Congress of the Molecular Biology Association of Turkey, İzmir Institute of Technology, 12-14 September 2014.